UNIVERSITA' DEGLI STUDI DI PADOVA

Dipartimento di Ingegneria dell'Informazione

Corso di Laurea Magistrale in Bioingegneria

Comparative Analysis of FEM Models with Homogeneous and Structured Bone in the Foot-Ankle Complex for the Study of Stress Fractures in the First Metatarsal

Relatore: Prof.ssa Zimi SAWACHA

Correlatori: Proff. Annamaria GUIOTTO,
Andre JACQUES,
Guillaume RAO

Laureando: Francesca ARDITI

Matricola: 2053160

Anno Accademico 2023-2024

27 Febbraio 2024

Abstract

Le fratture da stress metatarsale nel piede o nella caviglia rappresentano il 20% delle lesioni negli atleti, tra cui corridori, ballerini e reclute militari. Il carico meccanico e le forze di flessione sperimentate durante la camminata giocano un ruolo cruciale nell'eziologia di queste fratture, sottolineando la necessità di un approccio analitico che simuli il movimento della corsa con particolare attenzione alle ossa metatarsali e alla loro composizione tessutale. La diagnosi di queste fratture coinvolge tipicamente strumenti di imaging medico come i raggi X o la risonanza magnetica (MRI), ma questi metodi forniscono immagini dirette delle strutture ossee post-infortunio. Per anticipare l'anamnesi, sono stati creati modelli tridimensionali rappresentativi della sezione anatomica del piede. Tuttavia, la maggior parte di questi modelli nella letteratura non tiene conto della geometria trabecolare, trattando l'osso come una struttura solida e non porosa.

Questo studio introduce un modello ad Elementi Finiti (FE) specifico per il soggetto che incorpora la geometria trabecolare per prevedere la distribuzione dello stress e le deformazioni ossee durante la corsa. Utilizzando immagini tomografiche computerizzate (CT) di un paziente, la struttura anatomica del primo osso metatarsale è stata ricostruita in tre dimensioni.

Il processo di convalida del modello è stato concepito attraverso una doppia strategia. Inizialmente è stato adottato un approccio visivo, confrontando graficamente gli stress tra il modello stratificato e il modello omogeneo, quest'ultimo riconosciuto come modello di riferimento nella letteratura. Successivamente è stata effettuata un'analisi numerica dettagliata, confrontando gli stress e le deformazioni medie dei due modelli. Questa metodologia combinata ha permesso di ottenere una valutazione completa e approfondita delle prestazioni del modello sia in termini di confronti visivi che quantitativi.

L'ispezione visiva ha rivelato notevoli differenze nei risultati, sia in termini di intensità che di distribuzione degli stress simulati, evidenziando una prestazione superiore del modello stratificato in conformità con le conoscenze biomeccaniche. La convalida numerica ha indicato che, a livello macroscopico, la risposta biomeccanica del piede è simile in entrambi i modelli, suggerendo che il tessuto trabecolare non influenzi significativamente la distribuzione delle forze di reazione al suolo. Tuttavia, gli stress medi hanno mostrato differenze significative. I valori del Rapporto di Stress ottenuti, Rcort e Rtrab, 2.44 e 0.17 rispettivamente, indicano una sottostima nella regione corticale e una sovrastima nella regione trabecolare del modello omogeneo rispetto a quello stratificato. Le deformazioni medie del modello poroso accentuano più prominentemente il comportamento

meccanico dei tessuti, dimostrando una maggiore alterazione nel tessuto poroso rispetto a quello denso.

In conclusione, il modello stratificato emerge come uno strumento promettente per l'analisi numerica della biomeccanica ossea, offrendo una prospettiva innovativa nel campo medico. Integrando conoscenze anatomiche approfondite, migliora l'accuratezza e la precisione delle simulazioni, riducendo le sottostime degli impatti biomeccanici e contribuendo a una prevenzione degli infortuni più efficace.

Abstract

Metatarsal stress fractures in the foot or ankle account for 20% of injuries in athletes, including runners, dancers, and military recruits. Mechanical load and bending forces experienced during walking play a crucial role in the aetiology of these fractures, emphasizing the need for an analytical approach that simulates running motion with a particular focus on the metatarsal bones and their tissue composition. Diagnosis of these fractures typically involves medical imaging tools such as X-rays or magnetic resonance imaging (MRI), but these methods provide direct images of the bone structures post-injury. To anticipate anamnesis, representative three-dimensional models of the anatomical section of the foot have been created. However, most of these models in the literature do not take trabecular geometry into account, treating bone as a solid, non-porous structure.

This study introduces a subject-specific Finite Element (FE) model incorporating trabecular geometry to predict the distribution of stress and bone deformations during running. Utilizing computed tomography (CT) images from a patient, the anatomical structure of the first metatarsal bone was reconstructed in three dimensions.

The model validation process was conceived through a dual strategy. Initially, a visual approach was adopted, graphically comparing the stresses between the layered model and the homogeneous model, the latter being recognised as the reference model in the literature. Subsequently, a detailed numerical analysis was carried out, comparing the average stresses and deformations of the two models. This combined methodology allowed obtaining a complete and in-depth assessment of the model's performance with respect to both visual and quantitative comparisons.

Visual inspection revealed notable differences in results, both in terms of intensity and distribution of simulated stresses, highlighting superior performance of the stratified model in accordance with biomechanical knowledge. Numerical validation indicated that, at a macroscopic level, the biomechanical response of the foot is similar in both models, suggesting that trabecular tissue does not significantly influence the distribution of ground reaction forces. However, average stresses exhibited significant differences. The Stress Ratio values obtained, Rcort and Rtrab, 2.44 and 0.17 respectively, indicate an underestimation in the cortical region and an overestimation in the trabecular region of the homogeneous model compared to the stratified one. Average deformations of the porous model more prominently accentuate the mechanical behaviour of tissues, demonstrating greater alteration in the porous tissue compared to the dense tissue.

In conclusion, the stratified model emerges as a promising numerical analysis tool for evaluating bone biomechanics, offering an innovative perspective in the medical field. By integrating in-depth anatomical knowledge, it enhances the accuracy and precision of simulations, reducing underestimations of biomechanical impacts and contributing to more effective injury prevention.

Summary

Figure Index

Table Index

Introduction

This thesis was elaborated during a five-month study period at the University of Aix-Marseille and developed in the laboratories of the Institut des Sciences du Mouvement in Marseille. The project originates from the clinical problem of stress fractures, particularly in the metatarsal bones of the foot. Approximately 10-20% of stress fractures occur in the metatarsal bones, due to their bony conformation; in fact, they have a long, thin diaphysis, which is subjected to high stresses and loads during sporting activities such as running, but also marching performed by military recruits.

The metatarsal bone has a structure with an outer shell of dense, compact cortical tissue, and an inner tissue with a sponge-like lamellar structure, known as trabecular tissue. The differential mechanical properties of these two tissues influence the bone's response to mechanical stress. Cortical bone provides strength and evenly distributes forces, while trabecular bone allows for greater elastic and plastic deformation.

To understand the stress distribution which occur at the bone during running, in silico simulations (such as Finite Element Analysis) can be used, as these quantities are not directly measurable in-vivo. However, many current FEM are not accurate, assigning to the bones geometry a single geometry average elastic modulus. This thesis proposes a solution to this problem by developing a FE model of the foot with diversification of bone regions.

The aim of the project was to validate three dynamic FEM of the foot by including the real layers of different materials of the First Metatarsal and comparing them with three homogeneous tissue models. These models represented different walking mood (stomping with the heel, stomping with the entire midfoot and stomping with the forefoot) obtained from the starting model (AMUFFEM) provided by the University of Aix-Marseille. Three-dimensional reconstruction of the bone was performed by manual segmentation of a subject's computed tomography (CT) image and subsequently inserted into the AMUFFEM. These models were simulated by applying subject-specific boundary conditions, obtained through in vivo gait analysis, and the specific mechanical properties of the first metatarsal tissues obtained from the literature were assigned.

For the data processing, six simulations of a right foot strike were performed, and the values of Von Mises stresses, principal deformations, and ground reaction forces (GRF) were extracted and processed with the Python programming language to generate representative graphs.

Finally, the results were evaluated qualitatively and quantitatively by comparing the homogeneous and stratified models.

The structure of the thesis is organised into the following chapters:

1. Stress Fracture
2. Biomechanics and foot anatomy
3. Finite Element Modelling
4. Proposed Methodology
5. Result and Discussion
6. Conclusion

Chapter 1

1 Stress Fracture

In the first chapter, we will explore the core of the clinical problem underlying the project, which will be developed in detail in subsequent chapters. It is crucial to fully understand the nature and importance of this clinical problem to enhance the implications, solutions and innovations presented in this work. One of the central aspects we will discuss is stress fractures, a clinical phenomenon that has received increasing attention in the field of sports medicine and orthopaedics. In addition to being simple observational injuries, stress fractures can have major consequences on an athlete's life, affecting his or her performance, physical well-being, and career path. We will explore not only the nature and specifics of stress fractures, but also the impact they can have on the athlete from a physical standpoint. Through this chapter, we will provide an overview that will allow the reader to gain an initial understanding of the clinical context and the urgency to explore this topic further. This analysis will prepare the ground for the following chapters, where we will explore in greater detail and analysis the issue of stress fractures in the context of athletes.

1.1 Metatarsal Fracture

Stress fractures of the foot or ankle account for about 10% of injuries in competitive and amateur athletes and 30% of injuries in military recruits. Repetitive submaximal mechanical loading brings about physiological adaptation of the bone, but when these forces exceed the bone's reparative capacity, the resulting imbalance between bone formation and bone resorption can lead to microscopic bone injuries. The accumulation of these micro lesions generates a series of damages that may manifest as reactive bone oedema, an incomplete or non-displaced fracture line visible with various imaging modalities or a displaced fracture clearly visible with plain radiography. Both intrinsic and extrinsic elements contribute to the occurrence of a stress fracture. Intrinsic elements are generally unchangeable and include the subject's age, gender, genetic predisposition, hormonal alterations, vascularisation of the affected area, health, and bone density. On the other hand, extrinsic elements are variable and include the athlete's diet, weight, medication intake, the sport discipline practised, type of training, use of protective equipment, biomechanics and technique adopted. In the past, bone scintigraphy was considered the reference method for identifying stress fractures due to its high sensitivity within the first 48-72 hours of initial symptoms. However, today MRI has taken over from bone scans, offering superior accuracy and the ability to examine the surrounding soft tissue for

other injuries. MRI is considered for initial evaluation when there is a clinical suspicion of a stress fracture, which requires a restrictive treatment protocol, such as a period of immobilisation without load or with plaster cast. It is crucial that MRI findings and clinical signs and symptoms are correlated, as stress reactions such as bone haematoma or generalised spinal oedema are different from stress fractures, but no less common.

Stress fractures represent a specific category of bone injuries that can occur in individuals subjected to excessive mechanical loading, especially in sporting contexts or prolonged physical activity. These injuries occur because of repeated microtrauma, which exceeds the bone's ability to adapt without an adequate rest period. In the context of stress fractures, it is essential to distinguish between two main categories: low-risk fractures and high-risk fractures. This distinction is not based solely on the severity of the injury, but also considers various factors such as the location of the injury, its ability to heal, and the potential impact on the athlete's overall health.

Low-risk fractures generally present a less severe clinical picture and tend to heal with adequate rest and appropriate management of physical activities. In these cases, it is possible for the athlete to return to sporting activity with a well-structured rehabilitation strategy. Low-risk fractures have a high propensity to heal regardless of the type of treatment. In this field, therapy generally involves a period of activity modification with full load. Often these types of fractures develop due to intrinsic factors such as low bone density, which contribute to fracture propagation. Common sites of low-risk fractures include the posteromedial tibial shaft, fibula, calcaneus, cuneiform, cuboid and neck or metatarsal rods (as distinct from the metatarsal bases).

Stress fractures in the metatarsal bones constitute 38% of all lower limb stress fractures. Typically, effective treatment involves rest or cast immobilisation, occasionally complemented by shockwave therapy. Torg classified stress fractures into three types:

- type I exhibits clear margins without signs of widening, sclerosis, or bone reaction.
- type II presents a widened fracture line with bone reaction.
- type III shows extensive fractures with complete sclerosis.

While ultrasound's diagnostic role is recognized in some studies, MRI remains the preferred diagnostic tool, especially when X-rays may be inconclusive early on. Type I fractures often receive conservative treatment with a plaster cast, but surgical options arise for type II and III fractures or failed conservative treatments. Athletes may benefit from intramedullary screw placement for quicker recovery. Some experts propose alternative non-surgical treatments like extracorporeal shock waves

or electromagnetic fields, though their effectiveness remains debated. Predominantly affecting runners, dancers, and military recruits, these fractures result from perpendicular loading and specific anatomical factors that make the metatarsals susceptible. Typically, symptoms manifest as dorsal swelling, and diagnosis via X-ray becomes clearer weeks post-onset, with MRI reserved for diagnostic uncertainty or persistent symptoms.

In the context of athletes, stress fractures considered high-risk in the foot and ankle area represent problems that present significant challenges in the healing phase. Due to their complex nature, they often require a proactive management approach that may include different strategies such as limiting stress, applying bandages or immobilisation, and in certain scenarios, resorting to surgery. These fractures mainly emerge in regions subject to tensile stress or in areas with specific vascular characteristics, circumstances that decrease the chances of a proper healing process, i.e. non-union or bone remodelling. Among the most frequently affected locations are the tibial shaft, medial malleolus, talus, navicular, and several parts of the metatarsals, including the second, third, fourth and the proximal region of the fifth.

The primary strategy to prevent stress fractures in this sports context is geared towards modifying external risk factors. In addition to following specific diet protocols and well-structured training programmes, it is crucial to integrate a multidisciplinary approach. This implies collaboration with specialists such as endocrinologists to monitor possible bone diseases or metabolic deficiencies, psychiatric counselling to manage potential eating disorders, and continuous supervision by coaches and athletic trainers. The integration of such expertise and professionals ensures a comprehensive and targeted framework to optimise athletes' health and performance, while minimising the risks associated with these injuries[1], [2] [3].

Chapter 2

2 Biomechanics and Foot Anatomy

In this chapter, the structure of bone tissue will be explored in detail. Next, the locomotor system will be explored in depth, focusing on the bones of the foot. An examination of the morphology of both cortical tissues, characterised by a dense and compact structure, and trabecular tissue, with a sponge-like lamellar structure, will be provided.

In the context of the locomotor system, crucial anatomical elements such as ligaments, muscles and tendons involved in human gait will be analysed. Their functions and role in movement will be illustrated, providing a comprehensive basis for understanding the complex biomechanical system of the foot.

The chapter will proceed with an in-depth study of the mechanical properties of the two bony tissues, cortical and trabecular, highlighting the key differences between them.

Lastly, the chapter will conclude by introducing the biomechanics of the foot and the analysis of movement, creating a bridge between anatomical structure and functional dynamics.

2.1 Hard connective tissue: Bones

Bones perform a dual function of supporting and protecting organs, such as the skull and rib cage, and facilitate movement through the system of joints, which connect the bones, and the musculoskeletal system. The skeleton is divided into two main parts: the axial part, comprising the skull, spine and rib cage, and the appendicular part, consisting of the upper and lower limbs. From a morphological point of view, different categories of bones can be distinguished based on characteristic size ratios:

- **long bones** predominate in one dimension over the other two,
- **flat bones** show a predominance of two dimensions over the third,
- **short bones** have comparable dimensions.

In addition to their mechanical function, bones play crucial roles in metabolic and cellular functions. In fact, they serve as the seat for bone marrow, a tissue responsible to produce red blood cells, platelets, and white blood cells. This function is concentrated in the vertebrae, pelvis, skull, and rib cage in adults.

Bone tissue is part of the connective tissue category. Connective tissue comprises different types of tissues because they are characterised by specific features, events a common embryonic origin. The shared characteristic is the ability to connect various tissues structurally and functionally, but it also has functions of mechanical support, protection, and energy reserve. The common embryonic origin concerns the formation structure: they consist of cells and extracellular matrix (ECM), a collection of fibres and amorphous fundamental substance. The supporting connective tissue or bone tissue is an extremely dynamic and plastic type of tissue. It can modulate its structure because of organic and mechanical stimuli and consists of an *organic* and an *inorganic* part.

- The **organic** component is made up of cells specific to bone tissue, which are responsible for the growth, production, and reabsorption of the tissue itself, as well as extracellular matrix.
- The **inorganic** component consists of numerous mineral salts, such as Calcium phosphate, Magnesium, Sodium citrates, Magnesium citrate and Potassium citrate.

33% of the bone's dry weight is the organic component, which determines its strength and elasticity; while 67% of the dry weight is the mineralised component, which gives it firmness and hardness [4].

The outer surfaces of the bones are covered by a thick connective tissue capsule with interwoven fibres, the **periosteum**, which has the task of protecting the bone and supporting the trophic action mediated by the blood vessels in which it is rich. While in the outer face of the periosteum there are few cells and many collagen fibres (fibrous layer), in the inner face there are few fibres, numerous blood capillaries and osteoprogenitor cells. Connective fibres called **Sharpey's fibres** branch transversally from the periosteum, forming an anchoring system to the bone. Finally, the inner surfaces of the bone consist of the **endosteum**, a layer of squamous cells and connective fibres [5]

In the organic component, we have said that there is the presence of the extracellular matrix, composed of different types of glycoproteins, which play a fundamental role in the mineralisation processes of bone tissue; proteoglycans, which help in the orientation of collagen fibres; and

hyaluronic acid. The most abundant protein present in EMC is collagen, which is present as type I collagen fibres and has a diameter of 5-10 microns in fibrous bone tissue and a smaller diameter of 60 microns in lamellar tissue.

Bone tissue is made up of several specific cells. In more detail, *osteoprogenitor cells* or pre-osteoblasts have a mesenchymal origin and are present in the free surfaces of bone: they are found in the periosteum and endosteum: when reactivated, they provide for the formation of new bone tissue; in addition, they have stem-like properties that allow them to proliferate and differentiate into osteoblasts.

Osteoblasts are precursor cells of osteocytes, they provide both the production of organic matrix and the deposition of inorganic matrix and thus have osteogenic functions by producing type I collagen, osteocalcin, osteopontin and bone sialoprotein. When osteoblasts have finished forming bone, becoming trapped within gaps in the matrix they produce, they become osteocytes.

Osteocytes are cells that make up 90-95% of total bone cells and have a particular morphology and position. They present an irregular shape, with a conspicuous nucleus and a cytoplasm with several extensions. In addition, from the lacunae in which they are housed, numerous microscopic canaliculi branch off, through which the cytoplasmic extensions of different osteocytes contact each other through communicating junctions and with blood capillaries present in the bone channels allowing metabolic exchanges.

Lastly, *osteoclasts* are multinucleated cells, derived from pre-osteoclasts, which originate from haematopoietic stem cells and are influenced by various factors. Their function is to absorb bone tissue through an enzymatic action. The action of resorption begins with an erosive action of the cell on the bone, resulting in a gap (Howship gap) in which the cell sites; a rippled rim adheres to the bone tissue resulting in a “sealed zone” where acidification of the environment due to substances released by the osteoclast results in resorption [4], [5]

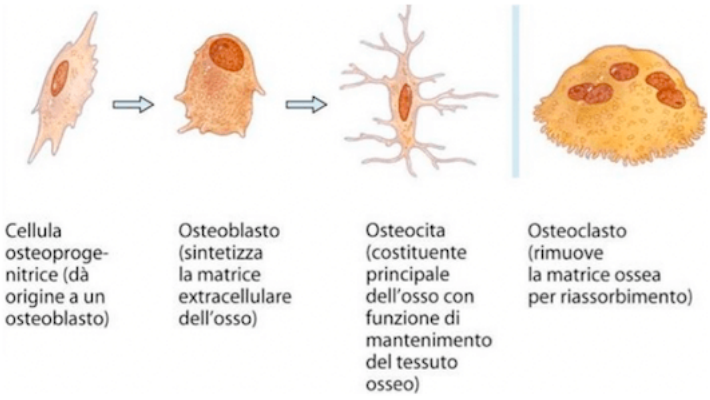

Figure 1: Graphical representation of the cells that make up bone tissue [6].

2.2 Locomotor apparatus and foot anatomy

The locomotor system represents the outcome of the synergistic union between the skeletal and muscular systems, thus forming the fundamental anatomical basis for human motor functions. The main anatomical elements that combine to form this complex system include bones, cartilaginous tissue, muscles, joints, tendons, and ligaments. The musculoskeletal system plays a crucial role, providing the human being with stability, support, and the ability to move and locomote, as well as performing a fundamental function in protecting vital internal organs, such as the brain, heart and lungs. The bones, which make up the skeleton, are responsible for providing stability and protection to the body. On the other hand, muscles, as the organs responsible for movement, confer mobility not only to the skeleton but also to other organs, such as the eyes. The interaction of these two components allows for a dynamic balance in the functioning of the locomotor system, ensuring a multifunctional role of the apparatus, which is essential for the well-being and functionality of the human body.

The anatomical section of the foot emerges as a fundamental ergonomic tool in the learning process of walking, especially in the developmental stages. Its role becomes crucial since the evolution of the vertebral curves and, consequently, of the entire posture, is closely related to the way the foot contacts the ground. This contact constitutes the anchor point to the ground on which the entire weight of the body rests, transmitting considerable loads to the ground and playing a key role in the antigravity control system.

During evolution, spanning some 350 million years, the demands of standing and bipolar walking led to the feet supporting twice the body weight compared to their original function of supporting a quarter of the weight. This transformation involved a transition from a prehensile to a stabilising (anti-

gravity) form, while maintaining the complexity of the foot musculature. Thus, the feet have become the most evolved and responsive mechanism to the environment and external stimuli in modern man, representing the most effective means of harnessing the energy required for locomotion, efficiently extracted from the force of gravity.

The feet are an essential part of our body, playing a crucial role in providing stability, balance and support. Their anatomy is remarkably complex, consisting of several parts, each of which performs specific functions. The structure of the feet, comprising bones, joints, muscles and soft tissue, is fundamental to our ability to maintain an upright position and to perform everyday activities such as walking, running and jumping.

Three main sections can be distinguished in the structure of the foot (Figure 2):

- ◊ Forefoot: This section includes the five toes (phalanges) and five bones called metatarsals.
- ◊ Midfoot: This is the central area of the foot, forming a pyramidal set of bones that help form the arch of the foot. It includes three cuneiform bones, the cuboid bone and the navicular bone.
- ◊ Hindfoot: This section forms the heel and ankle, involving the Astragalus and Calcaneus.

The complex interaction between these three sections allows the foot to adapt to different surfaces and perform a wide range of movements, providing the necessary basis for our locomotion and interaction with our surroundings.

Figure 2: Foot sections [7]

2.2.1 Foot bones

With a total of 26 bones, or 25% of the bones present in the human body, the foot is an articulated and complex bone structure that can be divided into three basic components: the tarsus, the metatarsus, and the phalanges.

- The ***tarsals*** are a group of seven bones located near the ankle: it includes the hindfoot and midfoot sections and is composed of short, irregular bones. In particular, the talus, calcaneus, three cuneiform, cuboid and navicular. The talus (or ankle bone) transfers the weight of the body onto the foot. It is connected superiorly to the two lower bones of the leg, the tibia and fibula; inferiorly, it is connected to the calcaneus, the bone that forms the heel. The five bones of the midfoot form the arch of the foot, which acts as a shock absorber.
- The ***metatarsals*** are located towards the toes and help connect the toes to the ankle. They are the first, second, third, fourth and fifth metatarsal bones of the forefoot section. The metatarsals are long, dorsally convex bones consisting of a body, a base (proximal) and a head (distal). These bones help establish balance when walking or running.

- The ***phalanges***, located at the end of the forefoot section, are the bones that make up the toes: there are 14 of them, two in each big toe and three in each other toe. These are called the proximal, middle, and distal phalanges.

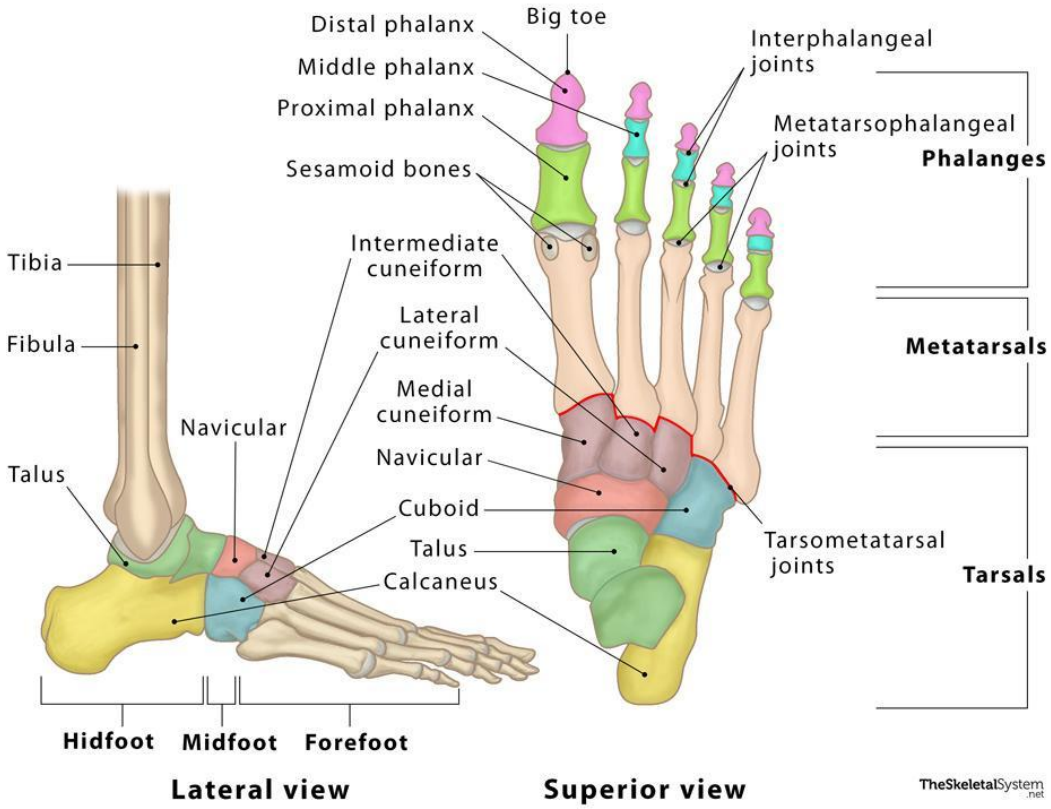

Figure 3: Foot bones [8]

From a structural point of view, it is possible to classify bone tissue into two distinct categories: trabecular tissue and cortical tissue. These different types of tissue are optimally distributed, organised, and shaped to provide the necessary mechanical properties with as little material as possible.

The fundamental difference between trabecular and cortical bone lies in the microstructural architecture. However, from a histological point of view, both share the same constituents. The different microstructural architecture results in significant differences in mechanical properties, giving cortical bone greater strength and stiffness. Cortical bone makes up 80 per cent of the total bone mass, while trabecular bone accounts for the remaining 20 per cent. The main function of cortical tissue is structural in nature, providing support and protection to the body. In contrast,

trabecular tissue has as its primary function the homeostasis of mineral levels, only secondarily playing a structural role[4].

In summary, the complex architecture of bone tissue is designed to maximise the necessary mechanical properties by differentiating the functions of cortical and trabecular tissue according to their microstructural characteristics and the physiological needs of the body.

Microscopic observation of bone tissue allows us to distinguish between two types of tissue:

- ◊ Lamellar: lamellar tissue forms the mature bone that results from the remodelling of fibrous or pre-existing bone tissue. This is a more organised tissue, with an orderly and parallel orientation of collagen fibres, which are arranged in overlapping layers called bone lamellae. Between one lamella and another, small, interconnected spaces: the lacunae, house cells that, by means of a system of canaliculi, meet areas of the bone from which they can receive nutritive materials.
- ◊ Non-lamellar: Fibrous, or interwoven-fibre, bone tissue is immature bone and is normally found in the embryo, in new-borns, in the metaphyseal site (see below) and during fracture healing. Once laid down, the fibrous tissue is readily resorbed and replaced with lamellar bone tissue. Under the microscope, it appears as a series of fibres interwoven in the three dimensions of space in an almost random manner. The meshes of this 'three-dimensional spider's web' consist of thick collagen fibres (5-10 μm in diameter). Non-lamellar bone is, overall, more elastic and less consistent than lamellar bone, due to the smaller amount of minerals and the lack of a preferential orientation of the collagen fibres.

In adults, all bone tissue is of the lamellar type; we find the non-lamellar type during ossification or during fracture repair. Lamellar bone tissue can in turn be divided into spongy bone and compact bone. Their basic composition is the same, but their three-dimensional arrangement is different. This diversification makes it possible to optimise the weight and bulk of the bones according to the different stresses to which they are subjected [9].

Usually, cortical bone occurs in the outer layer of bones, in the dialysis of long bones and in the epiphyses of short and flat bones, while trabecular bone characterises the dipole of flat bones.

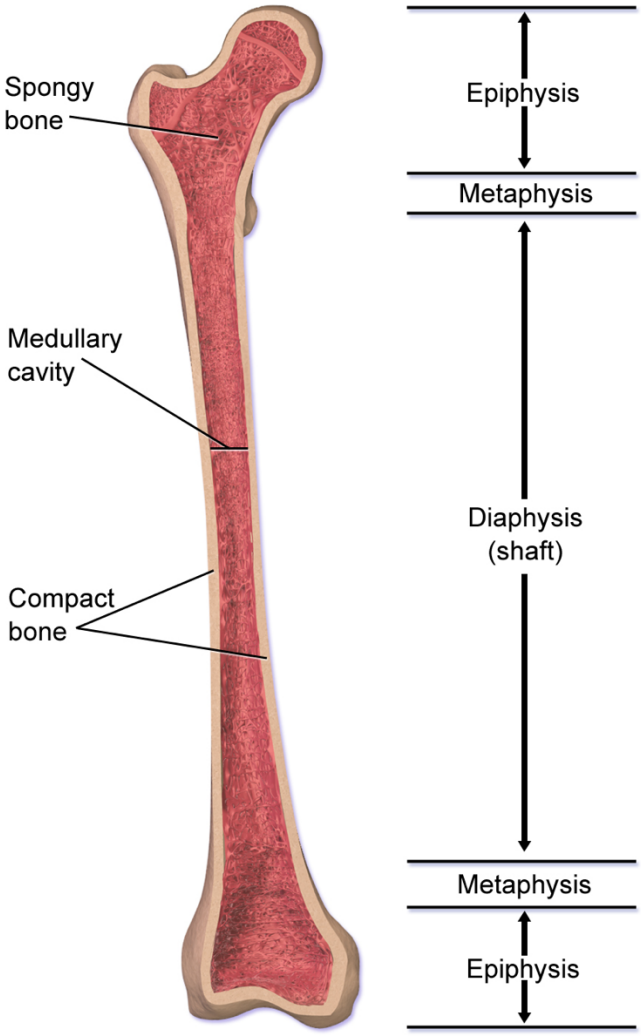

Figure 4: Representation of the main sectors of a bone, such as epiphysis and diaphysis, and depiction of the location of the cortical and trabecular layer [10]

2.2.1.1 Cortical Layer

The term “cortical” refers to the structure involving osteons aligned along a clearly defined axis, which are formed by concentric lamellae.

In the bone context, the cortical manifests itself as the outer layer of short, flat bones, and forms the diaphysis of long bones. The outer surface of the diaphysis is covered by the *periosteum*, a fibrous membrane whose fundamental role is to provide vascularity and nutrition to the bone. Inside the periosteum is the osteogenic layer, characterized by marked cellular activity. During growth phases, this layer allows the enlargement of the bone section and determines its shape. The periosteum plays a crucial role in the healing process of damaged bone, facilitating regeneration and repair of bone

tissue. The *endosteum*, on the other hand, is the membrane that lines the internal cavities of the bone, helping to maintain ionic balance and regulate bone metabolism.

Compact bone, also referred to as cortical bone, forms the solid and relatively dense outer walls of bone, providing strength. At the microscopic level, it displays a highly organized architecture, with the functional and structural unit known as an osteon or Haversian system. In the diaphysis, osteons align parallel to the longitudinal axis.

The osteon presents an intricate three-dimensional structure, characterized by several components. The central canal, or Haversian canal, extends along the osteon's longitudinal axis, housing blood vessels and nerves. Concentric lamellae of bony connective tissue surround the central canal, constituting the predominant part of the osteon. The number of these lamellae varies between osteons. Each lamella contains collagen fibres oriented in a specific direction, creating a combination of solidity and flexibility as adjacent lamellae have fibres oriented alternately. Osteocytes are situated in the gaps between the concentric lamellae. Canaliculi, small, interconnected channels within the bone tissue, link the lacunae to each other and to the central channel through the lamellae. These canaliculi facilitate intercellular contact and communication by housing the cytoplasmic projections of osteocytes.

Additionally, structures within compact bone, while not strictly part of the osteons, are present. Perforating canals or Volkmann’s canals, akin to the central canal but oriented perpendicular to the longitudinal axis, establish nerve and vascular connections between osteons. Circumferential lamellae, rings of bone arranged directly within the periosteum or endosteum, and interstitial lamellae, representing the remnants of partially resorbed osteons, are also noteworthy components [11].

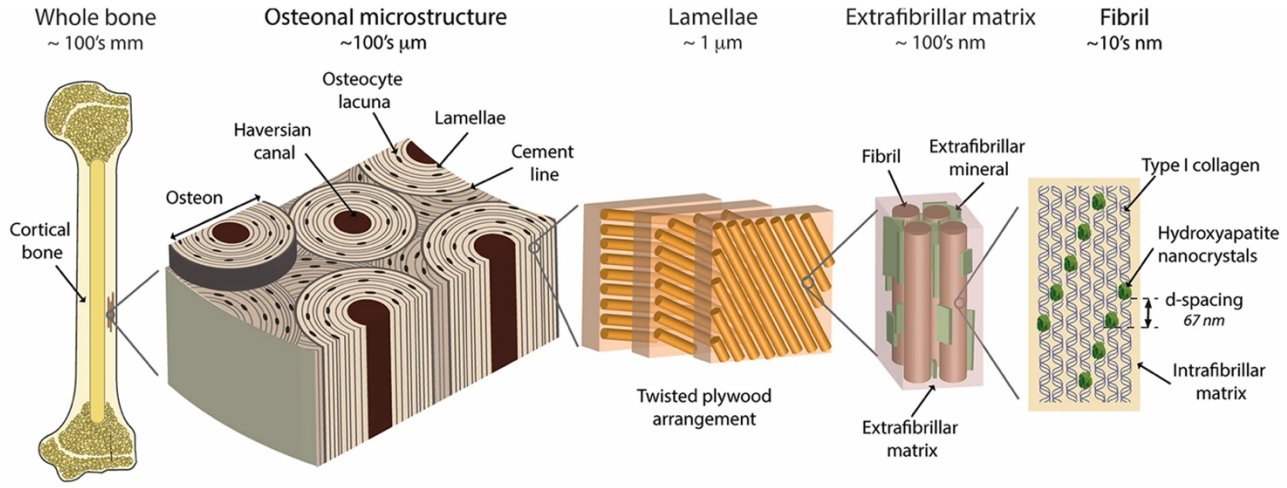

Figure 5: Graphic representation of the organisation of cortical bone. Specifically, one can see: the central canal, the concentric lamellae, the lacunae housing the osteocytes, the canaliculi, the lamellae and the composition of these [12].

Lamellae are made up of collagen fibres embedded in a substance consisting mostly of hydroxyapatite crystals oriented like fibres.

Collagen increases the ductility of the bone, improving its post-elastic behaviour; this is synonymous with safety due to its ability to absorb shocks and the limitation of the risk of complete breakage of the bone structure. Collagen fibres increase the toughness of the bone, the ability to resist the propagation of fractures in its structure.

2.2.1.2 Trabecular Layer

Spongy bone, unlike compact bone, does not have osteons, and its trabeculae consist of lamellae arranged to form a kind of spatial reticular lattice structure. Trabecular bone tissue is a special type of lamellar bone that is organised in such a way that it forms a particularly porous three-dimensional reticular structure.

Often, trabeculae form an intricate network of filaments and plates of bone tissue, imparting considerable resistance to mechanical stresses applied in different directions and distributing them over the entire bone structure. This type of bone is composed of thin trabeculae or spicules surrounding interconnected cavities containing bone marrow. These trabeculae are arranged following lines of force that run through the bone and undergo changes during the bone remodelling process.

The spatial conformation depends mainly on the type of mechanical conditions applied to the tissue, based on which the structure is optimised to achieve the greatest possible strength and lowest possible weight. The main trabecular bundles develop on the trajectories of the main tensile and compressive

stresses. This optimisation process results in highly differentiated density properties and orientation of the trabeculae depending on the location of the tissue sample.)

Spongy bone tissue owes its name to its less dense extracellular matrix and the presence of numerous intercommunicating cavities, giving it a sponge-like appearance with a soft texture. This type of tissue is found in the inner parts of flat bones (such as the skull, sternum, ribs, and pelvis), in the epiphyses of long bones and in irregular bones (such as vertebrae), except for the central part of long and short bones. Bony trabeculae, or spicules, form the main structure of the spongy bone tissue, forming an alveolar network. This tissue makes up about 20% of the skeleton, while 80% is compact bone tissue.

As shown in Figure 6, bone trabeculae are ossified and composed of osteocytes and extracellular matrix, forming gaps, and communicating through canaliculi. Osteocytes communicate and receive nourishment through canaliculi, which allow contact between the cytoplasmic projections of adjacent osteocytes through communicating junctions and blood capillaries in the bone channels.

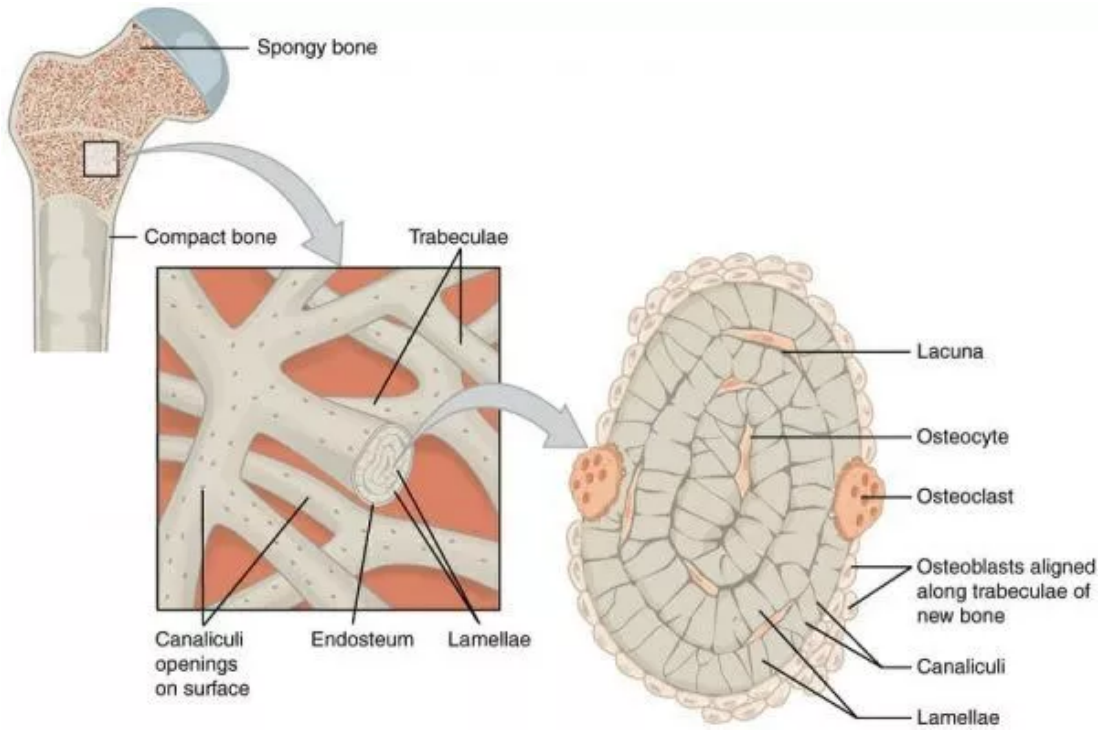

Figure 6: Representation of the spongy structure [13].

Although it constitutes a minority in the skeletal mass, the spongy bone tissue is metabolically active and is part of the lamellar bone tissue, conferring tensile and stress resistance. Its multi-directional arrangement of trabeculae allows it to withstand mechanical stress and cancel forces during compression.

Unlike compact bone tissue, spongy bone lacks Havers' canals and is not traversed by blood vessels and lymphatic ducts. Its lower density gives the bone lightness, facilitating muscle movement. However, calcium loss in spongy bone can make it brittle, causing localised pain and bone oedema formation, which can be detected by MRI [14], [15].

2.2.2 Foot Joints

Joints are complex anatomical structures that establish mutual contact between two or more bones. To prevent degenerative phenomena caused by wear, there is often indirect contact, mediated by fibrous or cartilaginous tissue and/or fluid.

Within the human body, joints are very numerous and present considerable structural differences, reflecting the variety of functions required by each one. In the foot, which contains as many as 26 bones, the joints play a crucial role in holding the different bony parts together, thus enabling the skeleton to fulfil its functions of support, mobility, and protection. The movements of the joints of the foot generally occur in the main planes: frontal, sagittal and transverse. There are two main categories of joints:

1. Synarthroses, which are characterised by a bony connection through a cartilaginous layer,
2. Diarthroses, which allow wider movements and consist of joint surfaces covered with cartilage, a joint capsule and a synovial cavity containing a lubricating synovial fluid.

In the context of the foot and ankle, various joints can be distinguished, each with specific functions and characteristics. Understanding this anatomical complexity is essential to fully appreciate the role of joints in providing structural support and facilitating movement in the skeletal system.

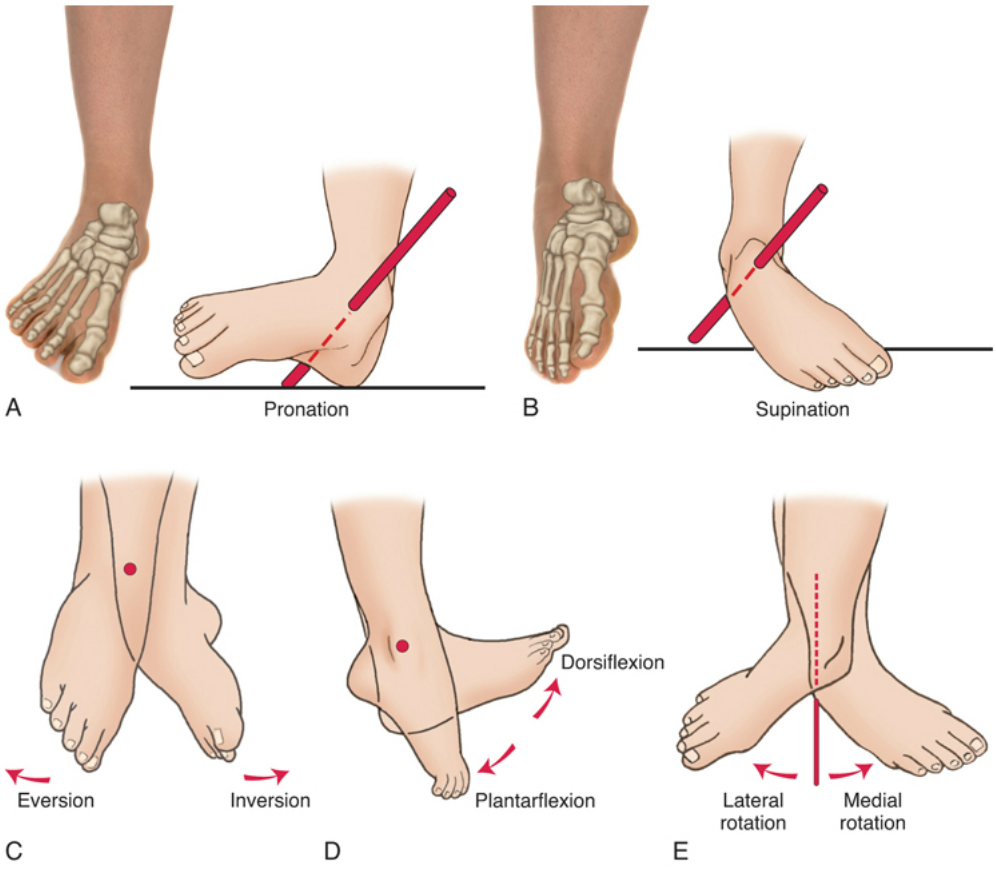

Figure 7: The different types of movement that the foot-ankle complex can make thanks to the joints present [16].

- The *tibiotarsi joint* is located between the tibia, fibula, and talus, and is a diarthrosis. The joint capsule, located between the cartilage-coated articular surfaces, allows movement of the foot in the sagittal and transverse planes. These movements include plantar flexion and dorsiflexion in the sagittal plane, and abduction and adduction in the transverse plane, with a range of motion of approximately 30°-50° for plantar flexion, 20°-30° for dorsiflexion, and 35°-45° for abduction and adduction.
- The *subtalar joint*, a diarthrosis between the talus and calcaneus, allows eversion and inversion movements in the frontal plane. The range of motion is about 20°-25° for eversion and about 50° for inversion.
- The *transverse tarsal joint* is a combination of two diarthroses: the talocalcaneonavicular joint between the talus, calcaneus and navicular, and the calcaneocuboid joint between the front of the calcaneus and the posterior surface of the cuboid. They contribute to the eversion and inversion movements of the foot.

- The *cuneonavicular joint* is a diarthrosis between the navicular bone and the three cuneiform bones, allowing some gliding movements. The cuboid navicular joint is a synarthrosis joint between the cuboid and the navicular bone.
- The *tarsometatarsal joints* are diarthrosis and are located between the tarsal bones and the bases of the metatarsal bones. The intermetatarsal joints involve the bases of the metatarsal bones, contributing to plantar flexion and dorsiflexion movements.
- The *metatarsophalangeal joints* are diarthroses joints between the heads of the metatarsal bones and the bases of the proximal phalanges, allowing flexion and extension of the toes at the metatarsal level. Finally, the nine interphalangeal joints connect the phalanges, allowing them to flex and extend [17].

2.2.3 Muscle complex

In this section, we will explore the muscles responsible for movements during the different phases of the walking cycle. Walking is a cyclic process of alternating rhythmic movements that allows the body to move forward. This occurs thanks to the generation of a propulsive force by the muscles, which involve the entire lower limb, not just the foot. All the muscles that originate in the skeleton of the leg end in the skeleton of the foot. There is therefore a cooperation of the crural muscles.

The *thrust phase* is made possible by the posterior muscles of the leg, which are responsible for the extension of the foot over the metatarsals, such as the twin muscles or gastrocnemius, soleus, peroneus longus, flexor longus of the toes and flexor longus of the big toe. On the other hand, leg extension is provided by the quadriceps femoris, as well as hip and thigh extension, we are talking about the gluteal muscles, biceps femoris in the long head, semitendinosus, semimembranosus, great adductor, piriformis, and quadratus femoris. The *lifting* of the limb forward is made possible by the thigh flexor muscles, including the rectus femoris, iliopsoas, sartorius, tensor fascia late and pectineus. Next, the ankle flexes forward through the action of the tibialis anterior, extensor longus, extensor longus hallucis, peroneus anterior, and extensor shorts hallucis.

The leg muscles can be divided into two main groups according to their position:

- an anterior group, consisting of the extensor muscles,
- a posterior group, consisting of the flexor muscles.

These two groups are separated by the tibia, fibula, and interosseous membrane. In turn, each group can be further subdivided into subgroups. The anterior group includes the anterior extensor subgroup and the lateral peroneal subgroup. The anterior muscles of the leg play a dorsiflexion role and

participate in the inversion of the foot, also contributing to eversion. On the other hand, the muscles of the posterior group are divided into superficial and deep flexor muscles. The classification can extend further because of innervation, distinguishing between muscles innervated by dorsal nerves and those innervated by ventral nerves.

The muscles located at the front of the leg are known as dorsi-flexors and participate in the inversion and extroversion movements of the foot. The anterior extensor subgroup, illustrated in Figure 2.5, consists of several muscles:

- *Tibialis anterior*: Characterised by its triangular shape, this muscle originates from the superior lateral surface of the tibia and inserts into the medial cuneiform and first metatarsal bone of the foot. Its main function is dorsi-flexion and inversion of the foot. It is innervated by the deep peroneal nerve and acts both as an antagonist and synergist of the posterior tibial.
- *Extensor digitorum longus*: Pinnate muscle originating from the lateral condyle of the tibia, the anterior superior surface of the body of the fibula and the superior part of the interosseous membrane. Its tendon divides into four parts that cross the back of the foot and insert into the second and third phalanges of the four smaller toes. This muscle is mainly involved in the dorsi-flexion of the toes, but also participates in the flexion of the foot. It is innervated by the deep peroneal nerve.
- *Extensor hallucis longus*: Thin muscle located between the tibialis anterior and extensor digitorum longus, originating in the anterior surface of the fibula and the interosseous membrane. It crosses the dorsum of the foot and inserts at the base of the distal phalanx of the big toe. Its main function is the extension of the big toe, but it also contributes to the dorsi-flexion of the foot and supports eversion and inversion. It is innervated by the deep peroneal nerve.

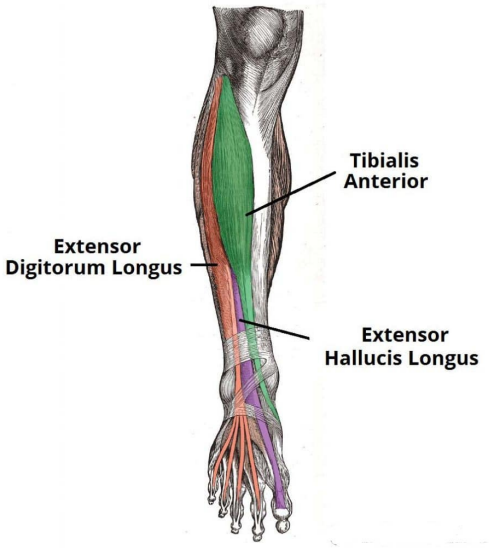

Figure 8: Anterior muscles involved in walking [18].

The posterior superficial muscle group is composed of:

- *Triceps surau*: it is configured as a complex union of two distinct muscles: The gastrocnemius, divided into two heads, derives its origin from the lateral condyle of the femur (lateral head) and from the medial condyle of the femur (medial head). Simultaneously, the soleus, with its point of origin on the Soleil line and the middle third of the posterior margin of the tibia, together with the upper quarter of the posterior fibula, integrates this muscular synergy. The union of these two muscles finds its convergence in the extremities, giving rise to a common tendon known as the calcaneal tendon or Achilles tendon. The latter enters the posterior surface of the calcaneus. Functionally, the triceps surae guides plantar flexion and emerges as the main creator of supination, i.e. the inversion of the foot. The tibial nerve represents the innervating element of this muscular complex.

The muscles situated at the back of the leg play a crucial role as plantar flexors of the foot. Within the deep posterior subgroup (depicted in Figure 9), the following muscles are notable:

- *Tibialis posterior*: Originating from the inner posterior borders of the tibia and fibula, as well as the interosseous membrane connected to these bones, the tibialis posterior transforms into a tendon that descends behind the medial malleolus. Eventually, it bifurcates into two segments: the medial component inserts into the tuberosity of the navicular, while the lateral component inserts into the medial cuneiform. Its primary functions encompass plantar flexion and inversion of the foot, and it receives innervation from the tibial nerve.

- *Flexor digitorum longus*: This muscle, initially thin and pointed at its origin on the posterior surface of the tibia, gradually increases in size as it descends. In the sole of the foot, it divides into four tendons, each inserting into the bases of the last phalanges of the second, third, fourth, and fifth toes. Its roles involve toe flexion, plantar flexion, and inversion of the foot, with innervation provided by the tibial nerve.

- *Flexor hallucis longus:* Arising from the inferior posterior surface of the fibula and the interosseous membrane, this muscle transforms into a tendon passing through the talus, calcaneus, and sole of the foot. Its ultimate insertion occurs at the base of the last phalanx of the great toe. Its functions include flexion of the great toe, and akin to the preceding muscle, it contributes to plantar flexion and inversion of the foot. Innervation is provided by the tibial nerve [11], [17].

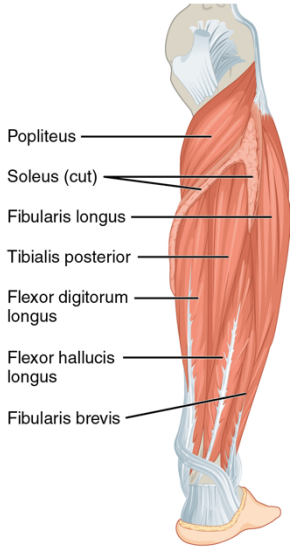

Figure 9: Posterior muscles involved [19] .

2.2.4 Tendon and ligament complex

Tendons and ligaments provide connections between muscles and bones, in the first case, and between bones and bones, in the second, to allow locomotion. The mentioned tissues are characterized by their dense and fibrous nature, serving as essential connectors in transmitting mechanical forces. This function is crucial for stabilizing the skeleton and facilitating body movement. The tendons involved take on the same name as the muscles previously explained, as they constitute a connective bridge between the muscles and the bones to which they are anchored. As for the ligaments, let's proceed to analyse some of them.

Ligaments that keep the tibia and fibula together and connect them to the tarsal bones

This set includes ligaments such as the anterior talofibular, posterior talofibular, and calcaneofibular, which together form the lateral collateral ligament. This ligament connects the fibula to the talus and calcaneus bones, preventing hyper-inversion of the subtalar joint and providing stability to the ankle. The tibionavicular, tibiocalcaneal, posterior tibiotalar, and anterior tibiotalar ligaments make up the medial collateral ligament (or deltoid ligament), a strong, flat, triangular band that provides stability within the ankle.

Ligaments that keep the talus together with the tarsal bones

This group includes the talonavicular ligament and the talocalcaneal ligament, which connect the neck of the talus to the dorsal surface of the navicular bone and join the talus to the calcaneus, respectively.

Other dorsal ligaments

This category encompasses several ligaments, including the bifurcate ligament, dorsal entocuneiform ligaments, dorsal cuneocuboid ligament, and others that contribute to the stability of the dorsal joints of the foot.

Tarsal plantar ligaments

This major group includes the long plantar ligament and the calcaneonavicular plantar ligament. The first is a long ligament on the bottom of the foot that connects the calcaneus to the cuboid and extends to the bases of the second, third, and fourth metatarsals. The second is a complex of three ligaments on the bottom of the foot that connect the calcaneus to the navicular bone.

Ligaments that hold the tarsal and metatarsal bones together

Divided into two subgroups, the dorsal and plantar tarsometatarsal ligaments constitute strong bands that extend from the tarsal bones to the metatarsals on the upper and lower surfaces of the foot. Other minor ligaments contribute to the stability of the joints in this region.

Ligaments that hold the metatarsal bones together

These ligaments, located at the level of the bases of the metatarsal bones, are composed of three parts: the metatarsal interosseous ligament, the dorsal metatarsal ligament, and the plantar metatarsal ligament.

This division of ligaments in the foot and ankle area plays a critical role in providing structural support and stability during foot and ankle movements [11], [17].

2.3 Mechanical properties of the bones

Cortical bone can be described as a structural compound, being composed mainly of two basic elements: hydroxyapatite and collagen. Hydroxyapatite is characterised by its remarkable strength and stiffness, presenting an elastic modulus of $E = 165\ GPa$. On the other hand, collagen, while having an elastic modulus that varies with deformation, can be approximated to a value of $E = 2\ GPa$ for typical deformations. Therefore, considering a weighted average between these two extremes, the elastic modulus of cortical bone tissue is around $E = 18\ GPa$. Collagen increases the ductility of the bone, improving its post-elastic behaviour; this is synonymous with safety due to its ability to absorb shocks and the limitation of the risk of complete breakage of the bone structure, while collagen fibres increase the toughness of the bone, the ability to oppose the propagation of fractures in its structure.

The mechanical properties of cortical bone tissue are influenced by several factors, including:

1. Load orientation and position: Bone tissue exhibits variable mechanical properties in response to angle, direction of loading and specific anatomical position. The influence of orientation and position of loading is reflected in the mechanical behaviour of cortical tissue, which is characterised by a pronounced anisotropy related to its specific structure. Haversian structures show a marked orientation in space, influenced by position in the bone and the local mechanical state, with the distal-proximal direction emerging as the main area for the development of tension states (Knets et al., 1981). Anisotropy of elastic moduli is assessed by uniaxial tensile tests along specific axes. Elastic and fracture limits emerge from the stress-strain curve during tensile or compressive tests, presenting a post-elastic region that varies with the direction of loading. Ductility is particularly pronounced in the longitudinal direction,

defining the axial orientation of the secondary osteons, while in compression the curve is influenced by work hardening and creep.

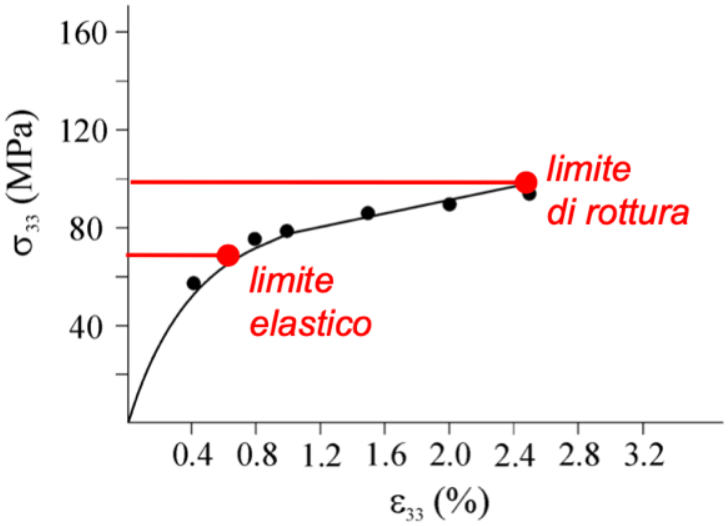

Figure 10: Elastic and fracture limits for cortical bone [4].

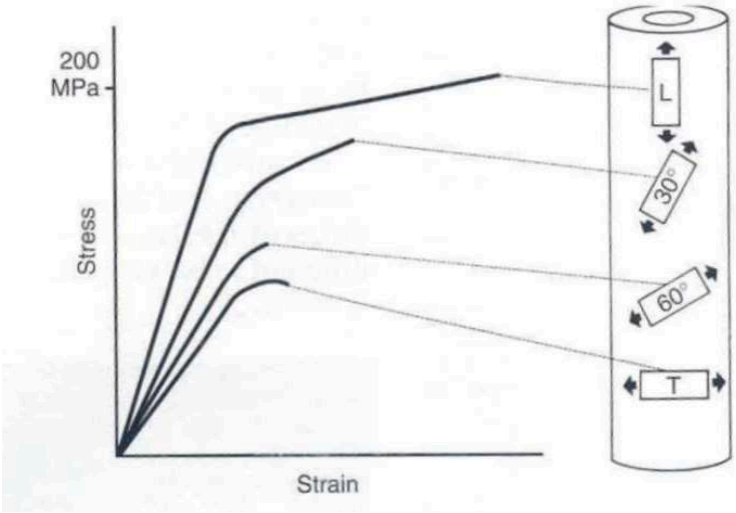

Figure 11: Behaviour of the post-elastic region depending on load orientation [4].

2. Effect of hydration: Bone strength is linked to the presence of two fundamental components at the sub-micrometric level: mineralised collagen fibrils (MFC) and the extra-fibrillar matrix (EFM). These elements undergo significant alterations influenced by age, the presence of pathologies or the use of specific drugs. The properties of MFC and EFM are complex and depend on various factors, including the degree of mineralisation, the accumulation of glycation products (AGEs) and the presence of proteins such as osteopontin. Age has a major impact on bone mineral content, which decreases with age and the use of bisphosphonates, commonly used in the treatment of osteoporosis. Concurrently, there is an increase in the

formation of AGEs, Advanced Glycation End-products are chemical compounds formed by combining sugars with proteins or fats, and a decrease in osteopontin, alterations that affect the composition of the extra-fibrillar matrix. The lack or reduction of osteopontin negatively affects the bone's ability to resist fractures.

3. Experimental data show differences of up to 20-25% in the maximum elastic modulus between the 25-34 and 60-95 age groups, indicating a substantial impact of age on the mechanical characteristics of bone. Similarly, a reduction in ultimate strength is observed, underlining the importance of understanding the complex dynamics of bone tissue to develop more targeted prevention and treatment strategies.
4. Effect of hydration: there is a significant change as the liquid fraction changes (by weight, w%). A transition from ductile to brittle behaviour is observed. A completely dry fabric (w% = 2.5%) exhibits behaviour typical of an elasto-fragile material, whereas in the presence of physiological hydration (w% = 10.5%) a wide zone of plasticity, characteristic of ductile materials, is observed.

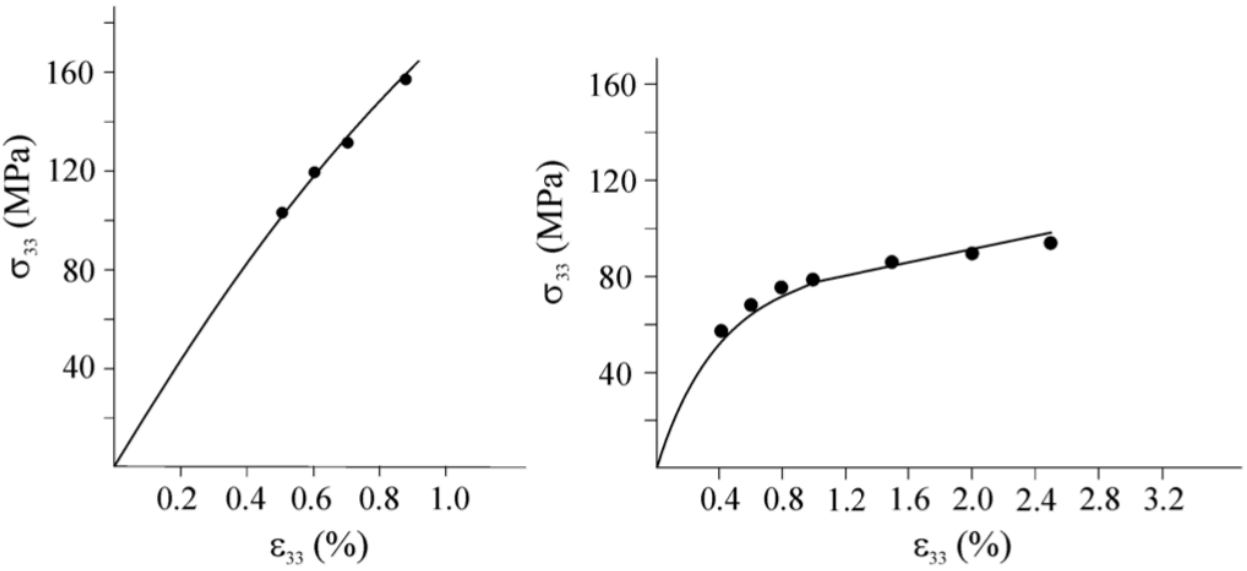

Figure 12: The first image shows the behaviour of elasto-fragile bone material, while the second image represents the behaviour of ductile tissue [4].

5. Influence of deformation speed: on the sample, this is manifested through changes in its stiffness. An increase in stiffness is observed as the strain rate increases.

Trabecular bone is characterised by unique mechanical properties compared to cortical bone. It has a lower elastic modulus, making it more deformable under applied loads and giving it a more ductile behaviour. However, the ultimate stress, which represents the maximum stress borne before fracture,

is generally lower than in cortical bone. Finally, the trabecular structure is adapted to respond dynamically to applied loads, manifesting structural adaptability in response to mechanical stresses.

1. Effect of density: trabecular bone is porous, and its mechanical response is influenced by this. Bone stiffness and strength have a marked dependence on structural density (the amount of bone tissue present in each volume).

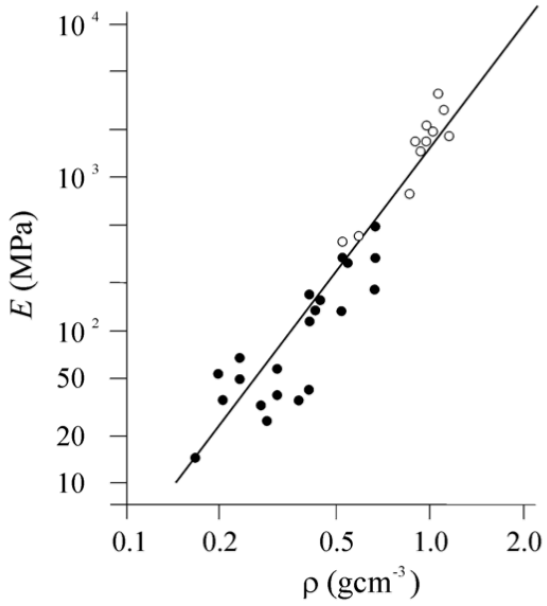

Figure 13: Correlation between density and elastic modulus, in tension (filled circles) and compression (hollow circles) in trabecular bone [4].

2. Effect of strain rate: the strain rate dependence is very low. This relationship, which combined with the density dependency relationship, allows us to write in empirical form:

$$E = 3790\varepsilon^{0.06}\rho^3 \qquad \sigma^- = 68\varepsilon^{0.06}\rho^2$$

where E (in MPa) is the modulus of elasticity, σ^- (in MPa) the axial compressive strength, ρ (expressed in g/cm^3) the structural density and, finally, the strain rate expressed in sec^{-1}.

3. Age effect: the structural configuration at the same site shows a marked dependence on the age of the subject. Increasing age is associated with a decrease in ultimate tension. Damage and repair of individual trabeculae is recognised as a normal physiological process that can have important clinical implications. Breakage of individual trabeculae tends to increase with the subject's age, attributable to fatigue phenomena (accumulation of damage due to cyclic loads). This phenomenon leads to an increased risk of fractures, especially in elderly subjects or those suffering from osteoporosis [4].

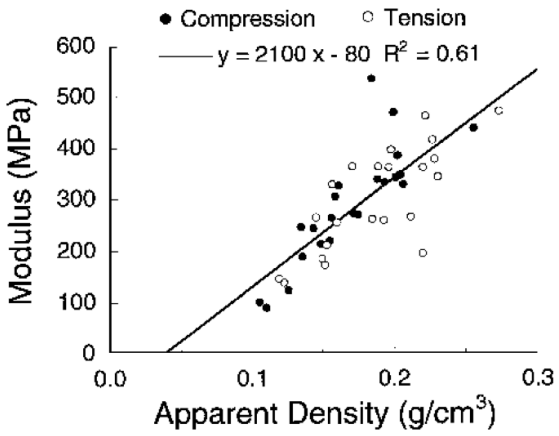

Figure 14: Values of elastic moduli, obtained in compression and tension, as the density of trabecular bone varies [4].

2.4 Biomechanics of the Foot and Motion Analysis

Movement analysis represents a fundamental technique for the quantitative assessment of musculoskeletal biomechanics during a movement. This method, increasingly popular and applied in numerous fields, finds its main application in clinical and rehabilitation, where it has a significant social impact considering the prevalence of musculoskeletal diseases and injuries in the population. The primary objective of movement analysis is to contribute to the resolution of health problems through an objective approach based on measurable movement parameters.

Movement analysis allows for the acquisition of both static and dynamic data: while static analysis is useful for assessing the balance and stability of a patient, dynamic analysis allows for the assessment of the degree of abnormality of a movement. In addition to its clinical use, motion analysis also finds application in sport, where it is used for the design of sports equipment, performance assessment of athletes and injury prevention. Finally, this technique has also found its way into animation and special effects in films, helping to create realistic and immersive sequences [20].

2.4.1 Gait Analysis

Gait analysis is the systematic study of human movement, involving both visual observation and specialised instruments to measure body movement, body mechanics and muscle activity. This type of analysis represents a sub-discipline of motion analysis, with applications mainly in the clinical and rehabilitation fields, aimed at providing an objective and quantitative assessment of human gait. It is widely used in sports biomechanics to optimise the running of athletes and identify possible posture or movement problems in people with injuries. The study of gait includes quantifying and analysing the measurable parameters of various types of walking, as well as interpreting the results to draw

conclusions about the status and characteristics of the individual under investigation, such as health, age, body size, weight, speed, and more, based on their gait pattern.

During walking, one-foot acts as a support point while the other advances until the next contact with the floor. Subsequently, the roles of the feet switch and during weight transfer both touch the ground. A step cycle (GC) is a sequence of events from the heel contact of one foot to the next heel contact of the same foot. This cycle is divided into two main phases: the stance phase, in which the foot remains in contact with the ground (0-60% of the GC), and the swing phase, in which the foot is not in contact with the ground (60-100% of the GC).

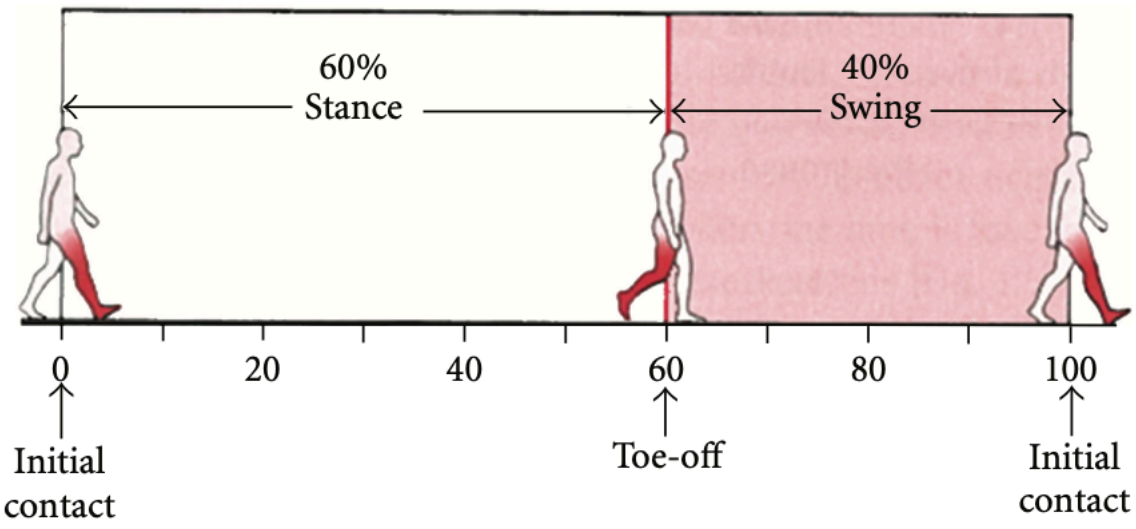

Figure 15: The gait cycle can be divided into the stance phase (weight-bearing) and swing phase (non-weight-bearing) [21].

By carefully examining the main steps of walking, we can identify four key events in the support phase:

- Initial contact: Corresponds to 0-2% of the gait cycle (GC) and corresponds to the first contact of the heel with the floor. The ankle is in a neutral position during this phase and the knee is slightly flexed and the hip is tilted about 30°.
- Loading response: This occurs between 2% and 10% of the GC. During this phase, the entire foot is in contact with the floor and the weight of the body is transferred to the supporting leg. It is a crucial moment for body weight loading, shock absorption and forward movement. The ankle flexes slightly downwards (plantarflexion), the knee flexes about 15° and the hip begins its movement from flexion to extension.
- Mid-Stance: This period, between 10% and 30% of the GC, involves aligning and balancing the body weight on the supporting leg as the leg approaches the upright position. During this

phase, the ankle moves slightly upwards (dorsi-flexion), the knee extends, and the hip continues to extend.

- Terminal-Stance: This phase occurs between 30% and 50% of the GC and includes heel lift and toe action. Initially, the ankle is in dorsi-flexion, while it subsequently flexes downward (plantar). The knee extends, preparing for the next movement, while the hip is in hyperextension.
- Pre-swing: This period, between 50% and 60% of gait, is the final phase of stance and lasts from the time of contralateral foot initial contact with the ground until the ipsilateral foot leaves the ground (toe-off). Pre-swing includes the second portion of double limb support in which the now trailing limb is rapidly unloaded in preparation for advancement during swing phase.

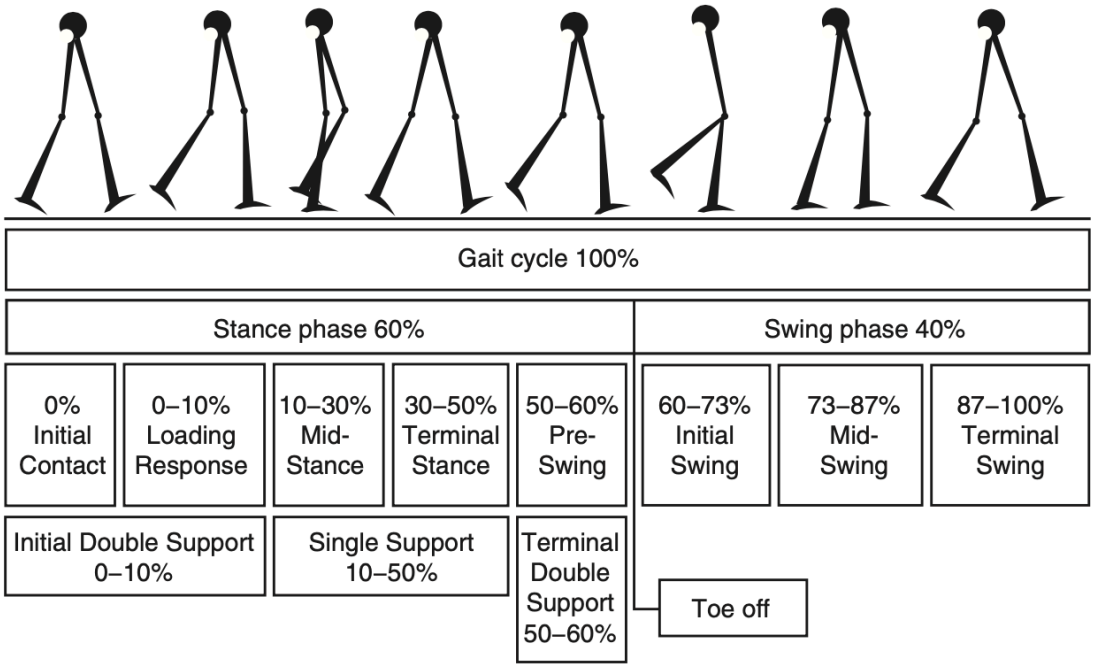

Figure 16: Normal gait cycle periods and timing [22].

The swing phase, on the other hand, comprises three distinct events:

- Initial Swing: This extends from 60% to 73% of the GC. During this period, the limb moves forward until it becomes parallel to the supporting leg, resulting from hip and knee flexion. The ankle is dorsi-flexed.
- Mid-Swing: This phase ranges from 73% to 85% of the GC and is characterised by the continuous advancement of the limb until the maximum degree of knee flexion. During this moment, the ankle is in a neutral position while the hip flexes further.

- Terminal Swing: This comprises the period between 85% and 100% of the GC, during which the leg completes its advancement until contact is made with the floor. During this phase, the ankle maintains its neutral position, preparing for heel contact, while the knee almost fully extends and the hip flexes.

It is essential to consider that the joint angles and GC percentages of all phases are reference values for normal conditions. Any deviation or alteration in movement can indicate abnormal situations, allowing an assessment of pathology and providing useful indications for treatment planning and evaluation. Based on the results of gait analysis, treatment development is reaching increasingly advanced levels in various patient groups, allowing quantitative and objective assessments of the severity of these pathologies [22], [23].

2.4.2 Ground Reaction Forces (GRF)

Ground reaction forces (GRF) are the forces that the ground exerts on a body when it meets it. These forces occur whenever a body interacts with a solid surface, such as when a person walks, runs, jumps, or simply stands. These act in opposite and equal directions to the forces exerted by the body on the ground according to Newton's third law of motion, which states that for every action there is an equal and opposite reaction. When a body, such as a person's foot, meets the ground, the ground exerts an upward force, which is equal and opposite to the force exerted by the body downwards (the weight of the body). This upward force is a component of GRFs.

GRFs are measured using force platforms embedded in the ground or surfaces on which activities are performed. These platforms can record the magnitude and direction of ground reaction forces during movement, providing important biomechanical information for analysing human movement, assessing sports performance, diagnosing musculoskeletal problems, and optimising movement technique.

They play a crucial role in gait analysis. Indeed, in gait analysis, they are measured using force platforms embedded in the ground or walking platforms. These measurements provide detailed information on how the body interacts with the ground during each step. GRFs show how body weight is distributed on each foot during walking. This can be useful for identifying load inequalities or weight distribution problems, which may be related to biomechanical problems or injuries. They can provide information on the moment at which foot contact with the ground occurs, as well as the sequence of events that characterise each phase of the walking cycle, such as heel strike, foot roll, and final push-off. Finally, they make it possible to assess the forces and moments acting on the body

during walking. This information is crucial to understand the loads on muscle, joint and bone tissues and to identify any abnormalities or imbalances that could contribute to mobility problems or pain.

In summary, ground reaction force analysis is fundamental to understanding the biomechanical details of walking and can be used to assess performance, diagnose musculoskeletal problems, and guide therapeutic intervention or optimisation of walking technique [24], [25].

Chapter 3

3 Finite Element Modelling (FEM)

This chapter will illustrate the concept of finite element analysis, outlining the steps that characterise this numerical methodology. The application of numerical models in foot biomechanics will also be discussed, highlighting both the advantages and disadvantages associated with this technique. Finally, in the final section of the chapter, the dynamic FEM model and reference model used in the realisation of this project will be presented, providing a complete picture of the methodological approach adopted.

3.1 Finite Element Analysis

Finite Element Analysis, known as FEA or FEM (Finite Element Method), is a numerical technique aimed at creating approximate solutions to problems described by partial differential equations associated with the behaviour of a physical system by reducing them to a system of algebraic equations. FEM is a numerical-engineering approach to solving physical problems, which allows the structural behaviour of a system to be studied by subdividing a complex object into many simpler elements, such as triangles or quadrilaterals in 2D and tetrahedra in 3D. Each element is characterised by a system of mathematical equations, which describe the local behaviour of the material or structure in question [26].

The analysis is reduced to the application of balance equations to each finite element, considering load and constraint conditions. Input data is entered into the simulation software at the beginning of the FEM analysis. This data includes descriptions of the materials and their quality, selected constraints, or mesh[1] quality, and must be extremely precise to obtain equally accurate results. Otherwise, unrealistic, and therefore unreliable results would be obtained. Finally, the equations are solved numerically by means of advanced iterative methods, resulting in an accurate representation of the overall behaviour of the system under investigation [27].

[1] Mesh: A polygonal mesh, in computer graphics, is a lattice that defines an object in space, consisting of vertices, edges and faces. Mesh is a representation of a larger geometric domain using smaller discrete cells. Meshes are commonly used to calculate solutions of partial differential equations and generate computer graphics renderings, as well as for analysing geographical and cartographic data. A mesh subdivides space into elements (or cells or zones) on which equations can be solved, thus approximating the solution over the entire domain. Element boundaries can be constrained to lie on internal or external boundaries within a model [47].

This method, being a virtual simulation technique, is widely used in the manufacturing sector, to design, test and optimise products and components, thus reducing development costs and time, improving quality, and ensuring the safety of the most advanced engineering solutions.

The FEM process is divided into three main phrases, namely pre-processing, processing, and post-processing.

1. Pre-processing: This phase involves the definition of a finite element model of the object. The model is divided into finite elements connected by nodes. The geometry, type of finite elements, type of analysis to be used (static, dynamic, thermal, linear, etc.), materials, constraint conditions and applied loads are defined.
2. Processing: during this phase, the equations describing the behaviour of the system are solved numerically for each finite element using structural calculation software.
3. Post-processing: phase in which the results obtained are visualised and analysed, obtaining information on stresses, deformations, heat flows and other parameters of interest useful for the evaluation of the system's performance.

Carrying out an FEM analysis correctly is not easy, as many pitfalls can be encountered in the process that could distort the results, e.g. particularly complex geometries to start from or constraints applied that do not correspond to the real ones. For this reason, it is important to rely on professional software for structural calculations with analysis and resolution of any problems.

Finite element analysis offers important advantages to designers and is therefore an indispensable tool for the manufacturing industry, such as design optimisation, reduction of development costs and time, increased accuracy and reliability, analysis of extreme loads or design of advanced materials [26], [27].

3.2 Types of finite element analysis

Finite element analysis for layered structures can be based on three different mechanical conditions, depending on the application of loads.

1. Static analysis: in the field of statics, the objective is to evaluate the behaviour of structures subjected to constant, or slowly applied, loads, without considering inertial effects or time-varying load velocities, so acceleration is considered constant. This type of analysis is important for understanding the stress distribution, deformations, and internal stresses in structures under static equilibrium conditions. The formulae and equations used in static

analysis include the equilibrium of forces (1), the deformation equations (2) and the constitutive relationships of materials (3). These formulae make it possible to calculate the constraint reactions, stresses, and deformations in the different parts of the layered structure, providing crucial information for optimising the design of the structures and ensuring that they can withstand expected loads without failure or excessive deformation.

$$\sum_i F_i = m_i a_i = 0 \tag{1}$$

$$\varepsilon = \frac{\Delta l}{l} \tag{2}$$

$$\sigma = E\varepsilon \tag{3}$$

Where:
ε is the unit strain
σ is the stress
E is the Young's Modulus

The deformations, however, are neglected in the next frame. Therefore, it is as if the model recovered instantaneously or had never received any load previously. This assumption is possible for analyses of small deformations.

2. Quasi-static analysis: quasi-static analysis is a type of analysis that considers loads applied gradually, but not necessarily constant over time. In this type of analysis, negligible or minimal dynamic effects are considered with respect to the rate of load application, hence inertial effects. At each instant, it is possible to approximate the behaviour of the structure as if it were in static equilibrium. This method is used in non-linear problems, where the system of non-linear equations can be approximated to a linear system.

3. Dynamic analysis: this is an approach that considers the dynamic effects caused by rapidly varying loads over time or vibrations applied to the structure. This type of analysis considers accelerations, velocities and rapid changes in loads that can influence structural behaviour. Factors such as the structure's natural frequencies, vibration modes, dynamic responses to load impulses and free oscillations of the structure are considered. The formulae used in the dynamic analysis of structures depend on the complexity of the structure, the loading conditions, and the dynamic properties of the materials. With this method, forces are non-zero (4), deformations (2) and constitutive relationships (3) must be considered; in fact, it is an analysis applied for large deformations.

$$\sum_i F_i = m_i a_i \neq 0 \quad (4)$$

3.3 Foot FEM

As stated in Chapter 2, the foot is a complex three-dimensional structure in which numerous bones, ligaments, tendons, then tissues and muscles interact to provide balance, stability, and propulsion to the body. The foot is the only point of contact with the ground; therefore, it is subject to repetitive constraints during walking activities, increasing the risk of developing acute injuries, such as stress fractures, plantar fasciitis, or osteochondral injuries. These injuries, as studied in Chapter 1, may result from abnormal loading that develops on the tissues and the inability of these tissues to regenerate. Therefore, it is of considerable interest to physicians to quantify the stresses suffered by anatomical structures during movement.

As we know, the total load on tissues depends on multiple factors, both intrinsic and extrinsic. In the case of extrinsic factors, the most important are the external forces, the geometry and mechanical properties of the anatomical structures, the loads, and the forces produced by the muscles. Due to the great difficulty of finding in vivo measurements of the loads acting on the anatomical structures of the foot, the implementation and use of biomechanical modelling is necessary [28].

More than three decades ago, the first applications of biomechanics to finite element analysis were introduced. Over time, the development of mathematical models, software and tools for FEA has made significant progress, leading to increasingly accurate and faster simulations. Several models, both two- and three-dimensional, have been developed in recent years in the specific field of foot biomechanics. For example, one of the first two-dimensional models was proposed by Patil et al. (1993) [29], who used two-dimensional membranes to represent the foot and applied simulative forces of the calf and tibialis anterior muscles. Other authors such as Goske et al. (2006) and Halloran et al. (2010) [30], [31] investigated the distribution of plantar pressure and combined musculoskeletal models with finite models of the foot. An early two-dimensional model based on motion dynamics was that of Qian et al. (2013) [32], which generated a gait simulation and was able to predict ground reaction forces, centre of pressure and plantar pressure with good agreement. However, 2D models may not accurately represent the complex 3D structure of the foot and its internal interactions during movement. Indeed, due to the absence of symmetry in the anatomical structure, it is unlikely to be able to conduct an accurate deformation and stress analysis using 2D models.

For this reason, more complex and realistic FE models are required, capable of representing reality as best as possible. 3D systems have been developed that couple both a musculoskeletal model and a 3D FE model of the foot. For example, Chen et al. (2001) [33] studied stress distribution during barefoot walking, while Cheung et al. (2004) [34] examined the effect of plantar fascia stiffness on biomechanics. Other authors such as Iaquinto and Waine (2010) [35] and Fernandez et al. (2012) [36] developed three-dimensional models to predict foot and ankle behaviour in specific situations. Several studies, such as Sawacha et al. (2011) [37], Guiotto et al. (2014) [38] and Scarton et al. (2018) [39] have developed three-dimensional FE models of the foot to help prevent diabetic foot by assessing kinematics, kinetics and plantar pressure and estimating internal foot stresses. These studies, however, exploit quasi-static simulations, focusing on precise instants of the gait cycle and not considering overall movement and energy flow [28]. Thus, the need arises to develop models even closer to reality, capable of exploiting the dynamism of movement.

3.3.1 Dynamics-based Model

From a computational point of view, providing a biomechanical model capable of estimating tissue loading considering all environmental characteristics, e.g., external forces, geometric and mechanical characteristics of tissues or muscle forces, is highly challenging due to their diversification. In fact, muscle forces that set the body in motion are usually estimated using neuro-musculoskeletal models of the body, while tissue loads are estimated using finite element (FE) analysis of the affected body structures. Deriving an appropriate clinical treatment based on results from an oversimplified model of the foot can be questionable. For this reason, dynamic simulations have begun to be exploited [28].

In 2013, Qian et al. [40] developed a dynamic model aimed at assessing the behaviour and internal loading conditions of the foot during locomotion, demonstrating a 20-30% improvement in the accuracy of peak plantar pressures compared to quasi-static simulations. Chen et al. [41] implemented a model driven by muscle forces and ankle joint reaction force, increasing the accuracy of predictions. This model, however, may underestimate the influence of the overall body movement on the foot by considering only the dynamics of the foot-ankle complex, and since a movement never repeats itself in the same way, it is useful to consider gait variability to analyse tissue load. Therefore, Van Waerbeke et al. [28] developed a 3D dynamic model of the foot driven by extrinsic muscular forces to estimate the stress suffered by the different internal structures of the foot during the stance phase, exploring the effects of gait variability.

3.3.1.1 Homogeneous Model

The three-dimensional AMUFFEM (Aix-Marseille University Foot Finite Element Analysis) model of the foot-ankle complex, guided by muscle dynamics, allows the study of internal tissue loads during dynamic activities such as running. This model includes bones of the foot, tibia and fibula, while the upper part is approximated to a solid beam. At the apex of this beam is a solid element equivalent to the mass, connected to the knee joint by a spring and damping with a hinge constraint, while the movement of the ankle is produced by the model.

The geometry of the model was obtained from MRI and computed axial tomography data of a healthy subject, with segmentation of the bones, ligaments and plantar fascia performed using Mimics© Software. Other anatomical parts, such as the heel pad and tendons, were constructed directly in the model generated in Abaqus©. There are nine muscles, such as digitorum longus, extensor hallucis longus, flexor digitorum longus, flexor hallucis longus, tibialis anterior, tibialis posterior, peroneus brevis and longus, and triceps suralis. The overall mesh was composed of tetrahedral elements and the various elements were connected by means of constraints and interactions.

The aim of the study is to explore the effects of intra-individual gait variability on the repetitive loads of the internal tissues of the foot during running, considering the intrinsic variability of the locomotion pattern its consequence in local tissue loads.

This allows the entire stance phase of the stride cycle to be dynamically simulated with boundary conditions derived from the static optimisation in OpenSim©. The input parameters included experimental data such as muscle forces, initial foot velocity, initial velocity of the centre of mass element before ground contact, angle between the sole of the foot and the ground now of contact, mass of the subject, and elastic and damping parameters of the knee joint. Model validation was performed by comparing the simulated ground reaction forces with experimental reference values.

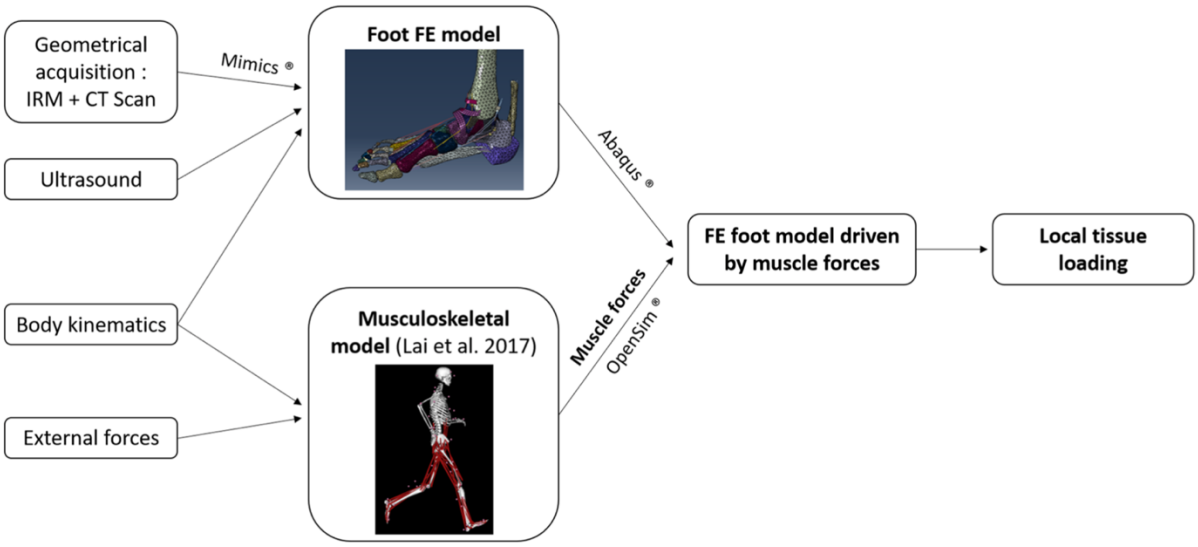

Figure 17: Complete model construction workflow, including FE part and tendon force estimates [28].

The highest stresses reported on the second metatarsal were specifically found in the neck and distal plantar part of the bone. These results are in line with Chuckpaiwong et al.'s study [42], which states that approximately 90% of stress fractures occur in the distal part of the bone. However, the stress values reported were approximately 40% higher than the average maximum stress estimates in Ellison et al.'s work, which did not include muscle forces [28].

It is important to note that the model used does not offer a detailed representation of the geometry of the bones. The latter are treated as a single region, with no distinction between cortical and trabecular tissue, and the elastic moduli are averaged between the components of the two materials.

Consequently, the study by Meardon et al. (2021) [43] provided inspiration for the present project. This study analysed bone stress in the tibia during walking and running in recreational runners of both sexes, using an integrated approach combining three-dimensional force and marker data with a musculoskeletal model and finite element analysis. This non-invasive method allowed bone stress to be estimated in detail, providing an in-depth view of tibial bone load distribution and contributing to the understanding and prevention of tibial bone stress injuries.

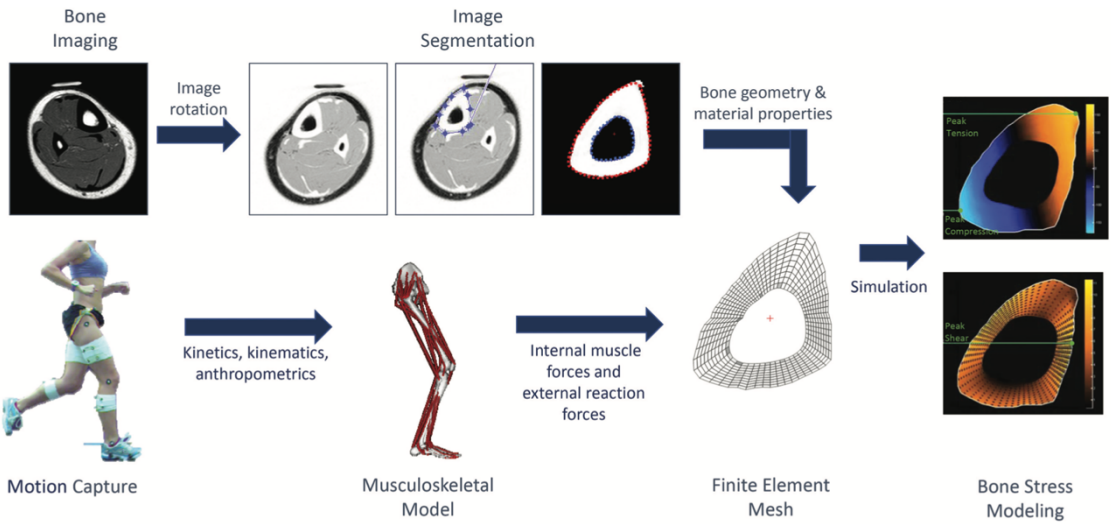

Figure 18: Graphical display of the workflow to estimate bone stress across the stance phase of gait in Meardon et al. model [43].

In conclusion, the importance of understanding tibial loads emerges as fundamental to preventing tibial bone stress injuries. This approach raised interest in recreating the foot-ankle complex three-dimensionally by means of finite element reconstruction, including an accurate representation of the cortical and trabecular geometry of the bones and exploiting the dynamicity of movement.

Chapter 4

4 Proposed methodology

In this chapter, the implementation of an individual-specific finite element (FE) model will be presented. Three different types of support will be analysed, such as Front, Mid and Rear support during running motion, incorporating the trabecular geometry for the specific first metatarsal bone within the model. Initially, the process of transforming a DICOM medical image into a three-dimensional bone reconstruction will be explained. Next, the transition from a surface mesh to a geometric mesh will be explained. Finally, the insertion of the extracted and processed elements into a pre-existing finite element model, provided by the Laboratories of the *Institut des Sciences du Mouvement UMR AMU-CNRS 728* at Aix-Marseille University, will be illustrated.

The objectives can be summarised in the following steps:

- Segmentation of bones from medical images to generate a three-dimensional reconstruction of them.
- Conversion of bone surface meshes into volumetric meshes to allow the import of objects into the simulation software.
- Using the muscle forces obtained as output variables from a static optimisation process to apply them to the finite element model. This phase aims to simulate walking and to formulate considerations based on the results obtained.

4.1 CT Image Acquisition and FEM Definition

In collaboration with the Department of Medicine and Radiology of Marseille, a file consisting of 720 files was collected, which, when combined, formed a Computed Tomography (CT) image of the foot of a healthy male patient. During the acquisition procedure, the patient was made to lie on a couch moving horizontally inside an open tube. To obtain quality images, it was necessary for the patient to remain still for the duration of the examination. The duration of the axial computed tomography (CT) scan was approximately 10 to 15 minutes.

The 3D FEM of the foot, provided by the University of Aix-Marseille, is activated by nine extrinsic muscles of the foot and nine tendons. It also includes the acquired geometry of the foot-ankle complex and the tibia. To simulate the impact of the head-arm-trunk complex, which was not considered in the

finite element model, we introduced a simple representation of the femur and an equivalent mass element of 70.8 kg, positioned approximately at the subject's centre of mass. A mass-spring system connects the virtual centre of mass to the lower tibia. This model was developed using medical imaging data of a single adult subject (30 years old, 1.80 m, 72 kg), frequently engaged in running (20 km/week) and with a hindfoot stance style. All procedures were conducted in compliance with the Declaration of Helsinki and were approved by the ethics committee of the University of Aix-Marseille. Informed consent was obtained from the participant and the MRI and CT scan data were acquired with the knee joint fully extended and the ankle joint in neutral position. In each acquisition, the ankle joint was maintained in neutral position by means of an anatomical cast of the lower limb.

The 3D FEM of the complete foot consists of 49114 nodes and 221398 elements and experimentally derived muscle forces were used to drive this model.

4.2 Segmentation in 3D Slicer

Bone geometries were extracted for the First Metatarsal and Calcaneus, using 3D Slicer software (version 5.4.0). The choice of 3D Slicer was motivated by its ability to offer a flexible and powerful working environment for creating three-dimensional models from complex medical data. This platform was preferred due to its open-source nature, which enables an immersive approach to medicine through 3D modelling capabilities, providing visualization, processing, segmentation, and registration of medical images and meshes. In addition, 3D Slicer offers a wide range of *toolboxes* specifically designed for defining regions of interest (ROIs) and extracting bone tissue.

The folder containing representative biomedical images of the right lower limb in DICOM format was loaded into the software. Subsequently, it was possible to visualize the anatomical sections through the three different views available in the software: axial, sagittal and coronal. Before starting to manipulate the medical images, the tools "*Intensity Segmenter*" and "*Segment Editor Extra Effects*" were downloaded and subsequently installed, which were useful for an initial general segmentation. "Intensity Segmenter" is a simple tool that segments an image according to the intensity value.

Segmentation begins by changing the contrast of the grey levels using the slider, moving it from right to left. From the drop-down menu in the top left-hand corner, “Segment Editor” is selected, i.e. the command used to highlight anatomical regions of interest. 3D Slicer's “Segment Editor” is a powerful tool used to segment, i.e. identify and isolate, regions of interest in three-dimensional medical images. Segmentation is the process of dividing an image into several regions representing specific anatomical or pathological structures. For both bones, segmentation was performed on the cortical layer,

designated as “CortM1” for the cortical metatarsus, “TrabM1” for the trabecular metatarsus, and “Calcaneus” for the calcaneus. In the case of the first metatarsal, segmentation of the trabecular layer was also performed to ensure the integrity of segmentation in the presence of different tissues.

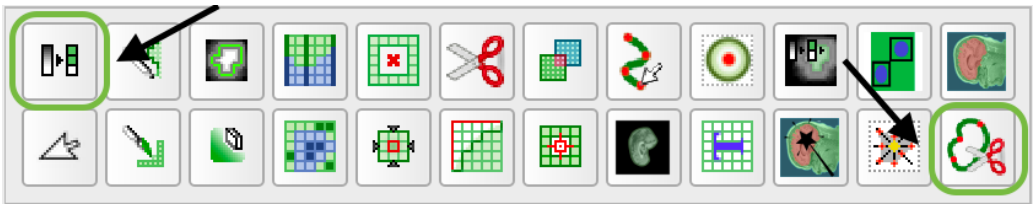

Figure 19: The command in the top right is the “Thresholding” command. The second at the bottom left is the “Surface Cut” command.

Before proceeding with the three-dimensional reconstruction of the elements, it was necessary to precisely define the anatomical region of interest. This process was facilitated using the “*surface cut*” effect available in the icon menu to the left of the visualisation screens. By selecting this command, the boundary points of the anatomical region were manually identified using markup points. Once the boundaries were defined, the “*thresholding*” command was activated, a function to modify the intensity of contrast between grey levels, and the optimal range was defined to ensure accurate and detailed segmentation. This procedure was essential to ensure a faithful three-dimensional representation of the anatomical features of the bones considered.

After the application of the automatic segmentation provided by the installed tool, it was possible to obtain an initial approximate 3D representation. However, to ensure a greater level of detail and accuracy, a second segmentation phase was performed. This time, the process was manual, carried out picture by picture using the 'paint' command. This procedure was adopted to obtain a representation of the bones of the first metatarsal and calcaneus as accurate and faithful to anatomical reality as possible.

Figure 20: Paint command used for the manually segmentation and Smoothing command for closing holes.

The CT images are processed to obtain a precise visualisation of the elements under examination. To achieve optimal segmentation and accurate three-dimensional reconstruction, we make use of the three planes previously mentioned. The strategic use of several planes is crucial, as relying solely on a single plane could lead to the formation of a disjointed and incomplete object. Such a result would compromise the effectiveness of subsequent steps, including meshing and testing.

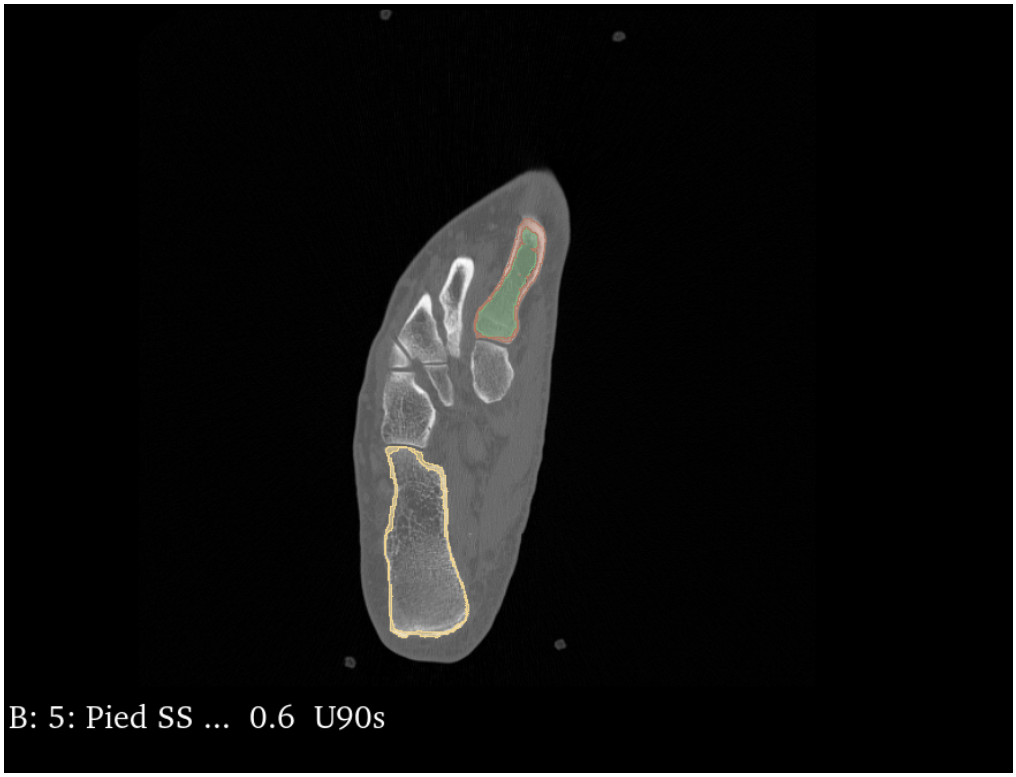

Figure 21: Axial plane view of the segmentation of the First Metatarsal and Calcaneus.

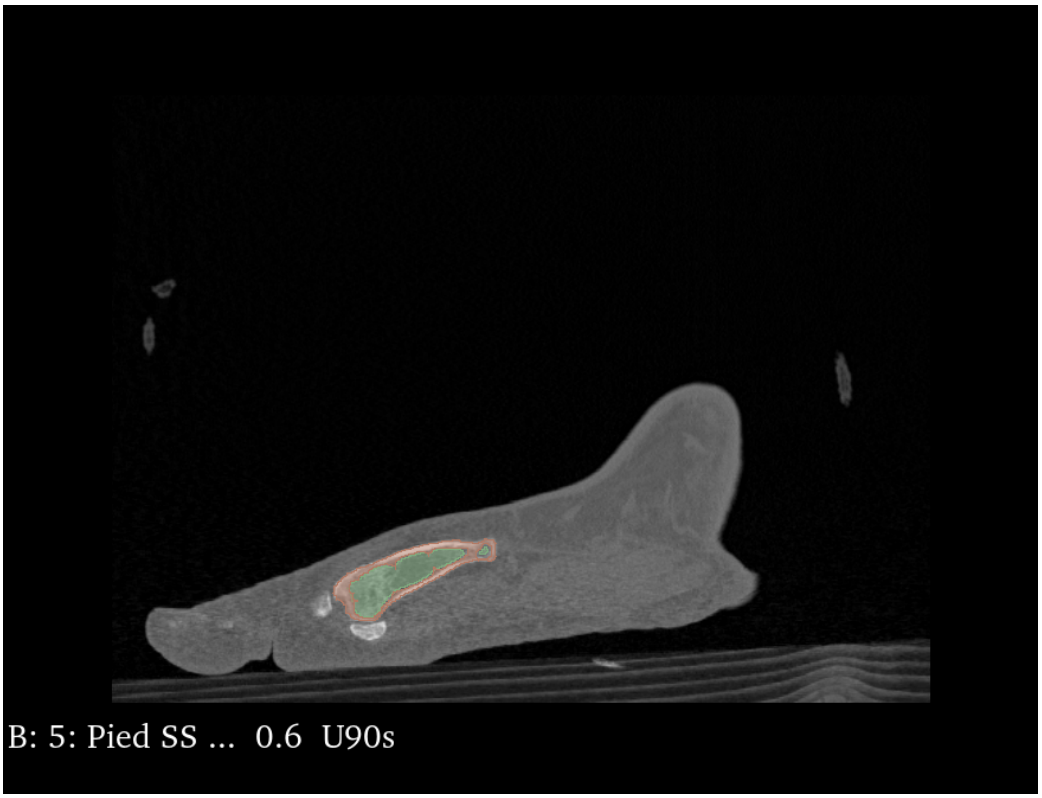

Figure 22: Sagittal plane view of the segmentation of the First Metatarsal.

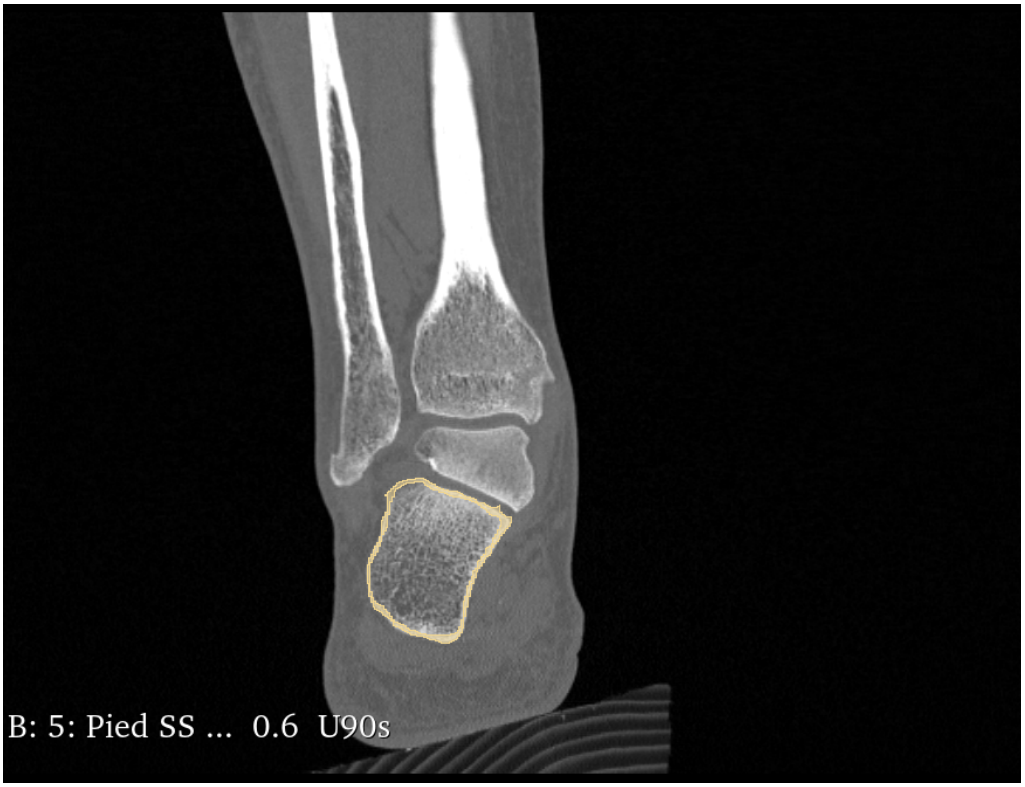

Figure 23: Coronal view of the plane showing a representative slice of the Calcagno.

Figure 19 shows a frame with three different segmentations superimposed, highlighting the boundaries of the cortical and trabecular tissue for the first metatarsal and the cortical alone for the calcaneus. This representation allows the different tissue distribution to be observed, providing a visual overview of what the three-dimensional reconstruction will look like.

Using the "*show 3D*" command, it was possible to display the newly segmented bones in the upper right screen. This three-dimensional visualisation provides a representative image of reality not only in terms of bone conformation, but also in terms of the position of the objects under examination. To ensure a more accurate and irregularity-free representation, a further modification was performed. Using the “smoothing” command from the icon menu, a smoothing was applied to close any holes in the bone reconstruction. This last step contributes to a more complete and consistent representation of the anatomical structures analysed, as shown in Figure 22.

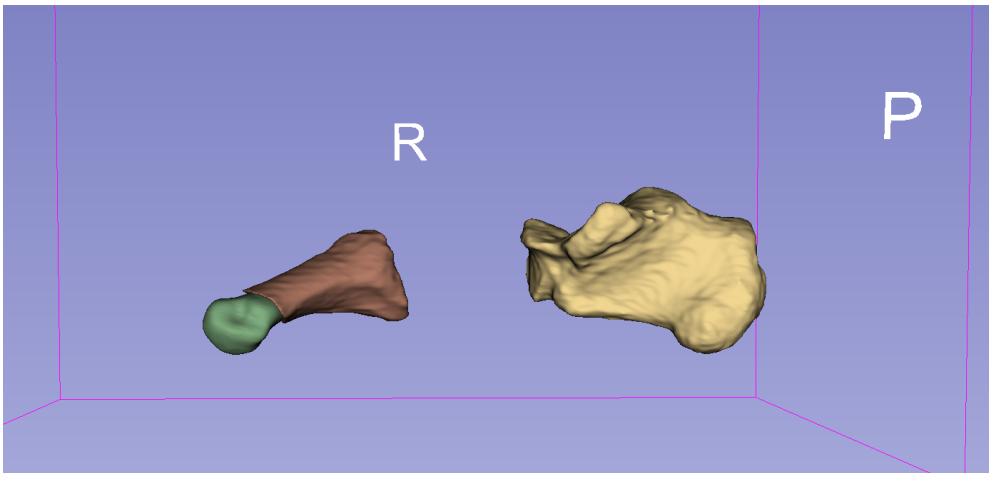

Figure 24: Screenshots of the bones reconstructed in 3D. In green is the trabecular layer of the First Metatarsal bone, in red the cortical layer of the First Metatarsal and in yellow the cortical layer of the Calcaneus bone.

The Slicer software facilitates the visual assessment of the dimensions of segmented objects through the “Volume Rendering” module. In the drop-down menu, different displays are available for the visualisation of CT and MRI images. In this specific case, a CT-AA type display was adopted, which allows the simultaneous visualisation of the entire skeletal model of the foot and the previously segmented bones. This choice aims to ensure that the reconstructions of the calcaneus and metatarsus maintain adequate dimensions with respect to the software's automatic 3D reconstruction, thus ensuring the integrity of specific bone dimensions in the 3D reconstruction without distortion. Next, once the three-dimensional bone reconstructions were obtained, the “Segmentations” module was used to convert and export the files from the *.nrrd* to the *.stl* format. This step is of crucial importance as it allows the generation of a volumetric mesh, an essential step for subsequent processes.

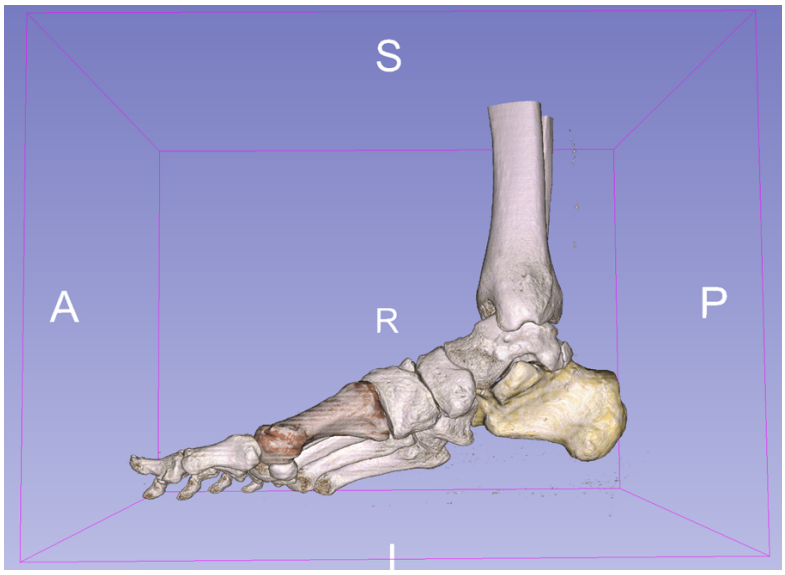

Figure 25: Bone rendering volume of the foot with visualization of the Calcaneus and Metatarsus in correct position.

4.3 Creation of the volumetric mesh

In this section, we will illustrate the methodology used to convert a surface mesh into a volumetric mesh, which is required for the manipulation and application of forces in simulation software. To generate physical bodies suitable for the application of a finite element analysis, it was necessary to convert *.stl* files, which represent a surface mesh, into *.inp* files, which represent a volumetric mesh. The first file type delineates the surface of a three-dimensional object by means of a network of triangles, consisting of vertices and faces (triangles) that define the exterior of the object. This type of file does not include information on the density or internal structure of the body but focuses exclusively on the external surface. On the other hand, a volumetric mesh provides details on the internal structures of the object. This type of mesh is composed of a three-dimensional network of elements, such as tetrahedra in our case, which define both the surface and the volume of the object.

For this study, we chose to use Materialise 3-Matic software (version 14.0) to produce an *.inp* file. Materialise 3-Matic is a sophisticated tool for 3D modelling and reverse engineering. The preference for this software stems from its ability to allow users to manipulate, optimise and prepare three-dimensional data for a variety of applications, including mesh conversion to CAD and correction of raw data for subsequent simulations.

As a first step, the output files from the previous software were imported, but only the cortical segmentation file was selected for both bones. This choice was guided by an understanding of the capabilities of the software, which allows the generation of a boundary between two different surfaces that coincide at one point, in our case we mean the inner cortical surface and the outer trabecular

surface, maintaining a correspondence between the nodes shared by the finite elements. This allows the creation of a second mesh within the bone, representative of the trabecular section. A geometric meshing step was performed to ensure uniformity in the dimensions of the elements. This was done by using the “Remesh” command in the horizontal menu at the top of the visualisation window, and then selecting “Uniform Remesh”. Next, a volumetric mesh was created using the "Remesh", "Create Volume" and "Solid Mesh" commands, as shown in Figure 24. A three-dimensional mesh of tetrahedral type was chosen, consisting of four vertices, six edges and limited by four faces. Each tetrahedron was assigned a dimension of 2 mm. This choice was guided by the consideration that a finite element size of less than 2 mm would offer greater accuracy in representing structural behaviour but would require computational resources that would slow down the simulation. Conversely, a dimension above 2 mm would speed up the simulation, but could generate less accurate results, especially in critical areas or with high gradients. Therefore, the cortical and trabecular parts were separated using the commands “Duplicate”, 'Separate' and “Shell to parts”. It was essential to reverse the mesh start direction for the trabecular section using the "Fix", "Invert normal" command.

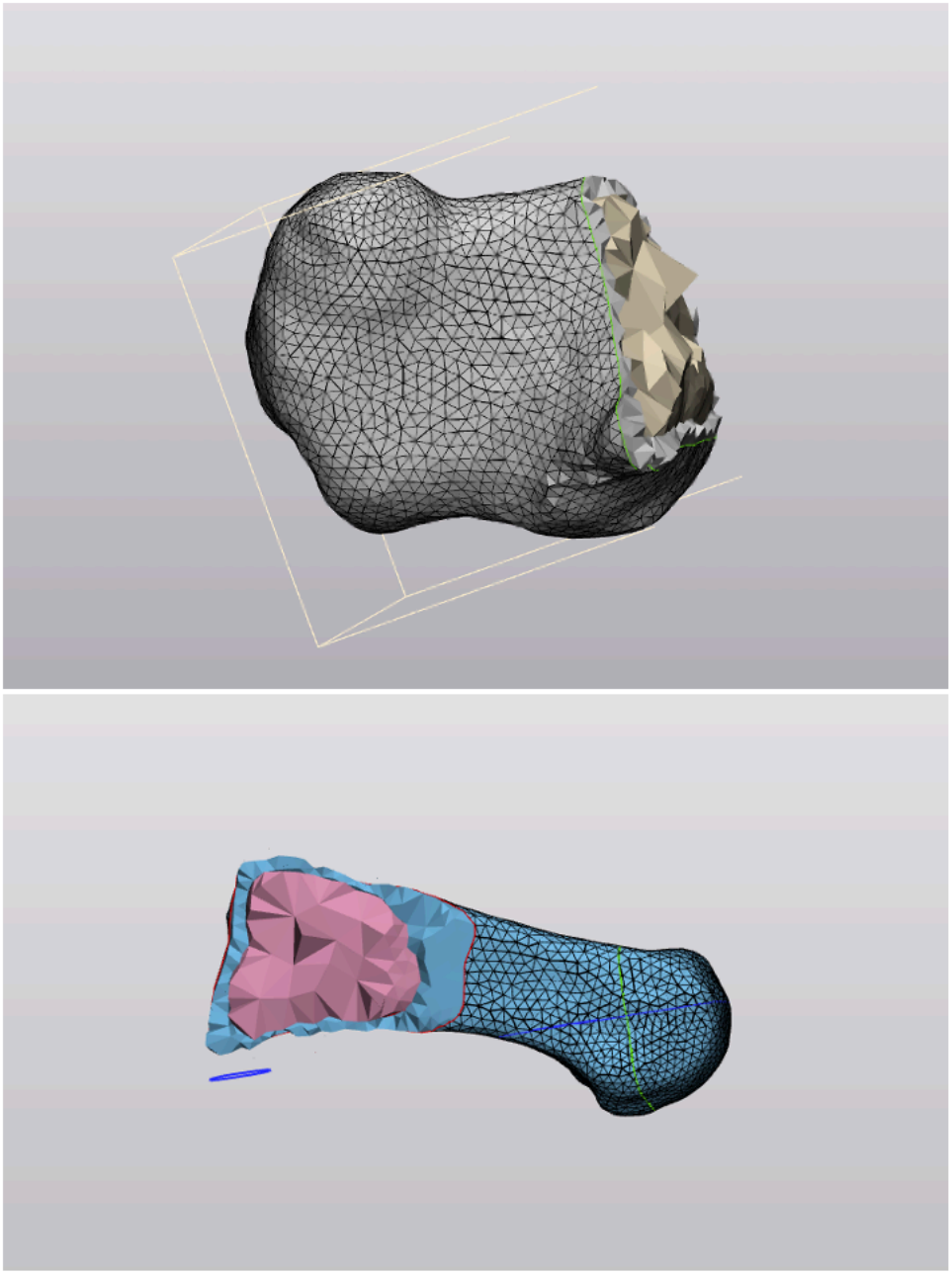

Figure 26: Visualizzazione della reticolazione a livello di volume.

Finally, two separate files were exported in .inp format. This procedure was essential to ensure the application of distinct materials within the Abaqus software.

4.4 Stroke simulation using the foot FEM

In this concluding section on the methodologies used, the Abaqus software is introduced. Here, all the steps performed to integrate the bones of the first metatarsal and calcaneus into the pre-existing model provided by the laboratories of the University of Aix-Marseille are outlined. The characteristics assigned to the test objects are made explicit, from the attribution of the materials used to the boundary

conditions, the latter having been previously configured to start the simulation of movements during walking and running. Abaqus© (version 6.14, Dassault Systems), is a finite element simulation (FEA) software developed by Dassault Systèmes Simulia Corp. This programme allows engineers to simulate the behaviour of real structures and components using the finite element technique. This approach allows a complex model to be broken down into smaller elements, thus simplifying the analysis.

The mechanical properties of the initial model were taken from the literature, including Young's modulus and Poisson's coefficient for linear models. Direct expressions of the mechanical models, based on stress-strain relationships and established potential formulations or polynomial representations, were extracted to obtain an accurate representation of material behaviour. To estimate the muscle forces of the nine extrinsic muscles, the OpenSim static optimisation tool was used, based on experimental data. Based on this information, the boundary conditions of the layered finite element model were set by considering the experimentally measured initial velocities in 2D (anteroposterior and vertical) and the muscle forces estimated from the pre-existing, time-dependent model acting on the foot. The application of the apparent weight of the model as an external vertical force was constant throughout the entire running simulation.

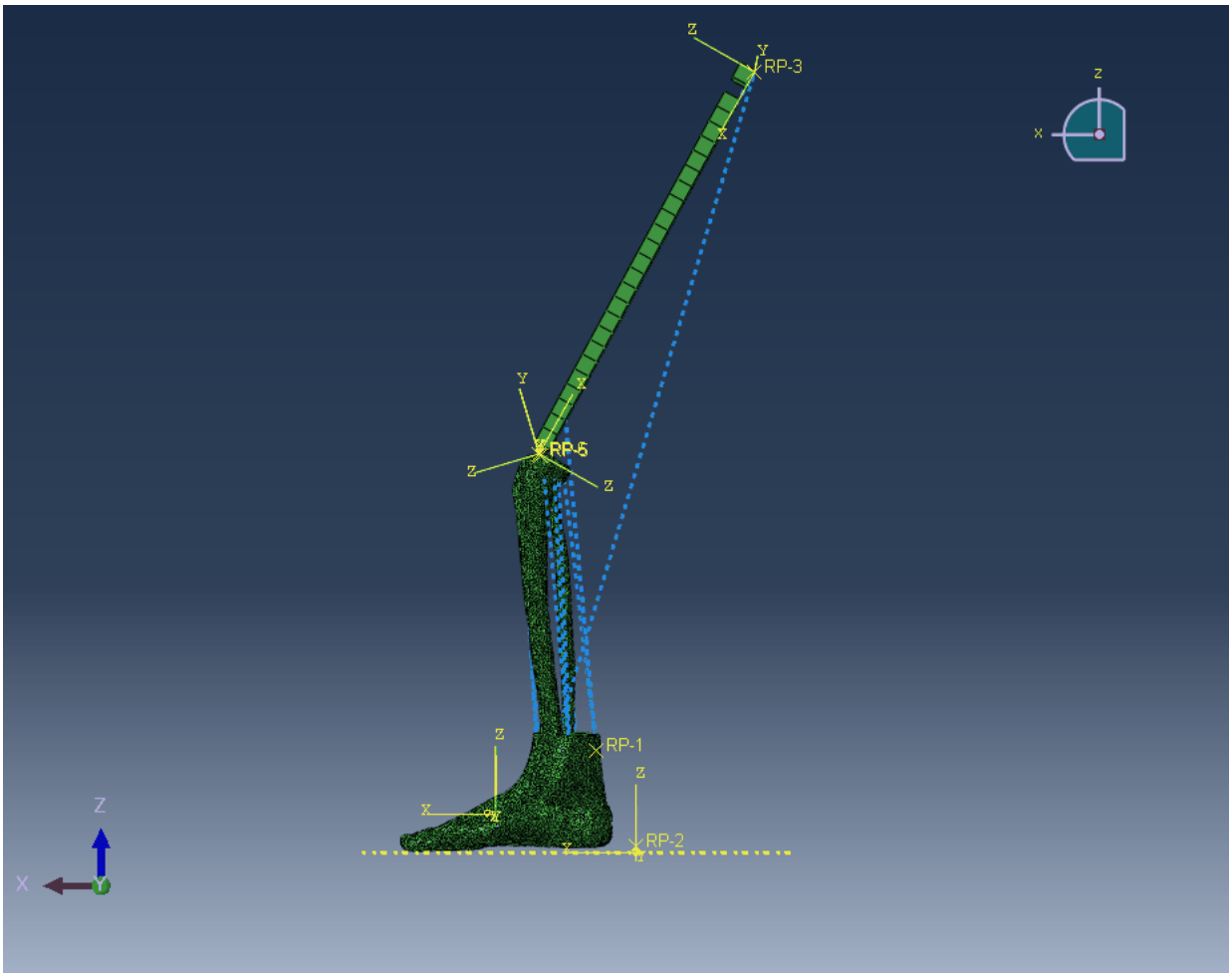

Figure 27: University of Aix-Marseille's FE Model.

During the development of the project, the option was chosen to start with the independent replacement of the First Metatarsal, excluding the import of the Calcaneus in order to avoid prolonged processing and model modification times. As a result of this decision, six separate models were created, three of which were composed of homogenous bone material and three of which were composed of different bone material. The models are named as follows:

1. LAYERS_FRONT_CT
2. HOM_FRONT
3. LAYERS_MID_CT
4. HOM_MID
5. LAYERS_REAR_CT
6. HOM_REAR

The models are distinguished according to the way the footrests on the ground. In particular, the aim is to examine the different stresses that occur in different types of running. The angles chosen are -

4.5°, 0.4° and 6.5°, which respectively indicate an approach to running with the forefoot, through the entire sole of the foot and from the hindfoot. The angles are based on experimental data, in fact, the angles between the ground and the foot were calculated during the static test to have a reference and then the angle during the dynamic test at the instant of contact with the ground. The difference between the two provided the angles used in Abaqus. For each angle, two separate models were adapted: one consisting of a single bone material and one consisting of two different bone materials.

- Identification of initial parameters: For these models, it was only necessary to define the initial parameters at the instant prior to contact. Subsequently, the movement of the foot is guided by muscular forces. The necessary inputs are the flexion/extension angle of the foot (Figure 25), defined by rotating the foot in the Abaqus assembly module; the initial velocity of the foot and center of mass, estimated by OpenSim; and the mass of the subject.

The models developed incorporated the new geometry of the First Metatarsal, manually inserted within the existing model, replacing the original. This step relied on the use of triads and rotation angles to accurately overlap the two meshes, subsequently eliminating the un-layered one. Once the geometry was properly placed, the constraints and interactions between the metatarsal bone and surrounding structures, such as tendons and ligaments, were restored. Constraints were reconstructed for the anterior tibial tendon, which generates upward traction during gait, resulting in bending of the big toe. Similarly, the constraints of the Long and Short Extensor tendons of the toes, responsible for the extensor movement, were recreated. The reconstructed interactions involved the tendons of the Extensor and Flexor muscles of the big toe. To ensure the precise execution of the movement and maintain the bone in position, interactions had to be generated with the metatarsal bone tissue and the flexor and extensor retinaculum. A crucial constraint was the connection between the trabecular and cortical geometry of the metatarsus to establish a solid connection between the two bony structures and enable optimal simulation.

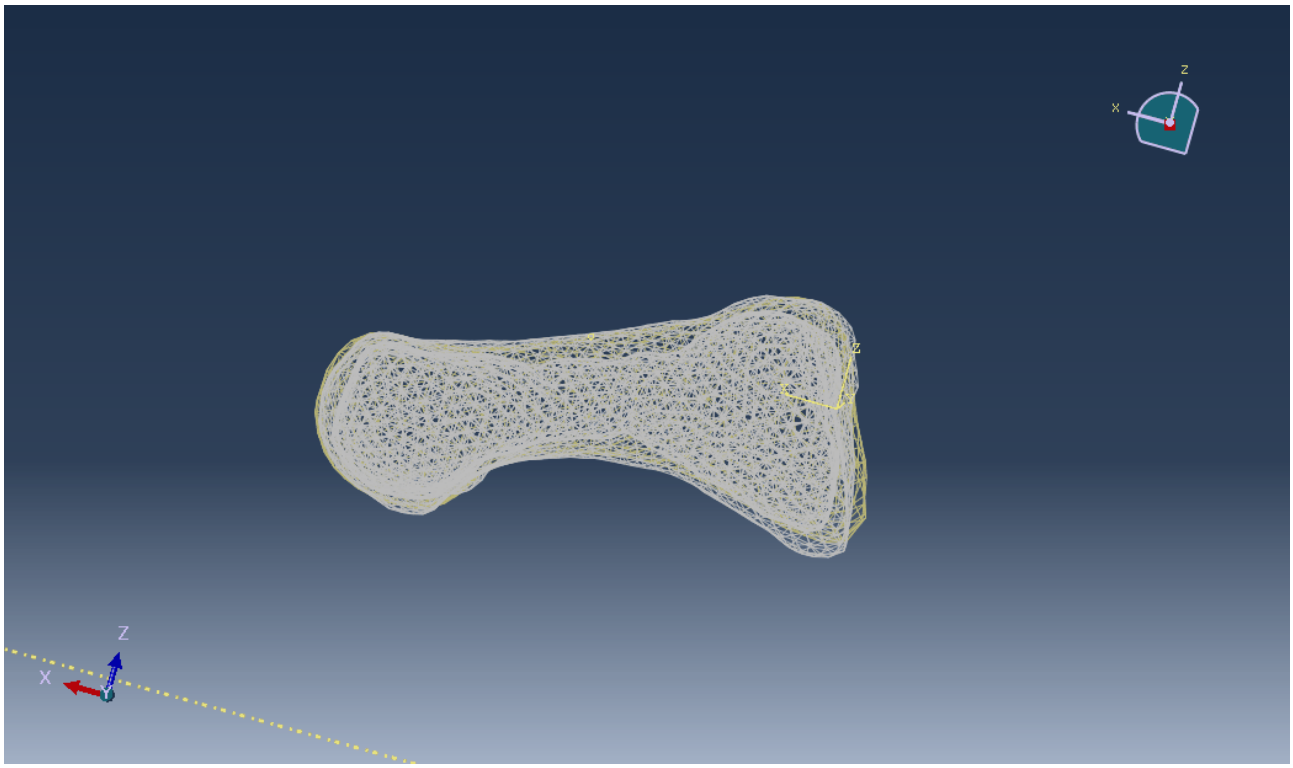

Figure 28: Overlap of metatarsal bones.

Therefore, the bone mechanical properties were assigned to the dense region and the spongiosa region, respectively. For all models, the mechanical properties were obtained from the literature, specifically the Young's modulus and Poisson's coefficient for the bone material were researched. The behaviour of the cortical and trabecular material was assumed to be homogeneous and linear elastic; density, elastic modulus and transverse contraction ratio are shown in Table 1.

Table 1: Material Behaviours.

	Density $[\frac{g}{mm^3}]$	**Young's modulus** $[MPa]$	**Poisson's ratio**
HOM CORT	0.0018	7300	0.3
HOM TRAB	0.0018	7300	0.3
LAYERS CORT	0.002	17000	0.32
LAYERS TRAB	0.001	350	0.25

According to the model of Gefen et al. (2000) [44], the elastic modulus for bone material is determined by averaging the cortical and trabecular values. For layered models, however, reference is made to the model of Lai Y-S et al. (2015) [45].

- Load definition: The only loads applied are the muscle forces. Since these are dynamic models, it is essential to have the values of the muscle forces for the entire stance phase of the stride cycle. Therefore, before generating the loads, their amplitudes must be determined. These amplitudes are implemented as functions in Abaqus, associating each time instant with the corresponding muscle force value. Subsequently, each load is defined with its amplitude in the Abaqus loading module.

- Definition of BCs: they were established for the plate and the mass-equivalent element. The plate remained fully constrained during the simulation, with all six degrees of freedom fixed at zero. The mass-equivalent element was allowed to move along the vertical and antero-posterior axes, while it remained locked along the mid-lateral direction. Only rotation around the mid-lateral axis is permitted, while other rotations are fixed at zero.

- Job creation: Finally, the models were ready to start the simulation. "Job-1s"' were created in the Abaqus job module for each type, respectively, and the job progress and partial results could be monitored via the "Monitor" item.

Thus, the boundary conditions for the six new models remain the same as for the reference model. Accordingly, the experimentally measured velocities and muscle forces obtained from static optimisation, provided by the University of Aix-Marseille, were assigned. After setting the boundary conditions, the impact and support phase of the running cycle was simulated. The model, driven by time-dependent muscle forces and ground contact, simulated a “step” (Step-1) consisting of 26 frames, representing time from 0 to 25 ms. Each simulation took approximately 12 hours to successfully complete. Upon completion of the simulations, the 'Job-1' files for each model were examined.

To evaluate this finite-element foot model, the antero-posterior and vertical ground reaction forces were inspected. The forces of the layered models were compared with those of the homogeneous models, which were validated with experimental data from the force platform of the starting model. A comparison of the stress evolution within the metatarsal was also conducted. The output data were extrapolated from the simulations and processed to validate them with scientific evidence and knowledge of biomechanics. They consisted of the temporal evolution of the stress suffered by the first metatarsal for all trials during the stance phase. The Von Mises constraints, the components of the stress tensor and the deformation constraints were brought back to the integration point.

4.5 Output processing

To validate the FEM of the foot, numerical data indicating ground reaction forces, stresses, and deformations of the first metatarsal had to be exported. The output data obtained was processed using the Python programming language, implemented through the PyCharm IDE (version 2023.3.1), ensuring an efficient and accurate process. The decision to adopt Python was motivated by its versatility and wide range of specialised libraries, allowing the process to be customised and optimised more effectively.

Data were downloaded from the “Job-1” files of each simulation in the form of *.rpt* files. These files collected the stress and strain values over time, for each individual finite element that made up the bone under test. The ground reaction force values, on the other hand, related to the internal model of the bone over time.

GRF - GROUND REACTION FORCES

Ground Reaction Forces (GRF) are the forces exerted by a supporting surface (such as the ground) on an object in contact with it. In the context of biomechanical analysis, GRFs are particularly important for understanding how the human body interacts with the ground during activities such as

walking, running or other dynamic movements. These were simulated and measured through the finite element (FE) models constructed, in the context of the biomechanical analysis of running. In the FE models, GRFs were simulated because of the interactions between the simulated foot and limb and the support surface, modelling the contact between these two surfaces. It was important to assign contact properties, such as friction and rebound coefficients, that influence contact behaviour. These parameters were derived from literature values and incorporated into the starting model.

```
import pandas as pd
import matplotlib.pyplot as plt

# Upload .rpt files
df1 = pd.read_csv( filepath_or_buffer: '/Users/francescaarditi/PycharmProjects/pythonProject1/GRF_Font_Layers.rpt', delimiter=r'\s+', skiprows=[0, 1], index_col=0)
df2 = pd.read_csv( filepath_or_buffer: '/Users/francescaarditi/PycharmProjects/pythonProject1/GRF_Front_Hom.rpt', delimiter=r'\s+', skiprows=[0, 1], index_col=0)
```

Figure 29: Import of libraries for manipulating and representing data and reading files.

The files containing the force values for each model were imported into Python using the *panda*[2]*s* and *matplotlib*[3] libraries. Once the data was read in, it was manipulated to create a plot graph, as shown in Figure 28, representing the trend of ground reaction forces over the time of the step.

```
# Plot
plt.plot( *args: df1.index, df1.iloc[:, 0], label='Layers')
plt.plot( *args: df2.index, df2.iloc[:, 0], label='Homogeneus')
# Title and Labels
plt.title('GRF FRONT')
plt.xlabel('Tempo [ms]')
plt.ylabel('Forza [N]')
# Legend
plt.legend()
```

Figure 30: Plotting function of data over time.

VON MISES STRESS

Von Mises stress is a concept used in stress analysis to represent the complexity of the stress state in a material. It is an equivalent stress measure that considers stresses in all directions. In fact, when a material is subjected to different stress components, e.g. normal stress and tangential stress, Von Mises stresses provide a single equivalent stress measure. This measure assumes that, for the collapse of a material, only the equivalent stress with respect to a given combination of stresses is significant.

[2] Pandas is an open-source library for data manipulation and analysis in the Python programming language. It provides flexible, high-performance data structures designed to make it easy and intuitive to work with structured or tabular data, such as spreadsheets or relational databases.
[3] Matplotlib is a data visualisation library in Python that offers a wide range of tools for creating graphs, plots and visualisations.

The formula for calculating Von Mises stresses (σ_{VM}) is given by:

$$\sigma_{VM} = \sqrt{\frac{1}{2}\left[(\sigma_1 - \sigma_2)^2 + (\sigma_2 - \sigma_3)^2 + (\sigma_3 - \sigma_1)^2\right] + 3\tau_{12}^2 + 3\tau_{23}^2 + 3\tau_{31}^2}$$

Where:

- $\sigma_{12},\ \sigma_{23},\ \sigma_{31}$ are the principal stresses along the three main directions,
- $\tau_{12},\ \tau_{12},\ \tau_{12}$ are the tangential stress components.

Again, the files containing the stress data were introduced and processed using the Python language. An initial code implemented allowed the files to be read and the average value of the stresses to be calculated at each time step. The script was executed to allow a direct comparison of the stress trend, i.e. the stresses in the cortical and trabecular regions for the two types of models were depicted within a single graph.

```
hom_data = pd.read_csv( filepath_or_buffer: "/Users/francescaarditi/PycharmProjects/pythonProject1/Hom_Front_ct_CortOnly.rpt", skiprows=5, header=None, sep="\\s+", index_col=0)
layers_data = pd.read_csv( filepath_or_buffer: "/Users/francescaarditi/PycharmProjects/pythonProject1/Layers_Front_ct_CortOnly.rpt", skiprows=5, header=None, sep="\\s+", index_col=0)

# Calcola la media dei dati filtrati per valori maggiori di 0.2
hom_data_filt = hom_data[hom_data > 0.2].mean(axis=1)
layers_data_filt = layers_data[layers_data > 0.2].mean(axis=1)

# Salva le medie in un file CSV
hom_data_filt.to_csv("media_Hom_Front_Cort.csv", header=['Mean'])
layers_data_filt.to_csv("media_Layers_Front_Cort.csv", header=['Mean'])

# STRESS PLOT CORT FRONT
plt.plot( *args: hom_data_filt, label="Hom_Front_ct_CortOnly")
plt.plot( *args: layers_data_filt, label="Layers_Front_ct_CortOnly")
plt.title("Von Mises Stress Front - Cortical")
plt.xlabel('Time Steps [ms]')
plt.ylabel('Von Mises Stress [MPa]')
plt.legend()
plt.show()
```

Figure 31: Manipulation of stress data.

PRINCIPAL DEFORMATIONS

Principal deformations refer to the maximum relative length changes in three orthogonal directions (usually denoted as ε_1, ε_2, ε_3), and are used to describe the deformation state at a specific point within a body. These deformations are used to analyse the behaviour of materials under applied loads. In simpler terms, when a material is subjected to a stress, the principal deformations indicate how much the material has stretched or compressed along specific directions. For a FEM, principal deformations can be obtained by analysing the strain tensor. The strain tensor, denoted as ε, is a matrix representing the deformations at each point in your model.

$$\varepsilon = \begin{bmatrix} \varepsilon_{11} & \varepsilon_{12} & \varepsilon_{13} \\ \varepsilon_{21} & \varepsilon_{22} & \varepsilon_{23} \\ \varepsilon_{31} & \varepsilon_{32} & \varepsilon_{33} \end{bmatrix}$$

Where:

- ε_{11}, ε_{22} and ε_{33} represent the deformations along the principal axes of the local reference system (normal deformations),
- $\varepsilon_{12}, \varepsilon_{13}, \varepsilon_{21}, \varepsilon_{23}, \varepsilon_{31}$ and ε_{32} represent the shear deformations.

Like the stresses, a script has been reproduced that generates a graph representing the average deformations over time for each type of support.

```
def genera_grafico(file_hom, file_layers, front_type):
    # Read first file rpt
    data1 = pd.read_csv(file_hom, skiprows=4, header=None, sep='\\s+', index_col=0)
    strain_Hom_Mid = data1.mean(axis=1)

    # Read second file rpt
    data2 = pd.read_csv(file_layers, skiprows=4, header=None, sep='\\s+', index_col=0)
    strain_Layers_Mid = data2.mean(axis=1)

    # Plot with two curves
    plt.plot( *args: strain_Hom_Mid, label=f'Homogeneous {front_type} Front')
    plt.plot( *args: strain_Layers_Mid, label=f'Layers {front_type} Front')

    plt.xlabel('Time Steps [ms]')
    plt.ylabel('Strain [με]')
    plt.title(f' Strain-Time | {front_type} Front')
    plt.legend()
    plt.show()
```

Figure 32: Code that generates a plotting of the deformation's curves over the time.

4.6 Performance metrics

To quantify and evaluate the differences between homogeneous and stratified FE models, two significant statistical metrics were used in this research: the absolute error and the stress ratio. These metrics played a crucial role in determining the accuracy and reliability of the results obtained from the models under examination.

Specific statistical indices were used to assess the precision and accuracy of the numerical model. These indices are of fundamental importance in the context of the analysis as they allow the difference between the two models to be measured objectively, providing an assessment of the error of one model compared to the other. The results generated by these metrics can be used to optimise the

model, assess the correct configuration of parameters, and monitor any improvements in performance over time.

AERR - ABSOLUTE ERROR

The absolute error (AERR) is a measure that provides a quantitative estimate of the discrepancy between the stresses predicted by the two models. Essentially, the absolute error provides an estimate of the absolute deviation between the actual data and the model prediction. An evaluation of this error allows one to quantify how much the model's predicted results may vary from experimental data or reference values.

$$AERR = |Real\ Value - Predicted\ Value|$$

A low absolute error, close to zero, indicates a more accurate forecast, while a higher error indicates a greater discrepancy between the model and the actual data.

In the context of this research, metrics are essential in understanding the degree of accuracy of the detailed, realistic model versus the more simplified model.

```
# AERR trabecular calculation
errore_assoluto_trab = [abs(v1 - v2) for v1, v2 in zip(media_Hom_Trab, media_Layers_Trab)]

# AERR Cortical calculation
errore_assoluto_cort = [abs(v1 - v2) for v1, v2 in zip(media_Hom_Cort, media_Layers_Cort)]
```

Figure 33: AERR calculation in Python.

R - STRESS RATIO

The stress ratio, or stress ratio, is an indicator that can be used to assess the difference between two conditions or models in terms of stress. It can be calculated as the ratio of the stress of one condition or model to another:

$$R = \frac{Stress\ value\ Layers\ Model}{Stress\ value\ Hom\ Model}$$

Where:

- R>1, indicates that the homogeneous model overestimates the stratified model,
- R=1, indicates that there is no significant difference between the models,
- R<1, indicates that the homogeneous model underestimates the stratified model.

```
if len(media_Hom_Front_Cort) != len(media_Layers_Front_Cort):
    raise ValueError("Le liste devono avere la stessa lunghezza.")

rapporti_per_steps1 = [v1 / v2 if v2 != 0 else float('inf') for v1, v2 in zip(media_Layers_Front_Cort, media_Hom_Front_Cort)]

# 2. Rappresentazione grafica del rapporto
steps = range(1, len(rapporti_per_steps1) + 1)

print(rapporti_per_steps1);

plt.figure(figsize=(10, 6))
plt.plot( *args: steps, rapporti_per_steps1, marker='o', linestyle='-')
plt.title('RATIO FRONT CORT')
plt.xlabel('Steps')
plt.ylabel('Layers / Front [MPa/MPa]')
plt.grid(True)
plt.tight_layout()
plt.show()
```

Figure 34: Calculation and graphical representation of R.

Figure 32 describes the code implemented to calculate the stress ratio values and the resulting graph showing the distribution of the data over time.

Chapter 5

5 Results and Discussions

In this chapter, we will examine the results of this study aimed at comparing two FEM, one with homogeneous First Metatarsal tissue FE model and one with stratified trabecular and cortical First Metatarsal tissue FE model, considering three different support conditions (Frontfoot, Midfoot, Rearfoot), and using the performance metrics described above.

Initially, we will conduct a qualitative analysis to validate the layered approach. We will observe and compare geometries using the Von Mises stress intensity scale, caused by the muscle forces inducing movement. The hypothesis is that the subdivision of the tissues and the different mechanical properties significantly influence the stress prediction. Next, we will perform a quantitative analysis. We will compare the data estimated by the 'Layers' model with that of the 'Homogeneous' model. We will collect and represent the stress data and calculate the absolute errors between the two model categories. This error will be the difference in stress measurements between the homogeneous and layered models for both the cortical and trabecular regions. It is important to emphasise that neither can be considered a true gold standard. Next, we calculate the error ratio. This step is crucial because it provides a numerical representation of the differences between the two models.

Following that, deformations will be presented through a strain-time plot, comparing them with the average deformations of a model previously described in the literature.

5.1 Quantitative Inspection

5.1.1 Visual Evaluation of von Mises Stress Distribution

Following the use of different materials constituting the bone of the first metatarsal, it was possible to carry out an initial visual analysis of the distribution and intensity of Von Mises Stress. Below are 12 images of the first metatarsal in the time steps in which the maximum stress occurs.

Front Homegeneus

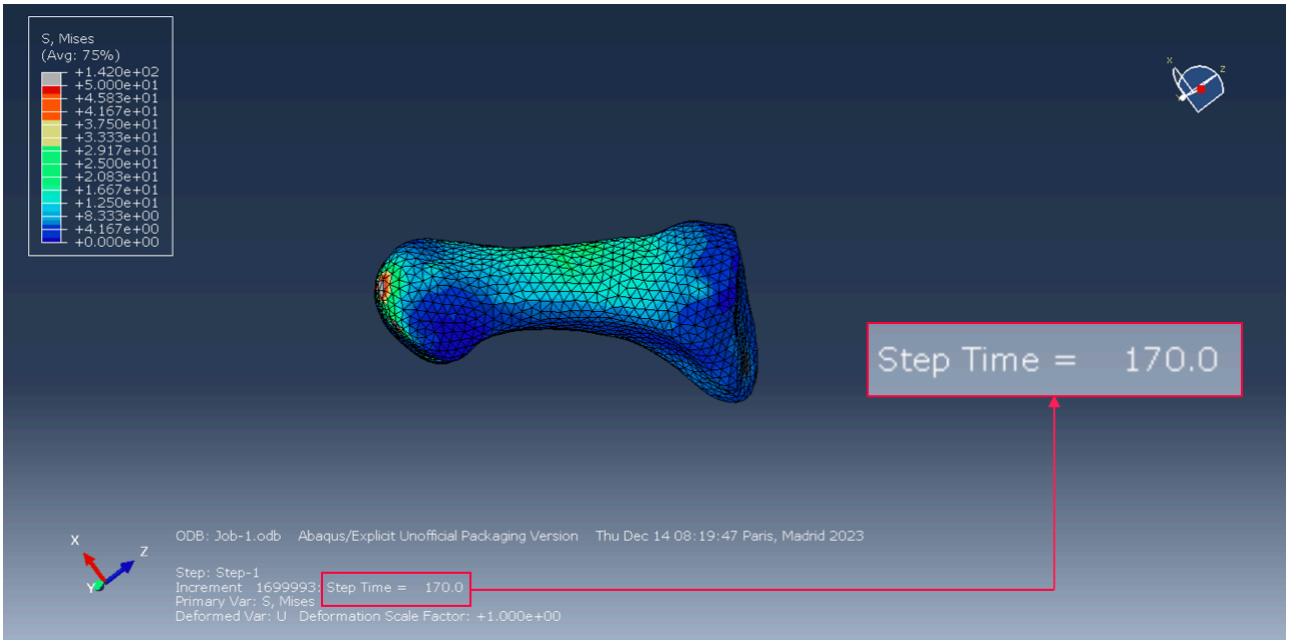

(A)

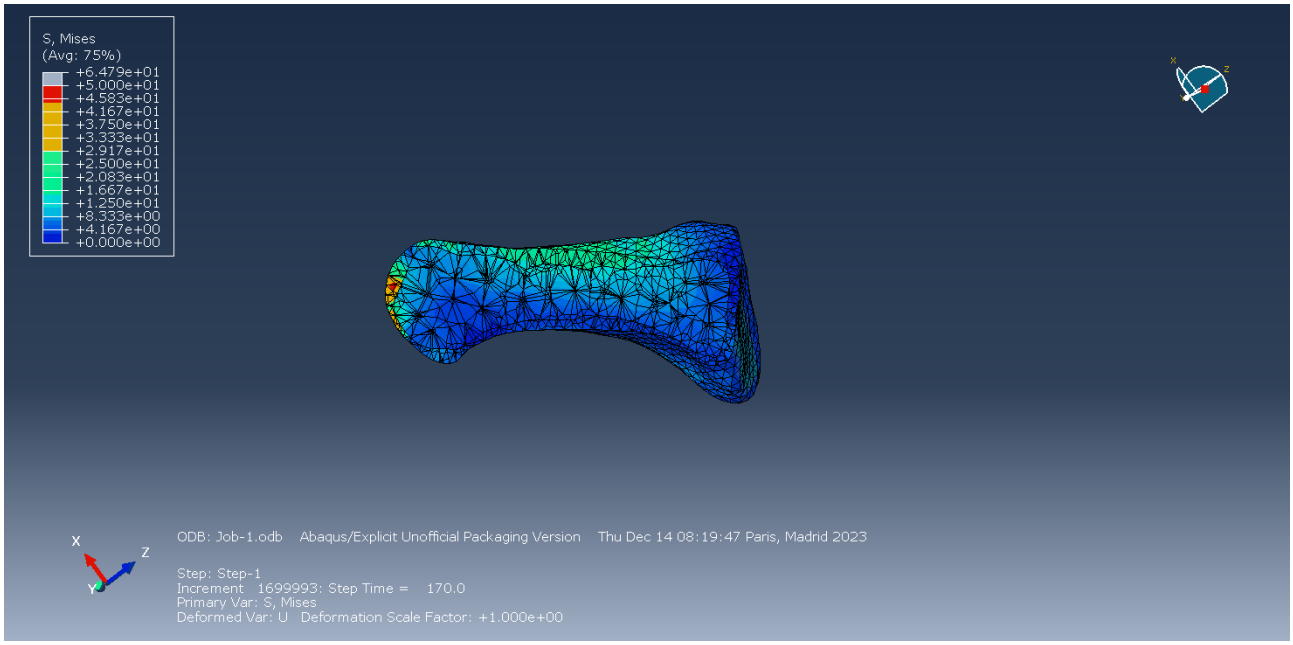

(B)

Front Layers

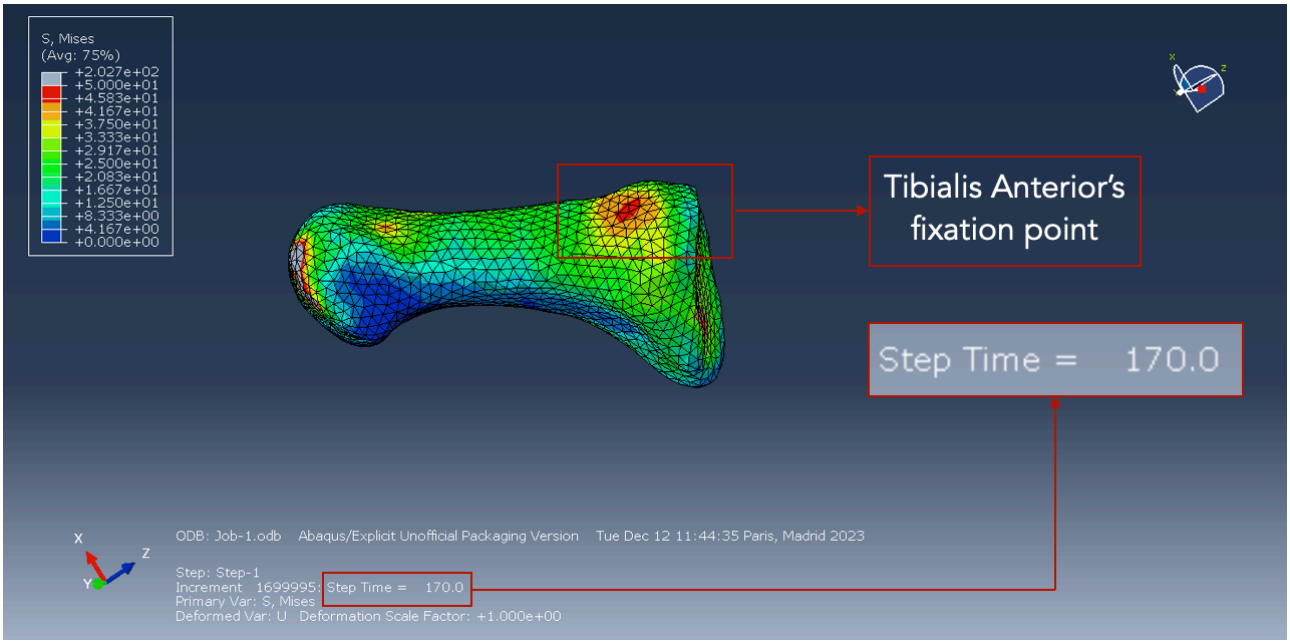

(C)

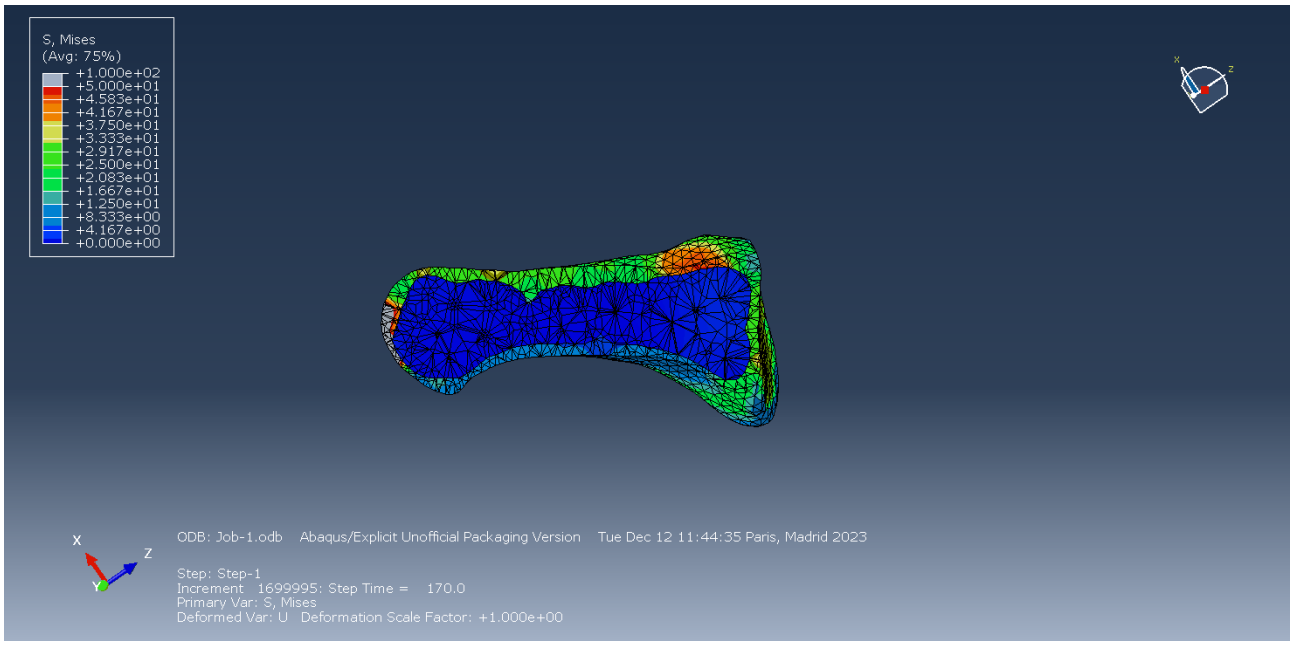

(D)

Mid Homogeneus

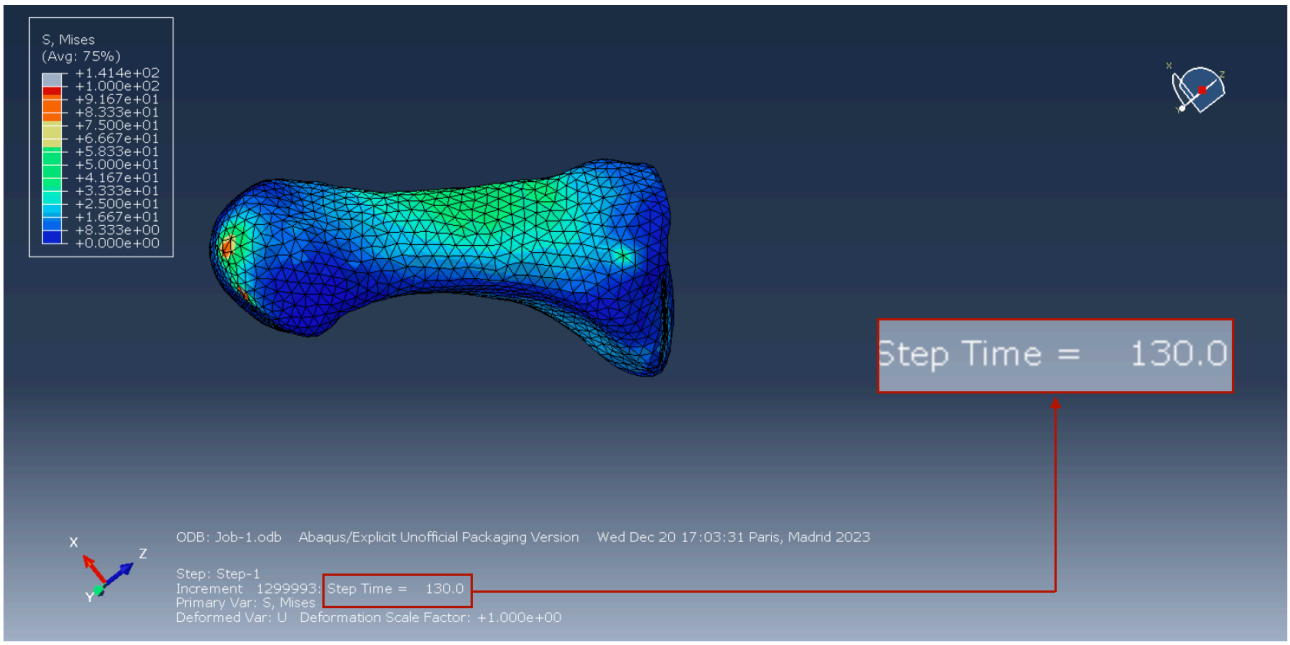

(E)

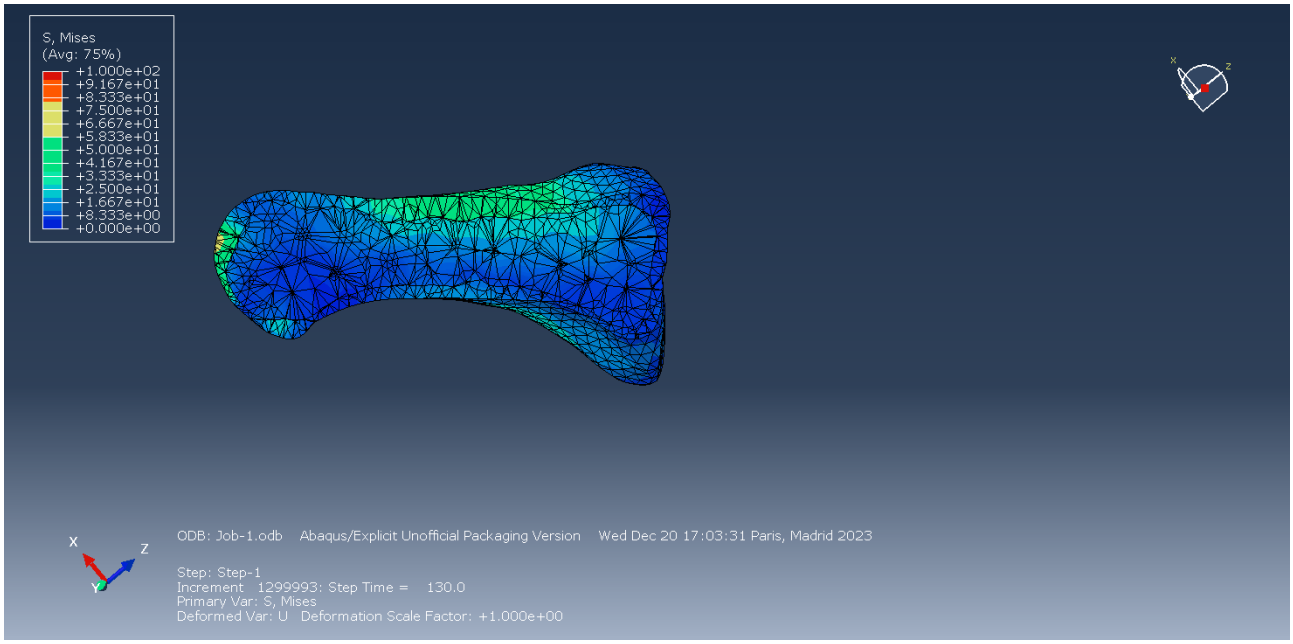

(F)

Mid Layers

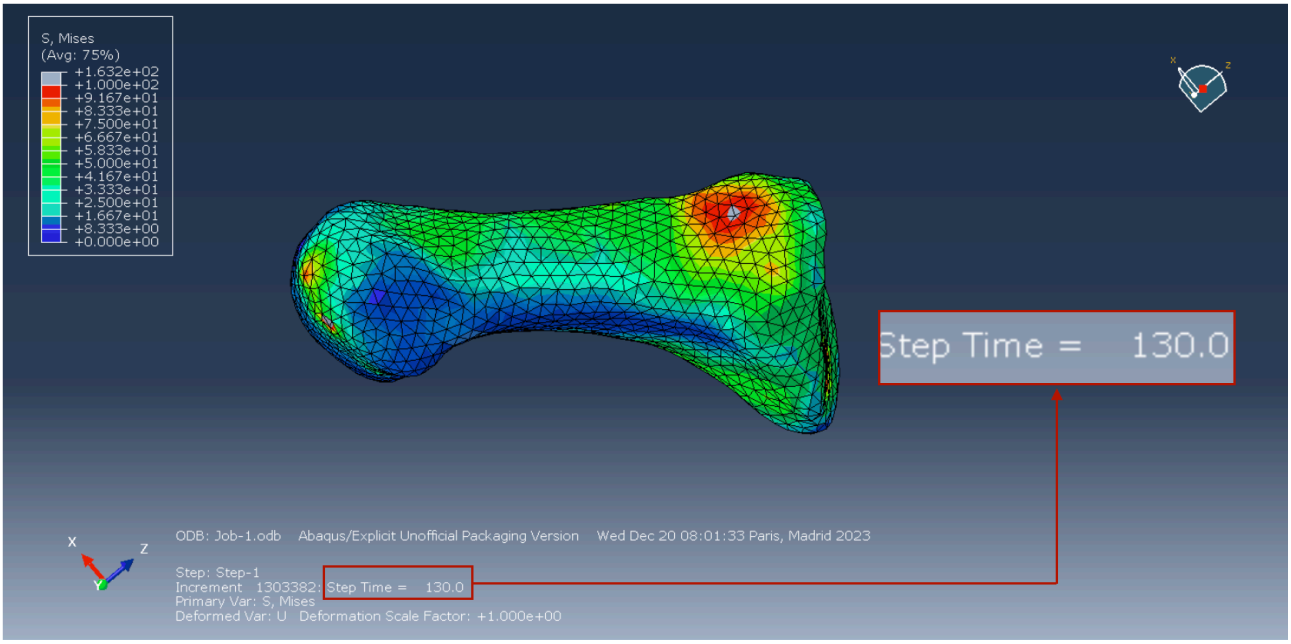

(G)

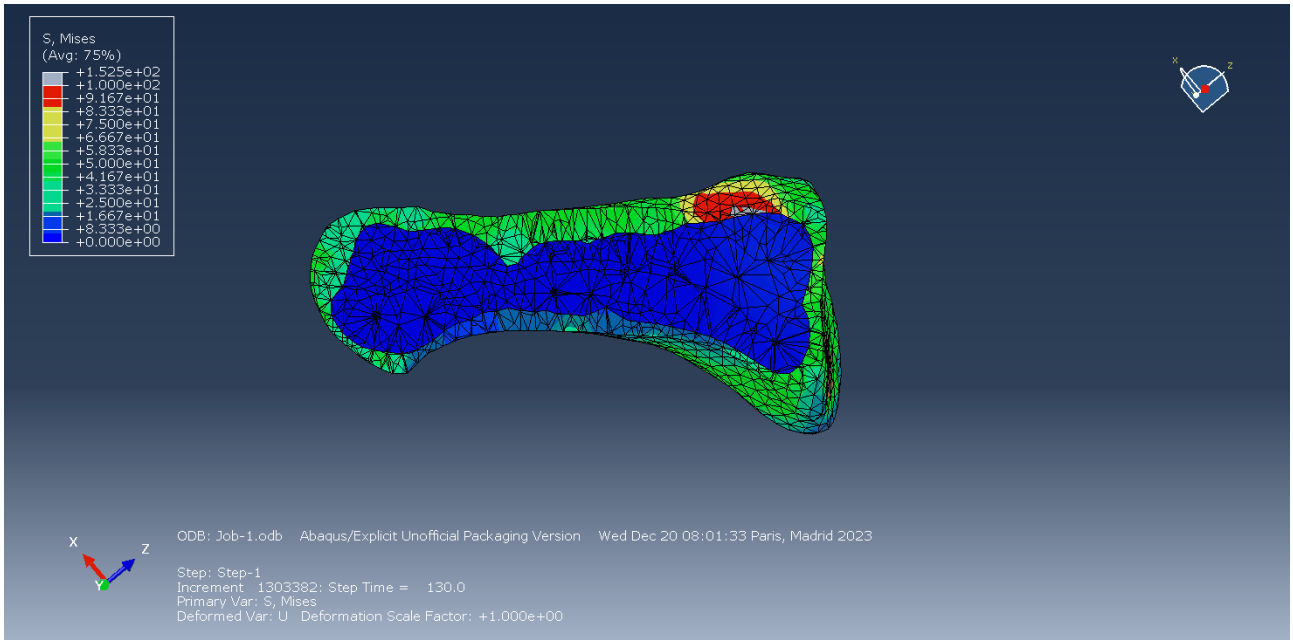

(H)

Rear Homogeneus

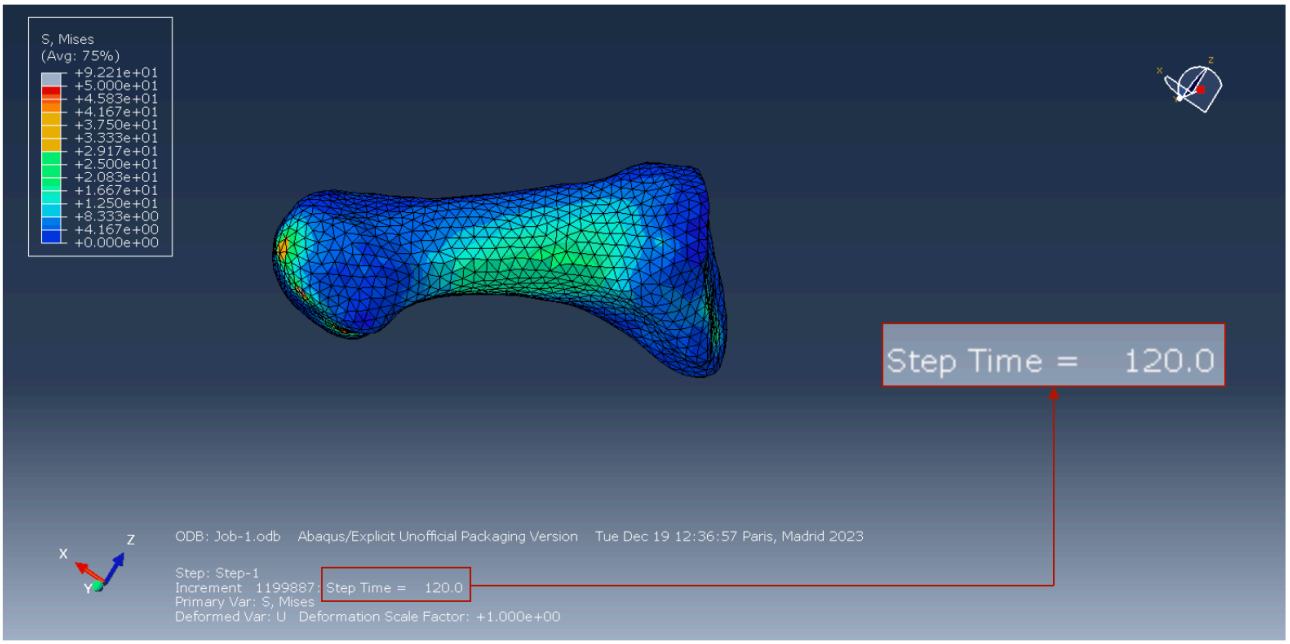

(I)

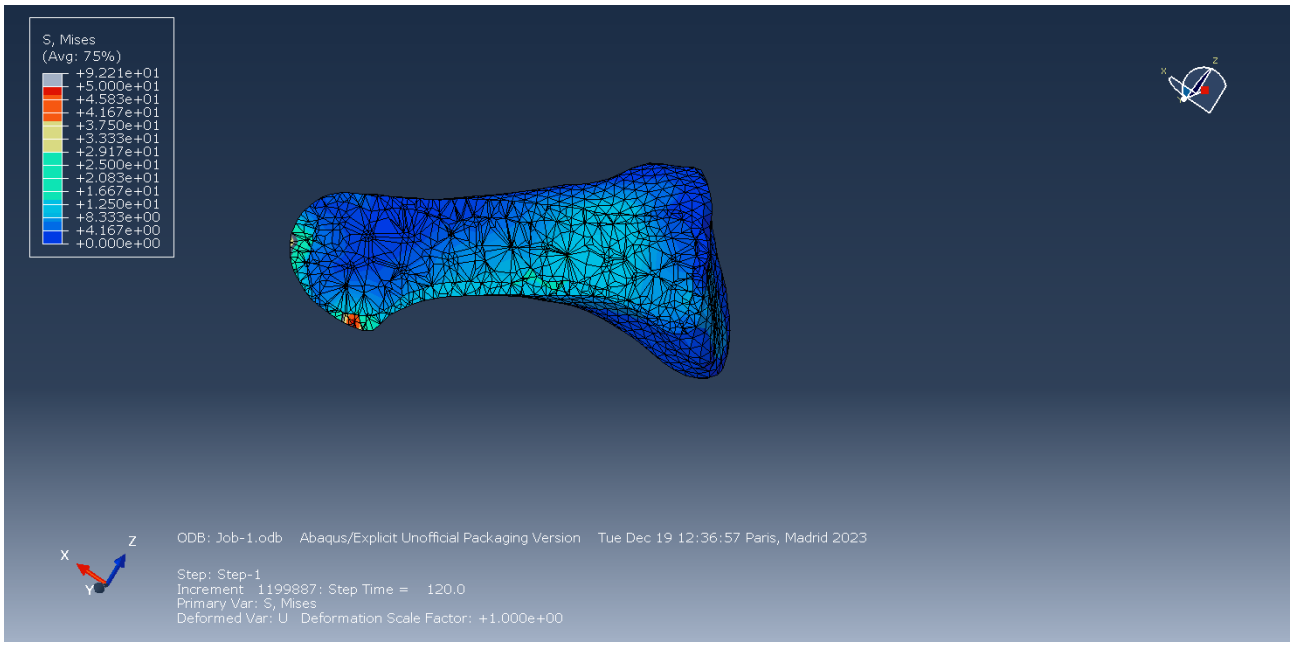

(J)

Rear Layers

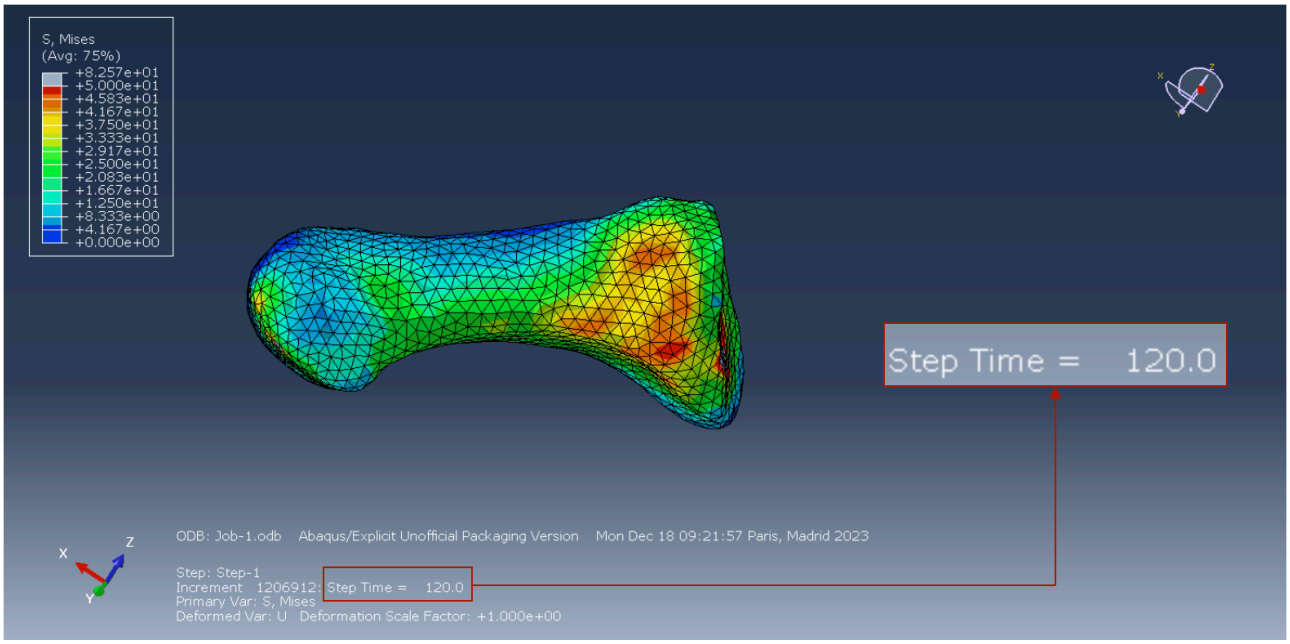

(K)

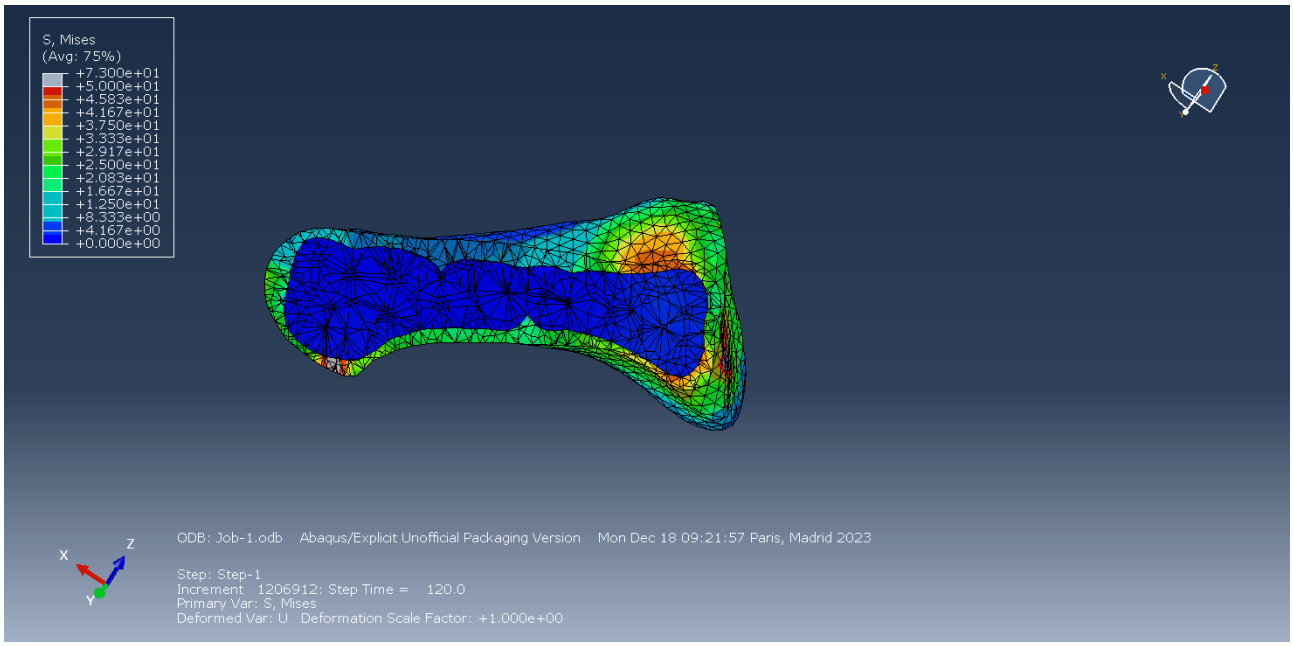

(L)

Figure 35: Comparison of Stress distribution in the Homogeneous and Stratified Model. The (A) (C) (E) (G) (I) (K) images show a complete view of the first metatarsal for all Front, Mid and Rear cases of the two model classes. Images (B) (D) (F) (H) (L) show the longitudinal section of the bone. In these cases, the distribution of internal stresses can be explored.

Looking at the images presented, it is evident that the maximum stress occurs at different times depending on the type of support during walking. Considering this consideration, it was crucial to

extrapolate the maximum stress behavior in the same time intervals for each type of support. As illustrated in the Figures, the extrapolated Step Times are 170.0, 130.0, 120.0 respectively, equivalent to 17ms, 12ms, 12ms.

For each model (Front, Mid and Rear), it was essential to set the stress scaling limits to clearly visualize the stress behavior. In fact, for the Front and Rear models, a scale of 0 to $50\ MPa$ was adopted, while for the Mid model, the scale ranged from 0 to $100\ MPa$. These scales were used to make the results more understandable and to distinguish high stress regions from lower stress regions. Typically, the scale is coloured in gradations from blue (low values) to red or grey (high values).

A first obvious result concerns the stress distribution between the homogeneous and the stratified models. In the former, stress shows an almost uniform distribution, extending linearly from the cortical shell to the inside of the bone without reaching high values. Specifically, in the three homogeneous types, stresses vary from $0\ MPa$ to $30\ MPa$, with a predominantly blue green colouring. In the models that also include trabecular tissue, the stress distributions appear visually different. The stresses are particularly high in the cortical region and minimal in the trabecular region, showing a great discrepancy in stresses. In the cortical, values between $50\ MPa$ and $90\ Mpa$ are reached, resulting in a large area of red staining, while in the trabecular tissue, the stresses stop at a maximum of $4\ Mpa$. The following findings suggest that the cortical layer is subject to much higher stresses than the trabecular tissue. Based on biomechanical and anatomical knowledge, it is possible to state that the differentiation between these two regions is fundamental. In fact, the cortical, being the outer layer, represents the densest and most compact part, which bears the highest mechanical stresses. The trabecular tissue, on the other hand, is the inner part consisting of a porous structure and possesses greater flexibility and absorbs forces more effectively. In confirmation of this, the images shown suggest that it is necessary and fundamental to assign each tissue its own mechanical characteristics.

A second significant result concerns the influence of the Tibialis Anterior tendon. This influence is considerably underestimated in models composed exclusively of cortical material because no abnormal stress levels are observed at the connection points between the tendon and the bone. In contrast, in layered models, an appreciable tensile action exerted by the tendon is evident, resulting in high Von Mises Stress values for the surrounding elements. Values of around $50\ MPa$ are recorded for the Front and Rear models, and around 90 MPa for the Mid model. The analysis of these results suggests that the effect produced by the tendon is considerably relevant, approaching the yield values of the cortical bone ($Yield\ stranigth = 100 - 150MPa$).

Table 2: Von Mises values.

Max MV HOM	Max VM LAY	Max VM Literature
30 MPa	50-90 MPa	100-150 MPa

As a result, a clear interpretation of the data emerges: models that consider both cortical and trabecular tissue can reflect the evolution of stresses more accurately and make it possible to identify in detail the areas subjected to greater stress, and consequently, the area most at risk of fracture.

5.2 Quantitative Inspection

To validate the visual interpretation of how stresses behave, a sensitivity analysis was performed. This method provides a means of assessing the strength of an evaluation, playing a crucial role in providing an objective assessment of the performance of the layered model.

5.2.1 Ground Reaction Force (GRF) Analysis

The first analysis performed concerns the Ground Reaction Forces (GRF) for the respective model classes. Ground Reaction Forces curves were represented in relation to the time taken to perform a running step.

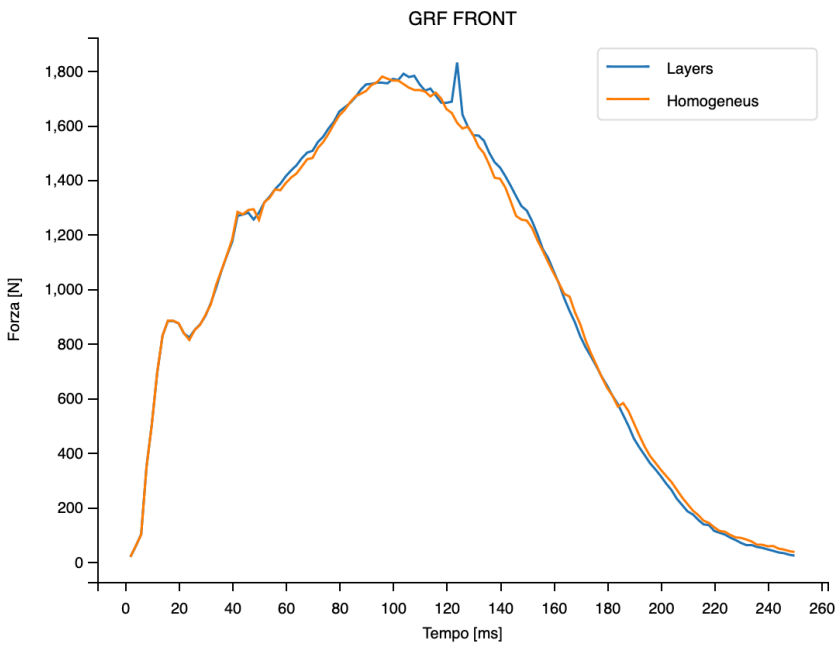

(A)

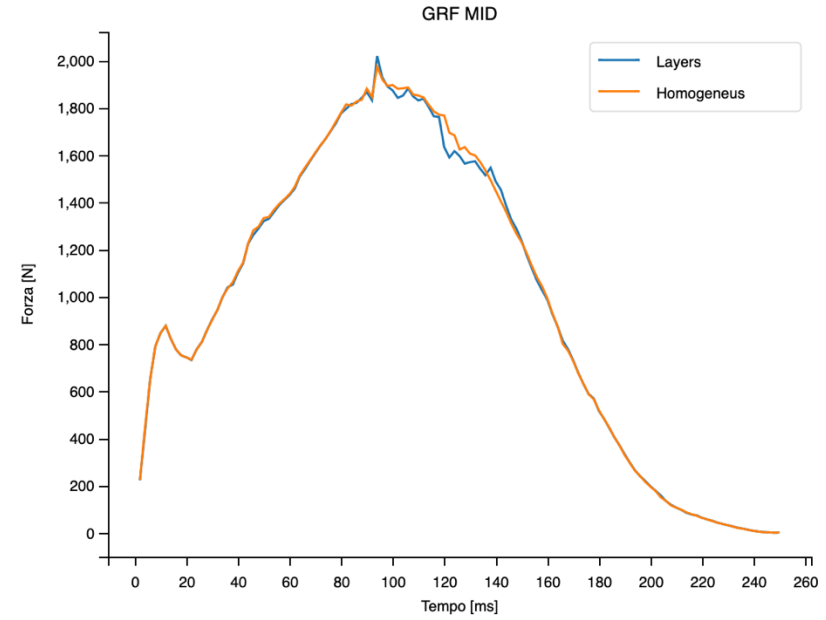

(B)

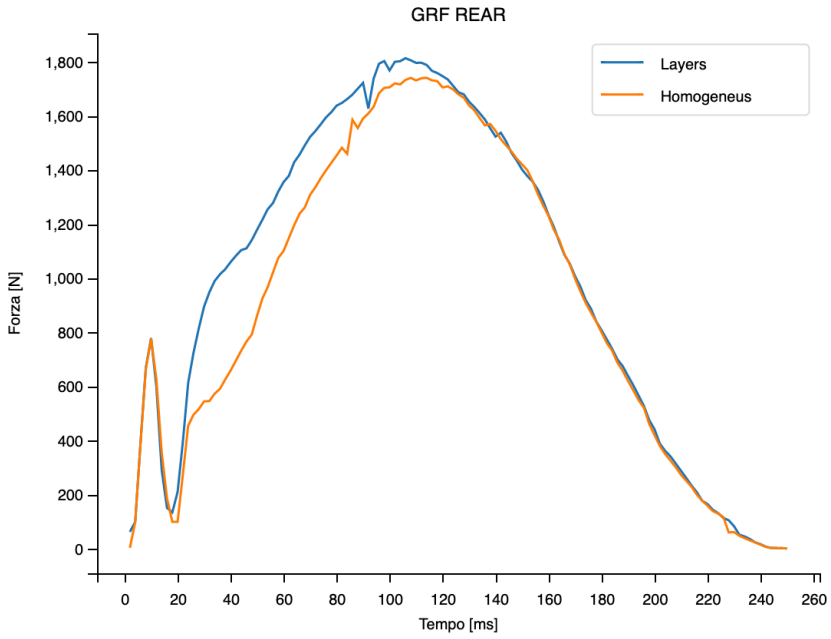

(C)

Figure 36: GRF for the three models Front Rear and Mid. Each graph shows the evolution curve of ground reaction forces over time for the homogeneous and stratified case.

The analysis of these forces makes it possible to examine in detail the biomechanics of the foot during the running motion. The remarkable overlap in Ground Reaction Forces (GRF) curves between the two models, despite significant differences in the composition of bone material, is a point of considerable interest and underlines the complexity of foot biomechanics during running. Firstly, the consistency in GRF curves suggests that both models are capable of effectively replicating the dynamic behaviour of the foot during the running cycle. This initial result suggests that, on a

macroscopic level, the simulation of the biomechanical response of the foot during running may appear similar, regardless of the detailed composition of the bone material. Furthermore, it suggests that the elastic behaviour of the cortical material is sufficient to accurately represent the response of the foot during running. Consequently, it appears that in the overall representation, the spongy tissue does not have a significant impact on the force distribution during running and does not lead to significant variations.

Thus, the comparison of GRFs generates similar results at the macroscopic level, despite substantial differences in model composition. These forces provide a global view of the load applied to the foot; therefore, they may not detect localized variations in biomechanical responses in different regions of bone tissue.

5.2.2 Von Mises Stress Evaluation

The apparent overlapping of the GRFs emphasizes the need to examine other biomechanical parameters in detail to gain a deeper understanding of the differences between the two models. To obtain a complete understanding of the biomechanical response, it is essential to examine the stresses.

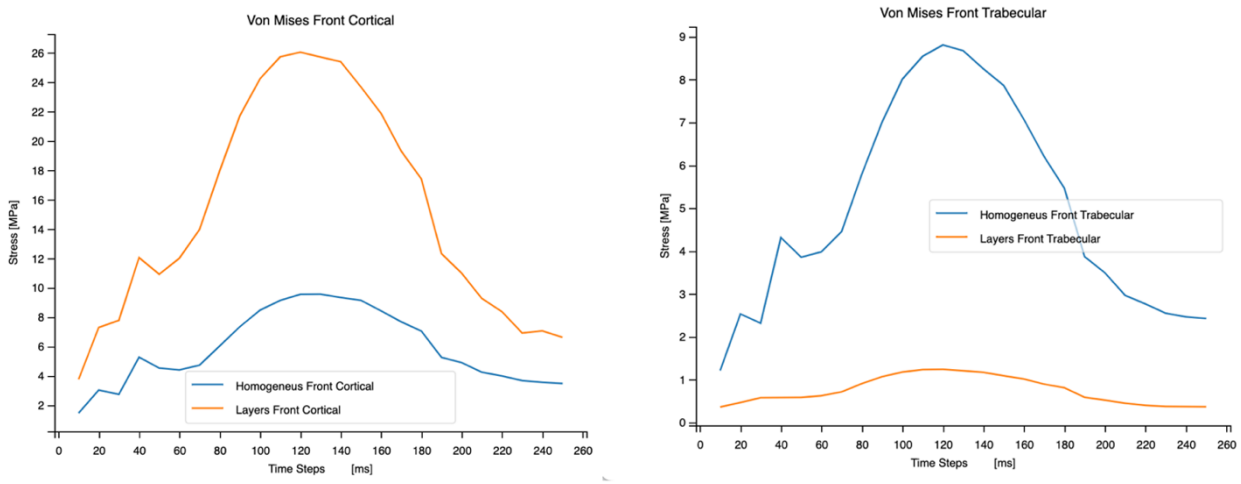

Figure 37: Von Mises stresses for the Front model divided by cortical and trabecular.

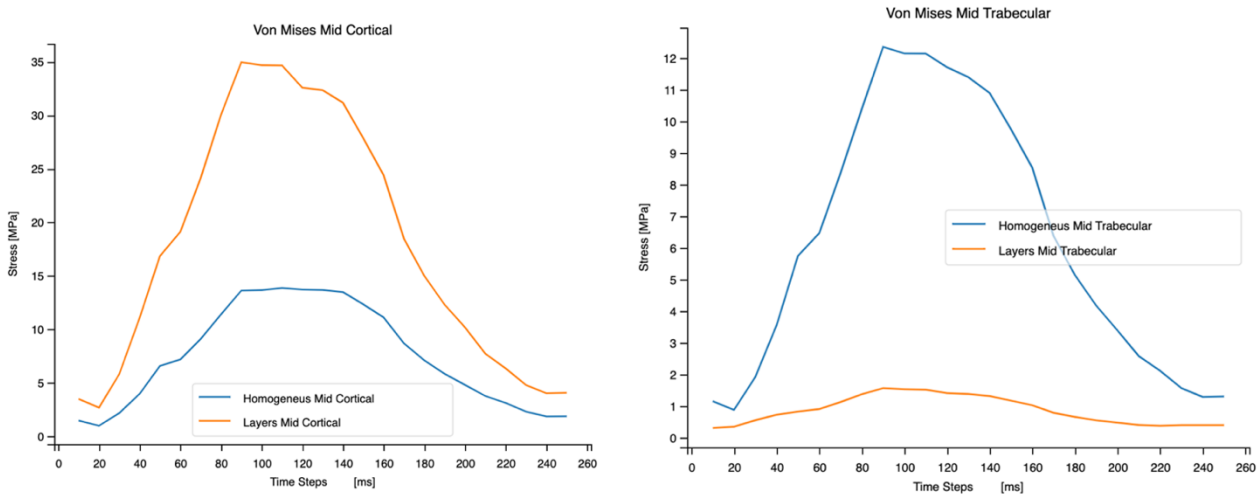

Figure 38: Von Mises stresses for the Mid model divided by cortical and trabecular.

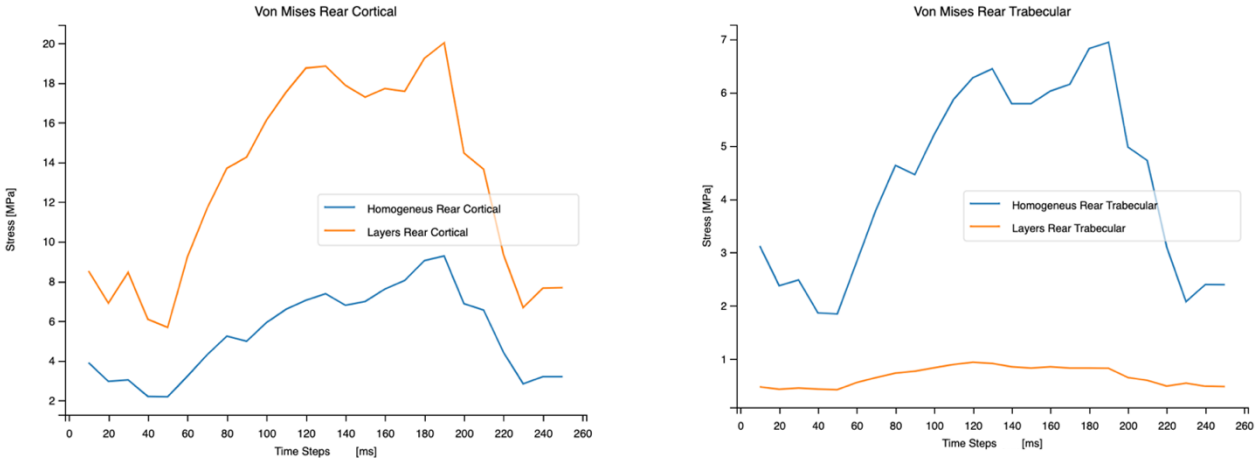

Figure 39: Von Mises stresses for the Rear model divided by cortical and trabecular.

The graphs above show the development of the average stresses in the cortical and spongiosis zones, respectively, for the two model classes, in relation to time. By plotting the following curves, it is possible to highlight the strong discrepancy between the two model types: within the layered model, the stress distribution shows a marked difference between the cortical and trabecular zones. High values are found in the cortical zone, whereas extremely low values are found in the trabecular zone. This variation reflects the different composition and density between these two bone tissues. A contrasting observation emerges from the homogeneous model, where stresses appear more uniform between the two regions.

What makes this discrepancy scientifically relevant is the consistency with known biomechanical principles and accumulated experimental evidence in the field of bone biomechanics. The presence of cortical and trabecular in the bones of the foot is well documented, with studies demonstrating dynamic adaptations in response to external stimuli. The cortical zone, which is denser and more rigid, tends to receive more stress, while the trabecular zone, which is more porous and deformable, can absorb load more effectively.

By considering this heterogeneity and replicating the diversity in the biomechanical response of the cortical and trabecular regions, the layered model emerges as a more accurate and realistic representation of the biomechanical complexity of the foot during running. This approach aligns with the natural adaptations of bone to the different biomechanical stresses that occur during physical activity.

Furthermore, the trend of the curves leads one to think that the homogeneous model falsely estimates the stresses and their distribution. In fact, it underestimates Von Mises stresses in the cortical tissue and overestimates them in the trabecular zone. To validate these assumptions, two evaluation metrics were calculated.

In particular, the Absolute Error (AERR) was calculated. At each Time Step, the difference in stress between each homogeneous model and its corresponding stratified model was evaluated.

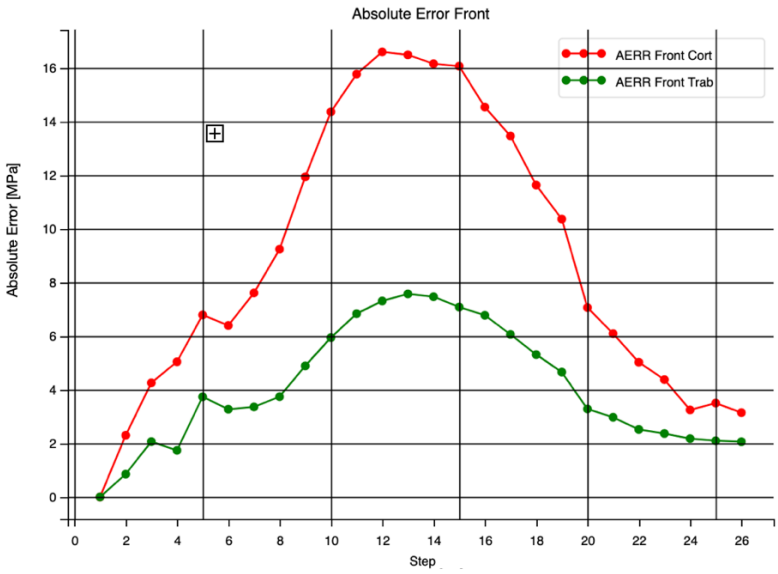
Absolute Error Front
AERR Front Cort
AERR Front Trab
Absolute Error [MPa]
Step
0
2
4
6
8
10
12
14
16
18
20
22
24
26

(A)

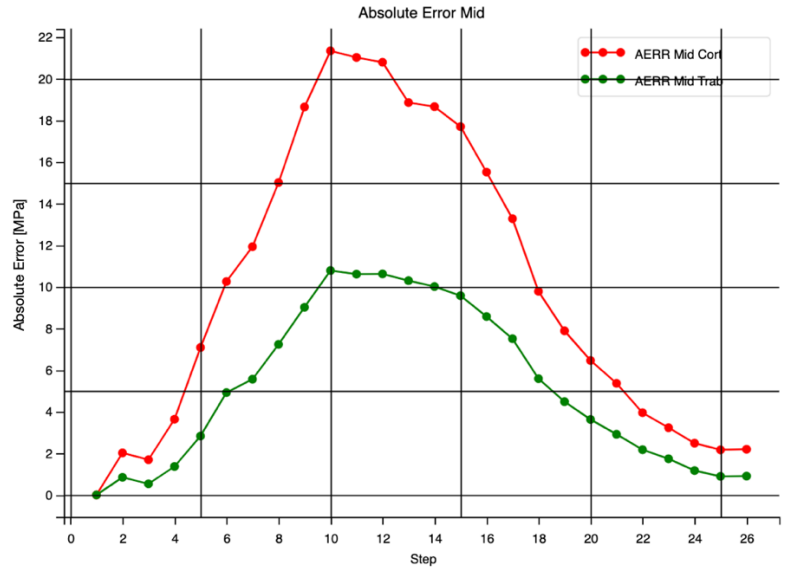

(B)

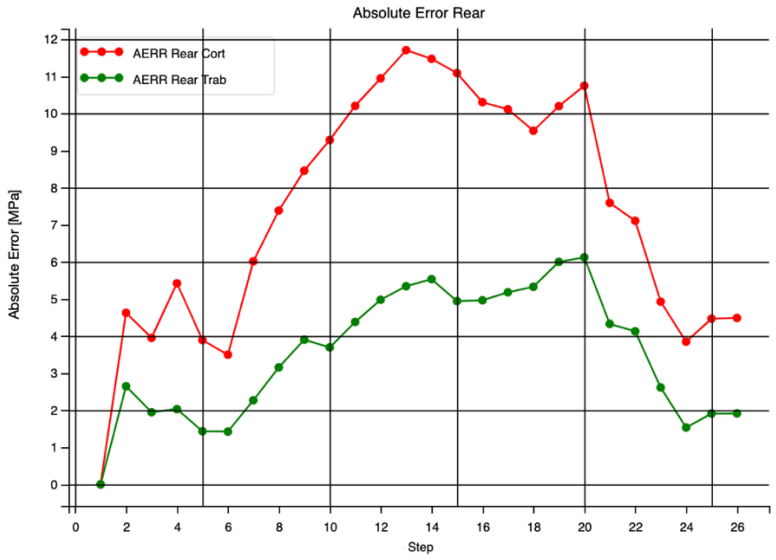

(C)

Figure 40: Absolute Error between the different classes of the models.

By analysing the graphs of the AERRs between the homogeneous and stratified models, interesting temporal trends emerge that capture the complex dynamics of the stress responses in the two models during the running cycle. These trends provide an important window into the diversity of the biomechanical response of the models, highlighting particularities in the stress distribution, especially during the critical phase of maximum pressure on the metatarsus.

A notable aspect noted is the increasing gap in stress values between the two models, reaching its maximum at a specific peak. This phenomenon indicates a significant difference in response between the stratified model, which considers the differences in composition and density between the cortical and trabecular zone, and the homogeneous model, which uniformly considers the entire bone structure. This marked deviation becomes particularly relevant during the maximum pressure phase

on the cortical metatarsal. The greater heterogeneity of the layered model makes it possible to more accurately and realistically capture the specific stress distribution associated with this critical phase of the running cycle. The cortical zone, which is denser and stiffer, experiences higher stresses, and the ability of the layered model to reflect these localised variations becomes clear.

However, what adds complexity and depth to our analysis is the subsequent decrease in the discrepancy after the peak pressure. This trend can be interpreted as a gradual convergence of the two models during successive phases of the time cycle. While the layered model deviates significantly during specific stress situations, it appears to converge with the homogeneous model at other stages, suggesting a greater similarity of biomechanical response in such contexts.

By analysing the Stress Ratio, we can define how much the homogeneous model underestimates stress in the cortical region and how much it overestimates it in the trabecular region. Particularly relevant is the calculation of the Ratio separately for the cortical and trabecular regions.

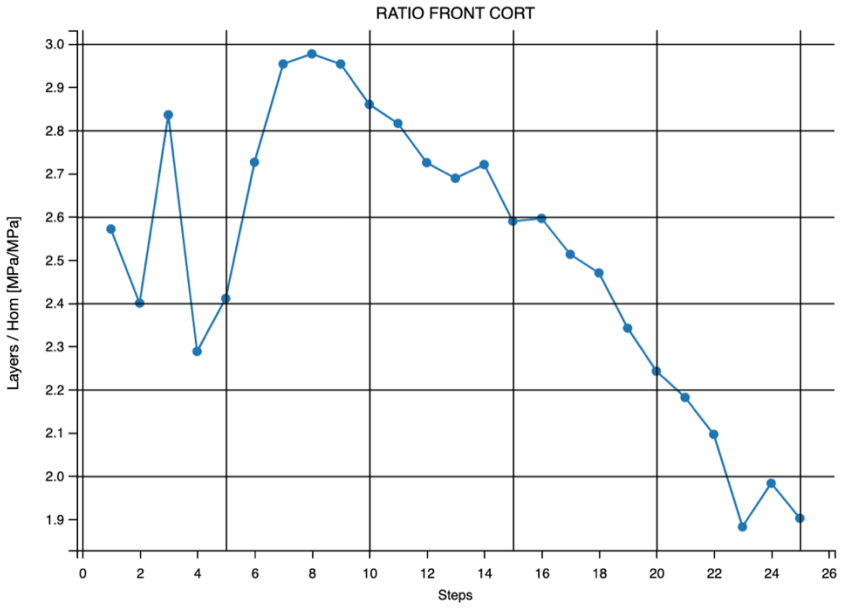

(A)

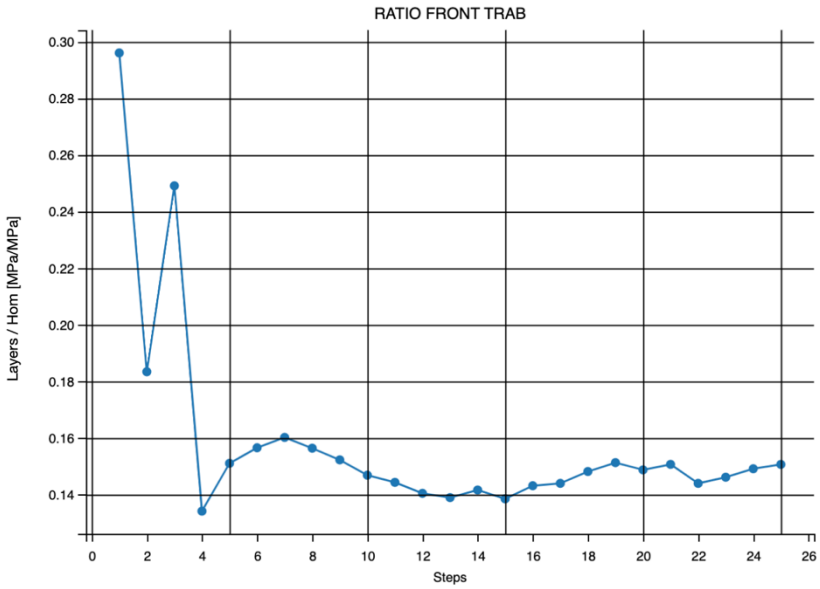

(B)

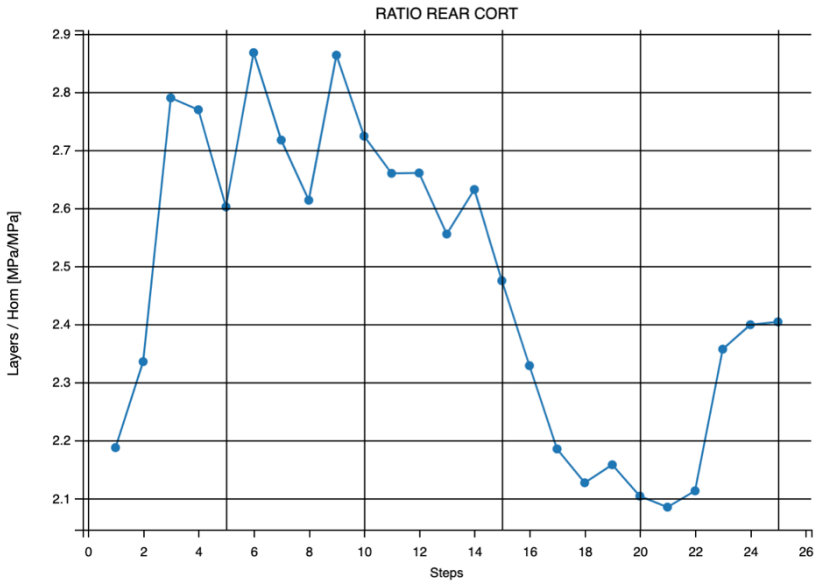

(C)

Figure 41: Cortical Stress Ratio for Homogeneus and Layers models.

Looking at the three graphs describing the stress ratio in the cortical area, an interesting picture emerges. All Stress Ratio (R) values are greater than 1, and the range is consistently between 2 and 3. This observation is significant as it indicates that the homogeneous model underestimates Von Mises stresses in the cortical region of the foot on average by approximately 2.5 times compared to a more detailed model that takes into account the difference in composition between the cortical and trabecular.

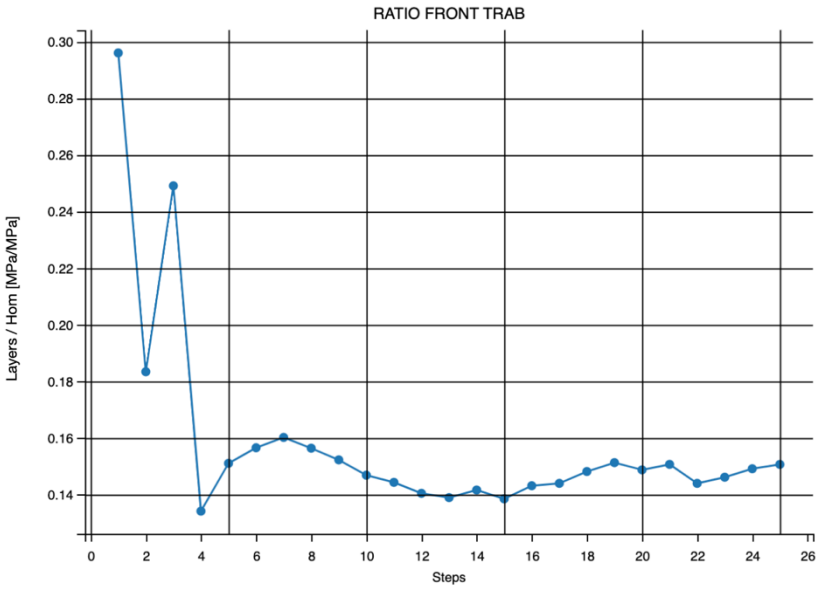
RATIO FRONT TRAB
Layers / Hom [MPa/MPa]
0.30
0.28
0.26
0.24
0.22
0.20
0.18
0.16
0.14
0
2
4
6
8
10
12
14
16
18
20
22
24
26
Steps

(A)

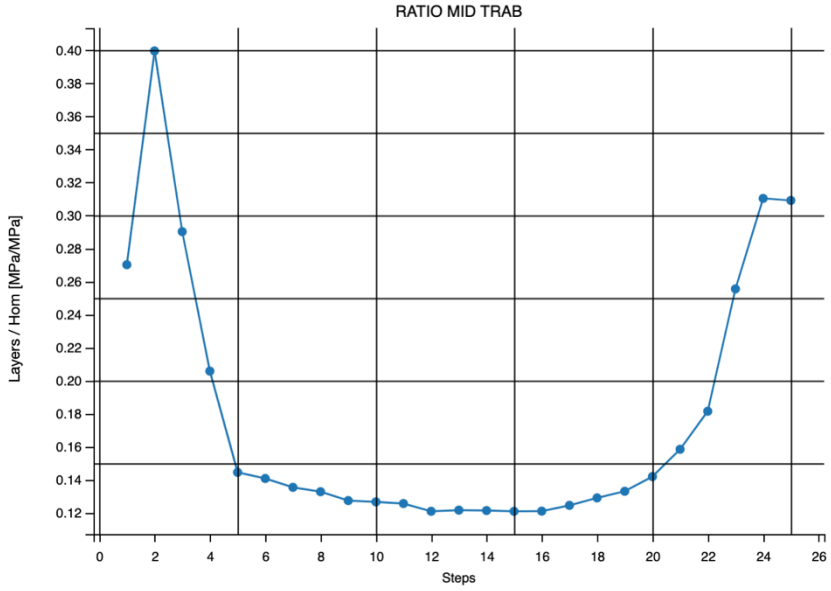
RATIO MID TRAB
Layers / Hom [MPa/MPa]
0.40
0.38
0.36
0.34
0.32
0.30
0.28
0.26
0.24
0.22
0.20
0.18
0.16
0.14
0.12
0
2
4
6
8
10
12
14
16
18
20
22
24
26
Steps

(B)

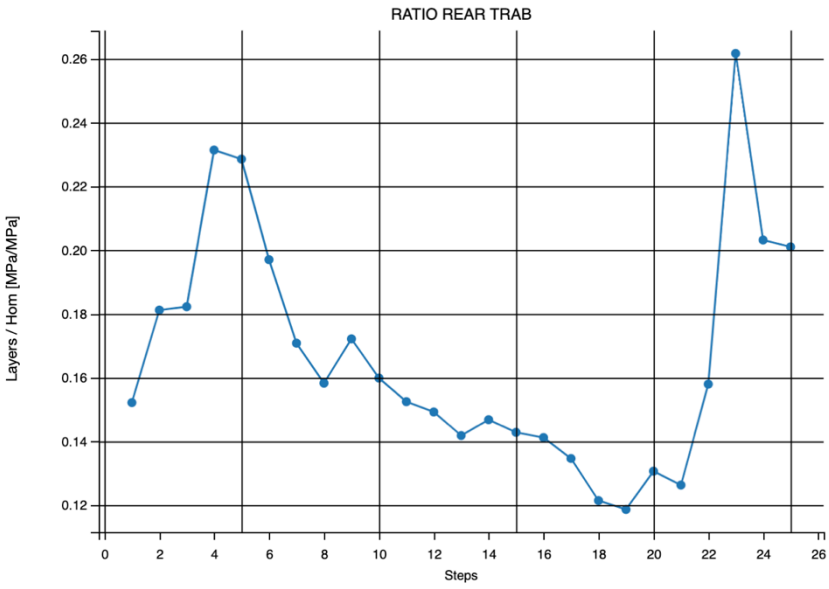

(C)

Figure 42: Trabecular Stress Ratio for Homogeneus and Layers models.

Differently, focusing on the trabecular region, the stress ratio in this area shows that the homogeneous model overestimates the stresses by up to eight times, with a value consistently between 0.12 and 0.2. This significant discrepancy highlights how the homogeneous model is unable to accurately capture the complexity of the biomechanical response in the trabecular region, showing an apparent inability to adequately model density and composition variations in this part of the bone.

Table 3: Ratio values.

REGION	**RATIO**		
CORT	R=2.44	R>1	Underestimate
TRAB	R=0.17	R<1	Overestimation

5.2.3 Deformation Assessment

Below are the average deformations for each time instant examined to observe the result from a numerical point of view.

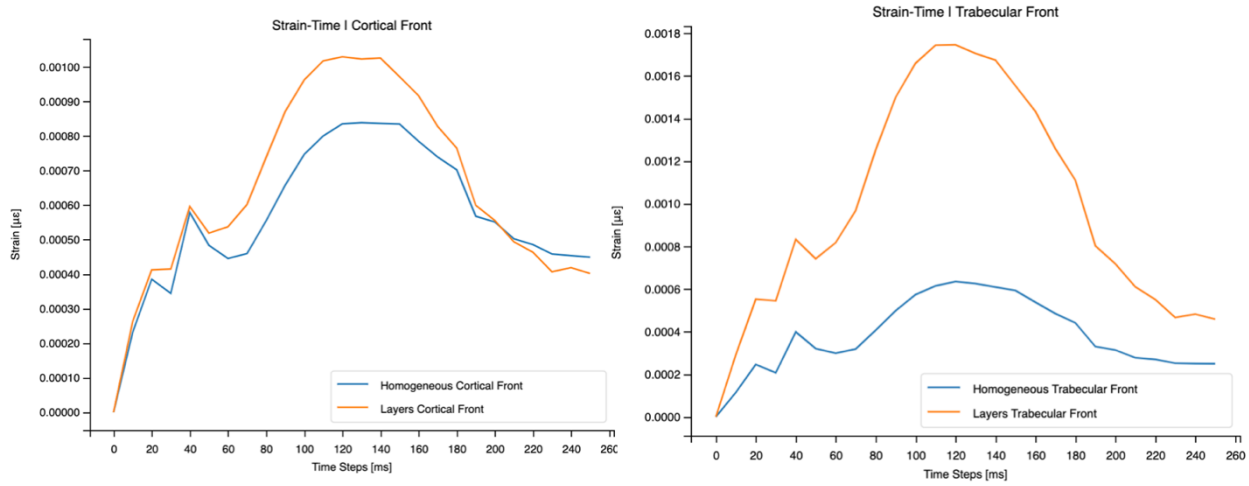

Figure 43: Deformations curves in Front models.

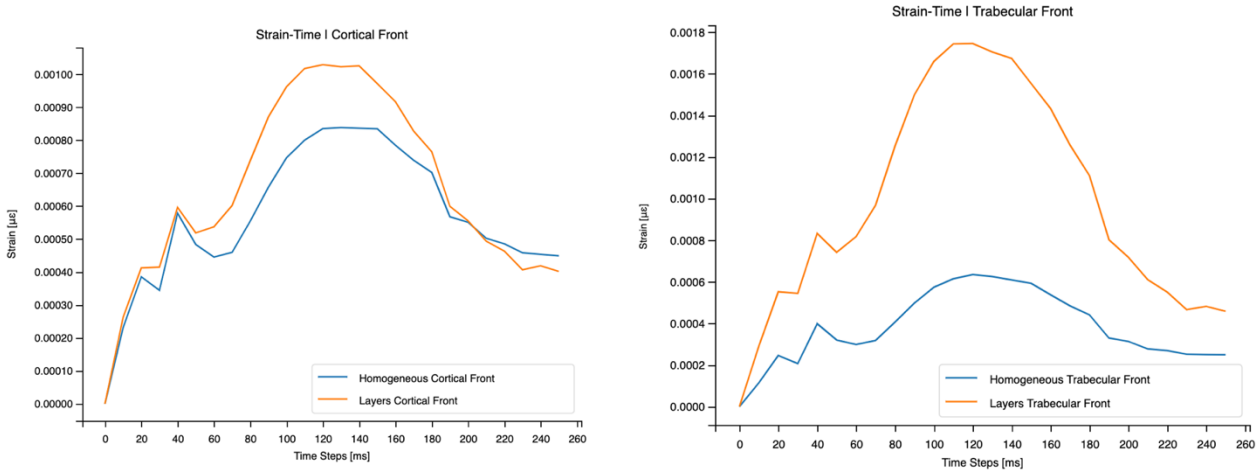

Figure 44: Deformations curves in Middle models.

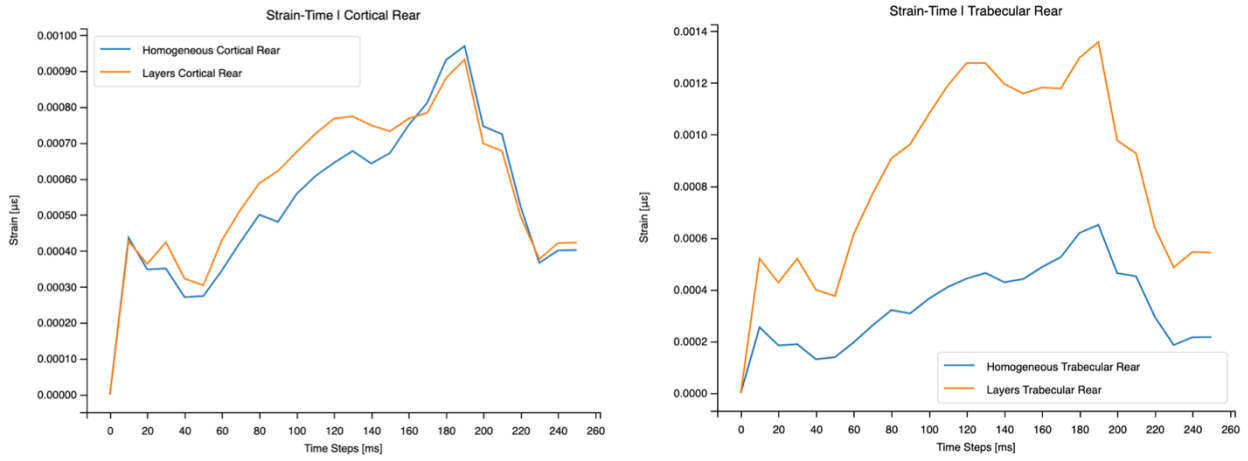

Figure 45: Deformation curves in Rear models.

A key point that emerged from the analysis is the significant difference in deformations between the cortical and trabecular regions in the two model classes, homogeneous and stratified. In cortical cases, the difference between the two model classes is smaller than in trabecular cases. This result is reflected in the established knowledge of bone biomechanics. In fact, we know that cortical tissue has a limited deformation capacity before failure. Its intrinsic rigidity limits the amount of deformation it can undergo before reaching a state of fracture or failure. Consequently, it is reasonable to expect differences between models to be less pronounced in cortical regions, as cortical behaviour is generally more uniform and predictable than trabecular.

On the other hand, the trabecular region, despite its lower stiffness, has a considerable deformation capacity, being able to deform up to 50 per cent in borderline cases. The average deformation curves clearly show that the layered models reflect this characteristic, with the outer shell reaching a maximum deformation of 0.14% and the spongiosa region being able to deform up to 0.24%.

In contrast, the homogeneous models present a different situation, misrepresenting the behaviour of the trabecular region. The maximum deformation observed in the trabecular region is 0.09%, showing a significant underestimation compared to the stratified models. This is consistent with expectations, considering that the homogeneous models do not accurately capture the variety of biomechanical responses and deformation capacity of the trabecular.

It was also possible to compare the overall deformation curves of the Front model with the Stress-Time curve extracted from the Y model. Miyazaki et al. The curves are defined from an average strain calculation between the cortical and trabecular region. The layered class model shows a deformation pattern like the model proposed by Y. Miyazaki et al [46].

However, the times of the model in the literature are higher than those extrapolated from the stratified model. This may be caused by individual variability.

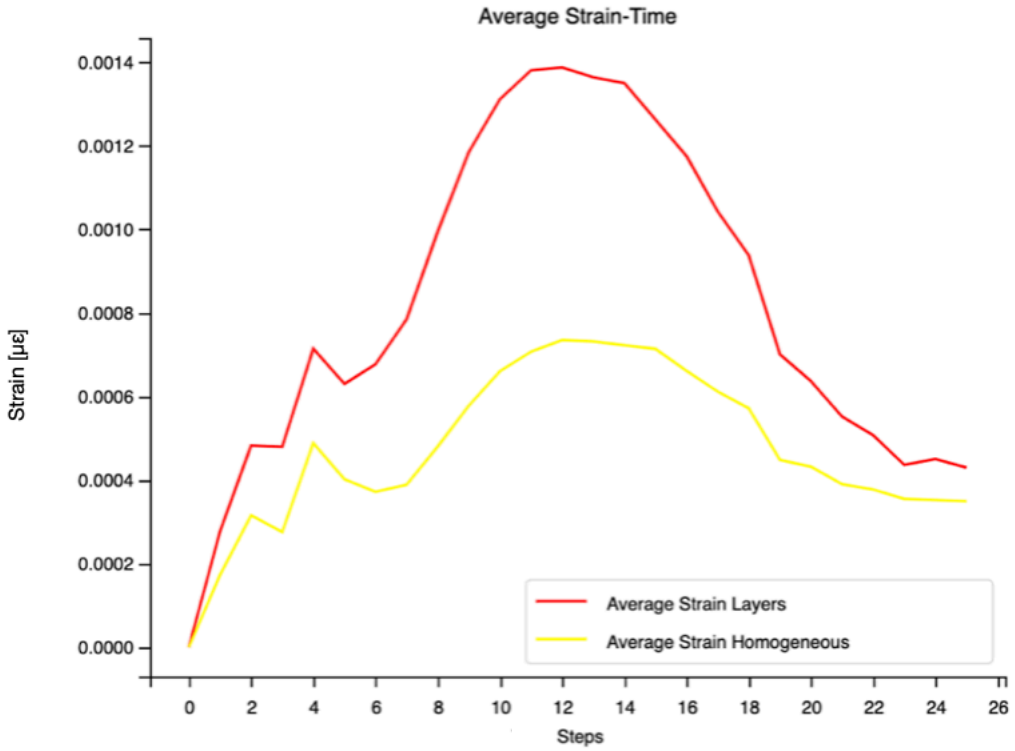

Figure 46: Deformations curves of Cortical and Trabecular regions.

As the figure shows, a maximum deformation occurs at half the support time, which shows a peak deformation of 0.14%, a value and behaviour like the model taken as a reference, which is in stark contrast to the maximum deformation value of the homogeneous model (0.07%).

Chapter 6

6 Conclusions

Metatarsal injuries often result from repetitive overloading of the anatomical structure and the limited ability to adapt to such stresses. Because of the challenges in accurately measuring these stresses in vivo, biomechanical modelling becomes crucial. However, current finite element modelling methodologies often have limitations as they fail to adequately represent the complexity of biomechanical reality.

The main objective of this project was to develop three FE models of the lower limb, distinguished by plantar load distribution modes and consisting of bone tissue diversity. These models were compared with homogeneous material models to assess which finite element analysis approach is most effective in predicting possible fracture sites.

The techniques used include the extraction of tissue geometries using 3D Slicer software, the creation of three-dimensional representations using Materialise 3-Matic and finite element modelling using Abaqus. Key variables considered in six different simulations include ground reaction forces, Von Mises stresses and estimated deformations.

To achieve the objective, two levels of validation were performed. Initially, the stratified and homogeneous models were qualitatively compared through visual observations of the regions of interest, showing that the stratified models more accurately reflect the mechanical behaviour of the fabrics.

Subsequently, a quantitative comparison between the models was performed, revealing significant discrepancies in stresses and strains. Although both types of models were able to effectively represent the dynamics of the running cycle, the stratified models showed a greater variation in stress and strain intensity between the different bone regions, compared to the homogeneous models. A ground reaction force (GRF) analysis confirmed that both types of models exhibited a similar macroscopic biomechanical response, independent of the variation in bone composition. At the microscopic level, there were significant differences in stresses between the trabecular and cortical regions in the stratified models, reflecting different tissue composition and density characteristics. In the homogeneous models, stresses appeared uniform in the two regions. In support of this, the stress ratio in the cortical zone was 2.44, defining an underestimation of the mechanical behaviour in the uniform models, 0.17 in the trabecular zone, suggesting an overestimation. The deformations also showed

significant differences, with a deformation of 0.24% in the trabecular zone for the stratified models, compared to 0.09% in the homogeneous models. The average deformation between the cortical and trabecular regions was found to be 0.14%, in line with the results of a study conducted by Y. Miyazaky et al.[46], which assigned different elastic modulus values for different bone regions.

In conclusion, the results indicate that layered models more accurately reflect tissue behaviour and biomechanical properties than homogeneous models. This suggests that the implementation of layered models could be a promising approach to simulate the mechanical behaviour of lower limbs more accurately.

However, it is important to consider some significant limitations that emerged from this study. The limited sample size, with only one patient per model, could compromise the representativeness of the population, making it crucial to enlarge the sampling to conduct a statistical analysis and generalise the results. Another limitation is the restriction of the anatomical location of the accurate reconstruction to the First Metatarsal. Consequently, it would be essential to define the trabecular and cortical geometry of all the bones constituting the lower limb, to obtain results more faithful to reality. A third limitation concerns the Young's modules used, taken from the literature, and referred to anatomical districts like the metatarsal bones, but their reliability is not guaranteed due to the considerable difficulties in performing mechanical tests on internal tissues such as trabecular tissue.

Future research could, therefore, include a better investigation of Young's modulus of metatarsal bones, as the coefficients used may not be precise enough, thus considering more accurate determination of the discrepancy between cortical and trabecular behaviour. This would allow engineers to obtain more accurate and efficient results, improving the diagnostic process and understanding of bone behaviour under repetitive stress. Furthermore, it will be essential to stratify all the bones that make up the foot to obtain stress-strain values relative to the entire anatomical district. Lastly, a larger number of subjects should be considered to conduct a statistical analysis and arrive at a gold standard model.

Bibliography

[1] J. Brockwell, Y. Yeung, and J. F. Griffith, “Stress fractures of the foot and ankle,” *Sports Medicine and Arthroscopy Review*, vol. 17, no. 3. Lippincott Williams and Wilkins, pp. 149–159, 2009. doi: 10.1097/JSA.0b013e3181b12727.

[2] M. J. Welck, T. Hayes, P. Pastides, W. Khan, and B. Rudge, “Stress fractures of the foot and ankle,” *Injury*, vol. 48, no. 8. Elsevier Ltd, pp. 1722–1726, Aug. 01, 2017. doi: 10.1016/j.injury.2015.06.015.

[3] P. Takkar and R. Prabhakar, “Stress fractures in military recruits: A prospective study for evaluation of incidence, patterns of injury and invalidments out of service,” *Med J Armed Forces India*, vol. 75, no. 3, pp. 330–334, Jul. 2019, doi: 10.1016/j.mjafi.2018.09.006.

[4] Centre for Mechanics of Biological Materials, “Meccanica dei tessuti biologici - Bone Mechanics.”

[5] Francesco Centorrino, “https://www.microbiologiaitalia.it/didattica/il-tessuto-osseo/.”

[6] “https://www.chimica-online.it/biologia/cellula-ossea.htm.”

[7] “https://www.theskeletalsystem.net/foot-bones.”

[8] “https://musculoskeletalkey.com/foot-and-ankle-11/.”

[9] S. M. Ott, “Cortical or Trabecular Bone: What’s the Difference?,” *American Journal of Nephrology*, vol. 47, no. 6. S. Karger AG, pp. 373–375, Jul. 01, 2018. doi: 10.1159/000489672.

[10] Physiopedia, “https://www.physio-pedia.com/Bone_Cortical_And_Cancellous,” 2023.

[11] V. D. O. Michael McKinley, *Anatomia Umana*, I edizione italiana. 2012.

[12] E. A. Zimmermann *et al.*, “Intrinsic mechanical behavior of femoral cortical bone in young, osteoporotic and bisphosphonate-treated individuals in low-and high energy fracture conditions,” *Sci Rep*, vol. 6, Feb. 2016, doi: 10.1038/srep21072.

[13] BD editors, “https://biologydictionary.net/spongy-bone/.”

[14] R. Oftadeh, M. Perez-Viloria, J. C. Villa-Camacho, A. Vaziri, and A. Nazarian, “Biomechanics and Mechanobiology of Trabecular Bone: A Review,” *Journal of Biomechanical Engineering*, vol. 137, no. 1. American Society of Mechanical Engineers (ASME), Jan. 01, 2015. doi: 10.1115/1.4029176.

[15] “https://www.chimica-online.it/biologia/tessuto-osseo-spugnoso.htm.”

[16] Niccolò Ramponi, “https://www.lascienzainpalestra.it/caviglia-anatomia-e-biomeccanica/.”

[17] “Tesi Francesca Bellà”.

[18] TeachMeAnatomy, “https://teachmeanatomy.info/lower-limb/muscles/leg/anterior-compartment/.”

[19] “https://en.wikipedia.org/wiki/Flexor_digitorum_longus_muscle#/media/File:1123_Muscles_of_the_Leg_that_Move_the_Foot_and_Toes_c.png.”

[20] J. K. Aggarwal and Q. Cai, “Human Motion Analysis: A Review,” 1999. [Online]. Available: http://www.idealibrary.comon

[21] V. L. Chester and M. Calhoun, “Gait Symmetry in Children with Autism,” *Autism Res Treat*, vol. 2012, pp. 1–5, 2012, doi: 10.1155/2012/576478.

[22] J. B. Webster and B. J. Darter, “Principles of Normal and Pathologic Gait,” in *Atlas of Orthoses and Assistive Devices, Fifth Edition*, Elsevier, 2018, pp. 49-62.e1. doi: 10.1016/B978-0-323-48323-0.00004-4.

[23] N. Prajapati, A. Kaur, and D. Sethi, “A Review on Clinical Gait Analysis,” in *Proceedings of the 5th International Conference on Trends in Electronics and Informatics, ICOEI 2021*, Institute of Electrical and Electronics Engineers Inc., Jun. 2021, pp. 967–974. doi: 10.1109/ICOEI51242.2021.9452951.

[24] J. S. Park and C. H. Kim, “Ground-Reaction-Force-Based Gait Analysis and Its Application to Gait Disorder Assessment: New Indices for Quantifying Walking Behavior,” *Sensors*, vol. 22, no. 19, Oct. 2022, doi: 10.3390/s22197558.

[25] A. Karatsidis, G. Bellusci, H. M. Schepers, M. de Zee, M. S. Andersen, and P. H. Veltink, “Estimation of ground reaction forces and moments during gait using only inertial motion capture,” *Sensors (Switzerland)*, vol. 17, no. 1, Jan. 2017, doi: 10.3390/s17010075.

[26] Redazione Tecnica, “https://biblus.acca.it/analisi-fem/.”

[27] Kate Brush, “https://www.techtarget.com/searchsoftwarequality/definition/finite-element-analysis-FEA.”

[28] C. Van Waerbeke, A. Jacques, E. Berton, and G. Rao, “Inter-strides variability affects internal foot tissue loadings during running,” *Sci Rep*, vol. 12, no. 1, Dec. 2022, doi: 10.1038/s41598-022-08177-1.

[29] L. H. Braak and A. Huson, “Stresses in a simplified two dimensional model of a normal foot : a preliminary analysis Citation for published version (APA): Patil, K. M Stresses in a simplified two dimensional model of a normal foot : a preliminary analysis STRESSES IN A SIMPLIFIED TWO DIMENSIONAL MODEL OF A NORMAL FOOT-A PRELIMINARY ANALYSIS,” *Mech Res Commun*, vol. 20, no. 1, pp. 1–7, 1993, doi: 10.1016/0093.

[30] S. Goske, A. Erdemir, M. Petre, S. Budhabhatti, and P. R. Cavanagh, “Reduction of plantar heel pressures: Insole design using finite element analysis,” *J Biomech*, vol. 39, no. 13, pp. 2363–2370, 2006, doi: 10.1016/j.jbiomech.2005.08.006.

[31] J. P. Halloran, M. Ackermann, A. Erdemir, and A. J. van den Bogert, “Concurrent musculoskeletal dynamics and finite element analysis predicts altered gait patterns to reduce foot tissue loading,” *J Biomech*, vol. 43, no. 14, pp. 2810–2815, Oct. 2010, doi: 10.1016/j.jbiomech.2010.05.036.

[32] C. T. Lim, J. C. H. Goh, Z.-H. Qian, L. Ren, L.-Q. Ren, and A. Boonpratatong, “IFMBE Proceedings 31 - A Three-Dimensional Finite Element Musculoskeletal Model of the Human Foot Complex,” 2010. [Online]. Available: www.springerlink.com

[33] W.-P. Chen, F.-T. Tang, and C.-W. Ju, “Stress Distribution of the Foot During Mid-Stance to Push-Off in Barefoot Gait: a 3-D Finite Element Analysis.”

[34] J. Tak-Man Cheung, M. Zhang, and K. N. An, “Effects of plantar fascia stiffness on the biomechanical responses of the ankle-foot complex,” *Clinical Biomechanics*, vol. 19, no. 8, pp. 839–846, 2004, doi: 10.1016/j.clinbiomech.2004.06.002.

[35] J. M. Iaquinto and J. S. Wayne, “Computational model of the lower leg and foot/ankle complex: Application to arch stability,” *J Biomech Eng*, vol. 132, no. 2, Feb. 2010, doi: 10.1115/1.4000939.

[36] J. W. Fernandez, M. Z. Ul Haque, P. J. Hunter, and K. Mithraratne, “Mechanics of the foot Part 1: A continuum framework for evaluating soft tissue stiffening in the pathologic foot,” *Int J Numer Method Biomed Eng*, vol. 28, no. 10, pp. 1056–1070, Oct. 2012, doi: 10.1002/cnm.2494.

[37] Z. Sawacha, G. Guarneri, G. Cristoferi, A. Guiotto, A. Avogaro, and C. Cobelli, “Integrated kinematics-kinetics-plantar pressure data analysis: A useful tool for characterizing diabetic foot biomechanics,” *Gait Posture*, vol. 36, no. 1, pp. 20–26, May 2012, doi: 10.1016/j.gaitpost.2011.12.007.

[38] A. Guiotto, Z. Sawacha, G. Guarneri, A. Avogaro, and C. Cobelli, “3D finite element model of the diabetic neuropathic foot: A gait analysis driven approach,” *J Biomech*, vol. 47, no. 12, pp. 3064–3071, Sep. 2014, doi: 10.1016/j.jbiomech.2014.06.029.

[39] A. Scarton *et al.*, “A methodological framework for detecting ulcers’ risk in diabetic foot subjects by combining gait analysis, a new musculoskeletal foot model and a foot finite element model,” *Gait Posture*, vol. 60, pp. 279–285, Feb. 2018, doi: 10.1016/j.gaitpost.2017.08.036.

[40] Z. Qian, L. Ren, Y. Ding, J. R. Hutchinson, and L. Ren, “A dynamic finite element analysis of human foot complex in the sagittal plane during level walking,” *PLoS One*, vol. 8, no. 11, Nov. 2013, doi: 10.1371/journal.pone.0079424.

[41] T. L. W. Chen, D. W. C. Wong, Y. Wang, J. Lin, and M. Zhang, “Foot arch deformation and plantar fascia loading during running with rearfoot strike and forefoot strike: A dynamic finite element analysis,” *J Biomech*, vol. 83, pp. 260–272, Jan. 2019, doi: 10.1016/j.jbiomech.2018.12.007.

[42] B. Chuckpaiwong, C. Cook, R. Pietrobon, and J. A. Nunley, “Second metatarsal stress fracture in sport: Comparative risk factors between proximal and non-proximal locations,” *Br J Sports Med*, vol. 41, no. 8, pp. 510–514, Aug. 2007, doi: 10.1136/bjsm.2006.033571.

[43] S. A. Meardon *et al.*, “Peak and Per-Step Tibial Bone Stress During Walking and Running in Female and Male Recreational Runners,” *American Journal of Sports Medicine*, vol. 49, no. 8, pp. 2227–2237, Jul. 2021, doi: 10.1177/03635465211014854.

[44] V. Filardi, “Finite element analysis of the foot: Stress and displacement shielding,” *J Orthop*, vol. 15, no. 4, pp. 974–979, Dec. 2018, doi: 10.1016/j.jor.2018.08.037.

[45] Y. S. Lai, W. C. Chen, C. H. Huang, C. K. Cheng, K. K. Chan, and T. K. Chang, “The effect of graft strength on knee laxity and graft in-situ forces after posterior cruciate ligament reconstruction,” *PLoS One*, vol. 10, no. 5, May 2015, doi: 10.1371/journal.pone.0127293.

[46] Y. Miyazaki, R. Sugizaki, M. Kawasaki, T. Nakagawa, Y. Saho, and T. Tateishi, “Fifth metatarsal strain distribution during cutting motions in soccer,” *Sports Biomech*, 2023, doi: 10.1080/14763141.2023.2241839.

[47] T. N. Alexander S. Gillis, “https://www.techtarget.com/iotagenda/definition/mesh-network-topology-mesh-network,” June 2021.